NTNU
Norwegian University of
Science and Technology

Modeling and Simulation of Anchor Handling Vessels

Lars Andreas Lien Wennersberg

Master of Science in Engineering Cybernetics
Submission date: June 2009
Supervisor: Thor Inge Fossen, ITK

Norwegian University of Science and Technology
Department of Engineering Cybernetics

Problem Description

The purpose of the thesis is to develop a simulator of an anchor handling vessel that is capable of simulating anchor handling operations under influence of environmental forces with realistic vessel motions. The following elements must be considered:

1. Give an overview of the best practice for anchor handling operations. Classification rules, regulations and operational procedures should be considered.

2. Based on a vessel model from the MSS Toolbox, develop and implement a simulator of an anchor handling vessel in MATLAB/Simulink. The simulator should contain the necessary modules for ballast tanks, roll reduction, cable systems and anchor handling equipment on deck.

3. Verify the simulator by simulating relevant anchor handling scenarios.

4. Present your findings and theoretical results in a report.

Assignment given: 12. January 2009
Supervisor: Thor Inge Fossen, ITK

Abstract

The topic of this thesis is modeling and simulation of anchor handling vessels. Computer simulations of anchor handling vessels can be used to evaluate the forces acting on them, and to gain valuable insight into their operational limitations. Introductorily, an overview containing important aspects of anchor handling operations is presented. The objective is to highlight important subjects that must be considered before a simulator is developed.

A simulator of an anchor handling vessel is successfully implemented in Matlab and Simulink. The simulator contains modules for ballast tanks, anti-roll tanks, cables, seabed and anchor interaction, winch systems and guide pins. The vessel model is matched up against a real anchor handling vessel to give realistic thrust characteristics. The simulator is capable of simulating both anchor deployment and anchor recovery operations in real time.

Catenary equations are used to model cables. A quasi-static polynomial approach with look-up tables is used for implementation. The method allows the use of different catenary models to simulate different phases of the anchor handling operation. A catenary model of two cables with a point load, imitating the effect of an anchor, is developed based on existing catenary models in the literature.

The simulator is verified through simulations. A set of case studies is used to evaluate the vessel performance during anchor deployment and recovery. The case studies consider operation in ideal and rough weather conditions, and it is shown how equipment failures and poor vessel configuration can lead to decreased vessel stability and loss of maneuvering capabilities.

I

Preface

This master thesis is written at the Department of Engineering Cybernetics at the Norwegian University of Science and Technology. It represents the end of my days as a student at NTNU. The years I've spent as a student in Trondheim have been very rewarding, both academically and socially.

First and foremost, I would like to thank my supervisors Thor Inge Fossen at the Department of Engineering Cybernetics and Øyvind N. Smogeli at Marine Cybernetics for their advices and support throughout the work on this thesis. They guided me in the right directions and gave me valuable help on technical modeling issues.

Marine Cybernetics presented me with the opportunity to write this thesis. I would like to thank Tor Arne Johansen at Marine Cybernetics/Department of Engineering Cybernetics for introducing me to the topic of anchor handling operations.

Thanks also to Carl M. Larsen and Odd M. Faltinsen at CeSOS, Rune Dahlberg at DNV and Ivar Fylling at Sintef Marintek for their literature suggestions and contributions.

Finally I would like to thank my fellow students for creating a good atmosphere and a constructive working environment.

_____

Lars Andreas Lien Wennersberg

Trondheim, June 2009

Contents

List of Figures

Nomenclature

Abbreviations

ABS	American Bureau of Shipping
AH	Anchor Handling
AHO	Anchor Handling Operations
AHTS	Anchor Handling, Tug and Supply
AHV	Anchor Handling Vessel
BP	Bollard Pull
BV	Bureau Veritas
CO	Coordinate Origin
DNV	Det Norske Veritas
DP	Dynamic Positioning
FDM	Finite Difference Methods
FEM	Finite Element Methods
FSE	Free Surface Effect
FSA	Finite Segment Approach
GL	Germandischer Lloyd
GP	Guide Pin
IMO	International Maritime Organization
LMS	Lump-Mass-Spring
LR	Lloyd's Register
MSS	Marine Systems Simulator
NED	North-East-Down
NMD	Norwegian Maritime Directorate
NWEA	North West European Area
OI	Offshore Installation
OSV	Offshore Support Vessel
PCP	Permanent Chaser Pendandt
PID	Proportional, Integral, Derivative
RL	Reference Load
RMP	Rig Move Procedure

Mathematical Notation

x	Scalar
$\mathbf{x}$	Vector
$\mathbf{X}$	Matrix
$x(t)$	Time domain
$x(s)$	Lagrangian coordinate
$\overline{x}$	Logical not

Lowercase

d	[m]	Cable diameter
d_a	[-]	Anchor damping constant
d_w	[-]	Winch damping constant
e	[0/1]	Guide pin error
g	[m/s^2]	Acceleration of gravity
g_i	[-]	Output of guide pin i
h_a	[m]	Vertical cable coordinate
h_b	[m]	Ballast tank height
h_d	[m]	Desired ballast tank water level
h_f	[m]	Free-surface tank height
h_w	[m]	Water column height for ballast and anti-roll tank
l	[m]	Length of cable span
l_a	[m]	Horizontal cable coordinate
m	[kg]	Mass
m_a	[kg/m]	Anchor mass
m_s	[kg/m]	Cable mass per unit length in water
n_b	[-]	Number of ballast tanks
n_g	[-]	Gear ratio
n_{gp}	[-]	Number of guide pins
p	[m]	Stretched Lagrangian coordinate
p_d	[m^3/s]	Volumetric pump flow set-point
p_p	[m^3/s]	Volumetric pump flow
r_d	[m]	Winch drum radius
s	[m]	Unstretched Lagrangian coordinate
s_d	[m]	Cable sag
t	[s]	Time
u	[0/1]	Guide pin control input
v_w	[m/s]	Linear work-wire speed
v_s	[m/s]	Stribeck velocity

Uppercase

A	[m^2]	Unstretched cross-sectional area of cable
A$_f$	[m^2]	Anti-roll tank area
A$_b$	[m^2]	Ballast tank area
A$_4$	[deg]	Amplitude of excitation roll moment
B	[N]	Buoyancy force
C$_\phi$	[-]	Roll condition of vessel
D$_g$	[-]	Gear damping constant
E	[Pa]	Young's modulus of elasticity
F	[-]	Falling slew rate
F$_B$	[N]	Breakout force
F$_C$	[N]	Coloumb friction level
F$_f$	[N]	Friction force
F$_P$	[N]	Vertical point load force
F$_S$	[N]	Stiction force level
H	[N]	Horizontal cable force
H$_s$	[m]	Significant wave height
J$_m$	[kgm^2]	Motor inertia
J$_w$	[kgm^2]	Winch inertia
K$_d$	[-]	PID controller derivative gain
K$_g$	[-]	Gear spring constant
K$_i$	[-]	PID controller integral gain
K$_p$	[-]	PID controller Proportional gain
L	[m]	Unstretched cable length
L$_s$	[m]	Stretched cable length
L$_{pp}$	[m]	Length between perpendiculars
R	[-]	Rising slew rate
R$_B$	[N]	Breakout resistance
$\mathcal{S}$	[-]	Set of active guide pins
T	[N]	Tension
T$_d$	[-]	Derivative time constant
T$_{gm}$	[Nm]	Gear torque on motor side
T$_{gw}$	[Nm]	Gear torque on winch side
T$_i$	[-]	Integral time constant
T$_m$	[Nm]	Motor torque
T$_p$	[s]	Water pump time constant
T$_{wd}$	[Nm]	Wire torque on winch drum
V	[N]	Vertical cable force
V$_b$	[m^3]	Ballast tank volume

W	[N]	Cable weight in water
W_b	[N]	Ballast tank weight
W_e	[N]	Effective cable weight
W_s	[N/m]	Cable weight per unit length in water

Greek

δ_g	[-]	Gear deadzone
∇	[m^3]	Displacement volume
μ_α	[-]	Mean value of α
ω_4	[rad/s]	Natural frequency in roll
ω_m	[rad/s]	Angular velocity of motor shaft
ω_w	[rad/s]	Angular velocity of winch drum
ϕ	[deg]	Vessel roll
ϕ_g	[-]	Gear deflection
ψ	[rad]	Vessel heading
ψ_c	[rad]	Cable angle
ψ_r	[rad]	Relative vessel-cable angle
ρ	[kg/m^3]	Water density
σ_0	[-]	Bristle stiffness constant
σ_1	[-]	Bristle damping constant
σ_2	[-]	Viscous friction constant
σ_4	[rad/s]	Wave encounter frequency
σ_α	[-]	Variance of α
θ_m	[rad]	Angular position of motor shaft
θ_w	[rad]	Angular position of winch drum
ζ_4	[-]	Relative damping constant in roll

Chapter 1

Introduction

1.1 Background and Motivation

A supply vessel is the most basic form of an offshore support vessel (OSV). Due to the variety of tasks and operations that are required to be performed at offshore installations (OI), supply vessels are often rigged with additional equipment to increase their versatility and capability of performing these tasks. Anchor handling vessels (AHV) or anchor handling tug and supply vessels (AHTS) are usually supply vessels with the additional capability of assisting offshore installations with anchor handling operations (AHO).

Rough weather conditions are frequently experienced at OIs. In addition, AHVs operate under strict time schedules. The desire to be on schedule could compromize the safety of the operation. Both AHVs and AHOs are subject to an extensive regulatory system aiming to eliminate all hazards related to such operations, and protect the involved parties. Despite these efforts, accidents causing injuries, loss of lives and material damages occur. This was last verified by the loss of the *Bourbon Dolphin* on April 12th 2007.

To prevent such accidents from happening again, computer simulations of AHVs may be of great importance. This requires that mathematical models specifically adjusted to match the characteristics of a given AHV and its assosiated equipment are implemented. Simulations can be used to evaluate the various forces acting on the vessel in specific situations as well as gaining valuable insight into the operational limits of the vessel. A further development of such simulations would be to incorporate a graphical interface and create a training simulator for the vessel crew.

1.2   Contributions and Scope of the Report

The main contribution of this thesis is the implemetation of an anchor handling vessel simulator capable of simulating both anchor deployment and anchor recovery operations. The simulator contains modules for ballast tanks, anti-roll tanks, cables, seabed and anchor interaction, winch systems and guide pins. A cable model of two cables with a point load, imitating the effect of an anchor, is developed based on existing catenary models in the literature. An algorithm-based model of guide pins is also developed based on functional descriptions in the literature. Relevant rules, regulations and operational procedures are reviewed, resulting in an entire chapter devoted to aspects of anchor handling operations that are essential to consider before an AHV simulator is developed.

1.3   Organization of the Report

In Chapter 2   an overview of important aspects related anchor handling operations is presented. The vessel equipment that should be modeled are identified. The rules, regulations and procedures related to AHOs and AHVs are summarized. A typical anchor deployment and anchor retrieval scenario is outlined.

In Chapter 3   the various catenary models are discussed and compared. In addition, a catenary model combining two cables and one point load is developed based on existing catenary equations. A quasi-static implementation approach using two-dimensional polynomials with look-up tables is presented.

In Chapter 4   the seabed and anchor interaction during anchor breakout is discussed. A dynamic friction model is suggested for modeling of the friction force.

In Chapter 5   the equations of the vessel model are presented. The coupling equations between the vessel and the cables are also developed.

In Chapter 6   the models of the vessels's deck equipment are presented. This includes the winch system and the guide pins.

In Chapter 7   mathematical models of ballast tanks and anti-roll tanks are presented and discussed.

In Chapter 8   the simulator implementation is briefly discussed. A set of case studies is designed and the results from the simulations are presented.

In Chapter 9   the results from the simulations are discussed.

In Chapter 10 the conclusion and suggestions for further work are presented.

Chapter 2

Anchor Handling Operations

This chapter contains an overview of various elements related to anchor handling operations, ranging from vessel design to operational procedures. The objective is to highlight important aspects of anchor handling operations that must be taken into consideration before a simulator is developed.

2.1 Vessel Design

AHVs have a very characteristic design. This is due to the specialized, yet various operations they are required to perform. In addition, the vessels must be capable of operating in rough environmental conditions. Design variations exist due to historical shipbuilding traditions and specific areas of operation. There are three main categories of anchor handling vessels [22]: the *North Eurpean Anchor Handling Tug*, the *American Anchor Handling Tug* and *the Anchor Handling Tug and Supply Vessel*. A detailed explanation of the particulars for each category is not provided, but some common features that are or at least should be present on any AHV are briefly discussed.

An AHV has a very large after deck. The starboard and port side of the after deck are enclosed by barriers intended to protect both the crew and equipment from the sea, since the after deck normally is situated close to the sea level. The stern of the vessel is open to the sea, allowing anchors and other equipment to be deployed and recovered easily. It is normal to have a stern roller positioned at the stern of the vessel. A winch house containing towing wires, winches and anchor handling equipment is situated on the forward section of the after deck. The accomodation and bridge is situated above the winch house. A typical anchor handling tug and supply vessel is illustrated in Figure 2.1. A more detailed and thorough explanation of the elements in AHV design is given in [22] and [16].

Figure 2.1. *Far Sapphire* Anchor Handling Tug and Supply Vessel. Photo courtesy to *Farstad.*

2.2   Anchor Handling Equipment

Since mooring systems differ, a specific operation requires a particular set of equipment and tools to accomplish the mission of deploying and retrieving anchors. The amount of equipment utilized in anchor handling operations is huge. A brief explanation of the equipment that should be part of an AHV simulator is given in this section.

Work Wire
The work wire is stored in the winch and used for deployment or retrieval of anchors, in addition to towing operations. There are usually several work wires on a vessel with different lengths and characteristics.

Winch
The winch usually contains both anchor handling drums and towing drums. The drums are normally connected to the same drive system. The anchor handling winch should have multiple gears to allow high pulling force at low gears. An arrangement with variable braking power should be present, allowing the winch to pay out work wire when the tension is excessive. The winch system may either be hydraulic, electric or diesel driven. The direction of rotation is normally overwind, so that the work wire has a small downwards angle towards the stern of the vessel.

Stern Roller
The stern roller is primarily used to guide chains and wires, contributing to less frictional damage at the stern of the vessel. It is also used to load and unload anchors.

Guide Pins
A guide pin is an arrangement for keeping the work wire in the centre/midship area of

the vessel. Several guide pins may be installed, allowing tighter control of the work wire position at the stern of the vessel.

Shark Jaw
The shark jaw is a device for connecting and disconnecting chain and wires, in addition to securing chain sections on the deck.

2.3 Rules and Regulations

All aspects of maritime operations are governed by an extensive regulatory system and a number of international conventions. The International Maritime Organisation (IMO) is an organization that promotes cooperation among governments and the maritime industry to improve safety at sea [43]. Most of the maritime conventions have been adopted by IMO, but they are only considered to be minimum requirements. Despite this, the normal practise is to follow the IMO conventions, even though each individual flag state can impose stricter rules. Most of the requirements in the regulatory system of IMO only applies to ships travelling between ports in different states. Traffic within national waters is therefore governed by the respective national authorities.

In Norway, the IMO conventions are implemented by authority of the Act No. 9 of 16 February 2007 on Maritime Safety, also known as the Maritime Safety Act [26]. The Norwegian Maritime Directorate (NMD) performs supervision and control of ships, but they also delegate some of the supervision responsibility to classifications societies. Five classification societies have supervisory authority in Norway: Det Norske Veritas (DNV), Lloyd's register (LR), Bureau Veritas (BV), Germandischer Lloyd (GL) and American Bureau of Shipping (ABS). The classification societies and the public authorities complement each others work in the process of classifying and supervising ships.

In the following, a review of the most relevant rules and regulations concerning AHVs are given. Specifically, the documents listed in Table 2.1 are considered.

Authority or Classification Society	Document
ABS	Rules for Building and Classing Steel Vessels Under 90 Meters (295 Feet) in Length [2]
ABS	Rules for Building and Classing Stell Vessels (2008) [3]
DNV	Rules for Classification of Ships [9]
NMD	Act No. 9 of 16 February 2007 on maritime safety [26]
NMD	Statuatory Regulations No. 695 of 15. September 1992 [27]
NMD	Guidelines for Safe Anchor Handling Operations [28]

Table 2.1. Documents used to review rules and regulations applicable to AHVs

Work Wire
The breaking strength of the work wire shall not be less than the reference load[1] (RL).

Winch
The winch shall be located as low as possible and as near as possible to the mid length of the vessel. The heeling moment arising when work wire is running in the athwartships direction should be minimized.

The winch shall have a drum release function that can be activated in all operational modes, including emergencies. It shall be possible to execute the emergency release during black-outs and at any combination of expected trim and heel. Identical control panels for releasing the winch drum should be present both locally on the winch and on the bridge. The winch brakes shall function normally without delay after an emergency release has been performed. There shall also be an arrangement for controlled release of torsion forces in the wires.

Situations where it is necessary to run out all work wire on the winch may arise. The work wire's end attachment should therefore be of limited strength, allowing the work wire to free itself from the winch.

Spooling Gear
All winch drums used for anchor handling shall be equipped with a remotely controlled spooling gear operable from the winch control panel at the bridge. The dimensioning of the spooling gear shall be such that it is able to spool at full winch load with the wire in the most unfavourable position with respect to the drum and the guiding pins. The spooling gear shall be able to pay out wire in a controlled manner during overload conditions.

Stern Roller
All AHVs shall have a stern roller or a similar arrangement that is individually fitted to each specific vessel.

Guiding Pins
All AHVs shall have guiding pins which function both for steel wire and chain. An acoustic alarm that is automatically activated when the guiding pins are used shall be presenent on the deck. A minimum of two guiding pins are required.

Wire and Chain Stoppers
All AHVs shall be equipped with remotely controlled wire and chain stoppers, e.g shark jaws. It shall be possible to perform emergency release from the bridge or at some other control station at the vessel. The emergency release shall function during blackouts and without using manual interventions. All wire and chain stoppers shall be dimensioned to sustain a safe working load[2] (SWL) that is 20 % higher than the maximum winch

---

[1]The reference load in the design and testing of towing gear is generally 2BP [2].

[2]The safe working load of a line is the load that can be applied without causing any kind of damage to the line. The safe working load for a device is the maximum load that can be sustained without risk of deformations and fractures.

power. The wire and chain stoppers shall not be used as the attachment point for wires and chains during anchor handling operations. An acoustic alarm that is automatically activated when the stoppers are used shall be presenent on the deck.

Ballast and Anti-Roll Tanks
All AHVs shall have a ballasting plan stating the sequence of how and when ballast tanks should be filled or emptied in order to obtain stability. The consequenses of using anti-roll tanks with respect to vessel stability shall be explained in the instructions for the vessel master.

2.4 Operational Procedures

Anchor handling operations are complex and thourough planning in advance is therefore crucial for the operation to succeed. The investigations in the aftermath of the *Bourbon Dolphin* accident concluded that several causes may have contributed to the capsizing [29]. Failures and weaknesses in the preparations and evaluations during the operation were identified:

- There was no vessel-specific anchor handling procedure for the *Bourbon Dolphin*.
- The planning of the Rig Move Procedure (RMP) was insufficient.
- No review of the RMP was carried out even though problems arised during the rig move.
- No risk evaluation of two vessel having to work closely was performed.

As a result of the *Bourbon Dolphin* comission report, the Norwegian Maritime Directorate issued a document containing guidelines for implementation of specific actions, aimed to ensure an acceptable safety level in AH operations [28]. In addition to regulations from public authorities and classification societies, other organizations have published information about their own experiences related to AH operations. *Guidelines for the safe management of offshore supply- and anchor handling operations NWEA* is a result of a collaboration between different organisations, aiming to ensure and improve the safety of supply and anchor handling operations in the North West European Area [19]. Note that these guidelines do not supersede legal requirements. In the following, some key information regarding the procedures of anchor handling are briefly outlined.

2.4.1 The Rig Move Procedure

Before any AH operation can commence, a rig move procedure must be made. The purpose of the RMP is to identify and clearify all aspects of a specific operation. Introductorily, the roles and resposibilities of involved key personell shall be defined and the purpose of the operation described. A step-by-step description of the operation shall be provided, with emphasize on maximum use of diagrams. Other information required in the RMP is [19]:

- Step-by-step illustrated descriptions for special operations.
- Drawings of anchoring arrangements.
- Catenary curves for relevant water depths showing the various cable tensions.
- Offshore installation draught during anchor handling.
- List of back-up equipment.
- Weather criterias and weather window.
- Time estimate.

The step-by-step description of the operation should contain the following elements:

- Positions, departures and arrivals.
- Water depths.
- Sea bottom conditions.
- Subsea infrastructure.
- Field-specific requirements.
- Anchor patterns with line lengths and operational manuals for running anchors issued by supplier.

2.4.2   Requirements for Anchor Handling Vessels

The RMP must also specify the requirements related to AHVs and the OI. The requirements for the involved AHVs should atleast contain the specifications of the following elements:

- Bollard Pull.
- Winch capacity, drum capacity and number of drums.
- Secondary winches, number and capacity.
- Guiding pins.
- Requirements for wire termination.
- Stern roller.
- Spooling gear.
- Minimum freeboard requirement for safety on deck.
- Requirements for deck crane used for equipment handling.

2.5   Deployment and Recovery of Anchors

2.5.1   Mooring Configurations

Mooring systems can have several different configurations. Previous experiences and specific requirements decide whether or not a particular configuration is selected for implementation at the OI. In this thesis a permanent chaser pendant (PCP) system is considered.

2.5.2 Assumptions

It is assumed that the OI[3] is moored with a PCP system, which is one of the least complex mooring systems. There are no subsea or surface obstructions present. It is also assumed that the OI is placed at the correct location with the correct heading. The deployment of the first anchor may be considered as a special case and will not be treated. The following deployment and recovery procedures focus on the tasks of the AHV and OI. Detailed descriptions of equipment involved in the operations can be found in [16] and [22].

2.5.3 Anchor Deployment

A standard anchor deployment operation can be divided into four sequential main phases:

Phase	Description
1	Receiving a PCP
2	Anchor deployment
3	Chasing back
4	Passing back the PCP

Each of these phases are described in the following.

Phase 1: Receiving a PCP

The deployment operation starts by the AHV maneuvering its stern towards the crane of the OI. The PCP is lowered from the crane and the AHV connects its work wire to it. Depending on the heading of the AHV, the appropriate guiding pins must be raised to guide the PCP during the connection phase. After a successful connection, the AHV begins to move slowly ahead. The OI crane lowers the anchor at the same time. The pull of the work wire and the slackening of the OI winch must then be combined to secure the anchor on the stern roller of the AHV. In this phase of the operation it is important that the tension of the work wire is sufficiently high in order to prevent the PCP to slip of the anchor, causing an anchor drop-through.

Phase 2: Anchor deployment

With the anchor secured on the stern roller of the AHV, the anchor deployment phase can begin. First, the OI pays out chain until the length is about two times the water depth[4] while the AHV maintains its position and heading, see Figure 2.2. Upon completion of this step, the AHV starts to maneuver itself into position for running out the chain, which is some point along the line between the OI and the proposed anchor target. The

---

[3]The term offshore installation is used for rigs, semi-subersibles, mobile operating units, barges and any other floating structure that is subject to mooring.

[4]Two times the water depth is a rule of thumb. Enough chain must be paid out from the OI to give the AHV sufficient maneuvering capabilities.

OI then releases the winch break and the AHV begins to move towards the anchor target along the preplanned track, as illustrated by Figure 2.3. At this point it is important that the anchor remains at the stern roller, that chain is running freely from the OI winch and that the AHV position is monitored closely.
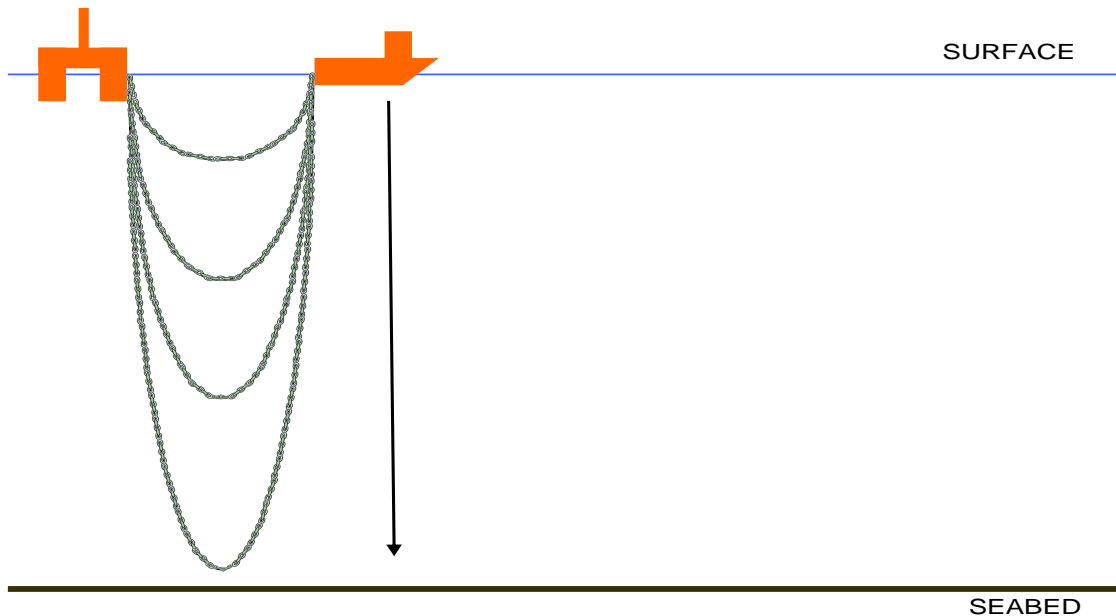
Figure 2.2. The offshore installation runs out chain until about two times the water depth is deployed. The AHV maintains its position during this process.

Once the AHV has reached its target position, power usage is lowered and the OI winch break is applied. At this point, the chain must be stretched. This is normally done by the AHV moving slowly forwards along the predescribed path. Alternatively, the OI winch can be used to obtain sufficient chain tension.

Once the chain is sufficiently stretched and the position of the AHV is correct, the actual anchor deployment can commence. The AHV deploys the anchor from the stern roller and begins to pay out its work wire while at the same time moving slowly ahead, see Figure 2.4. It is important that the tension of the work wire is sufficiently high for the anchor to be deployed with correct attitude. The anchor should land on the seabed under tension. When the anchor lands, a reduction in the work wire tension is experienced. The AHV continues to pay out work wire until 1.5 to 2 times the water depth is deployed. At this point the OI must use its winch to recover a certain length of the chain in order to obtain the correct mooring line tension. It is important that the AHV maintains its position at this point, since drifting off to starboard or port may cause the anchor position and heading to change.
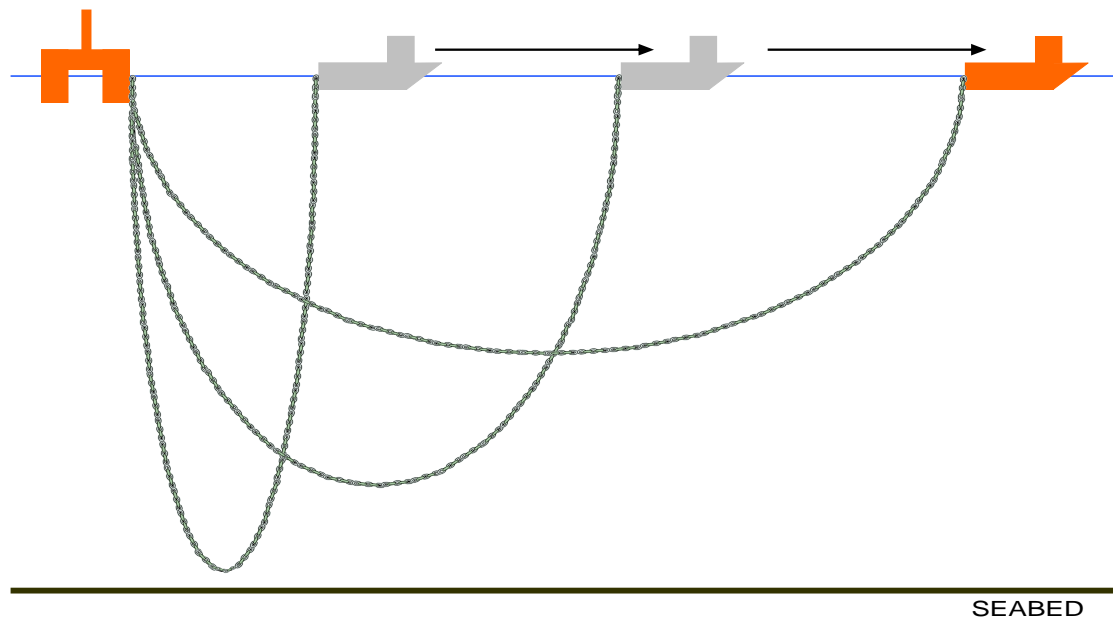
SEABED

Figure 2.3. The AHV runs out chain along the predescribed path while the offshore installation continues to deploy chain.

WORK WIRE
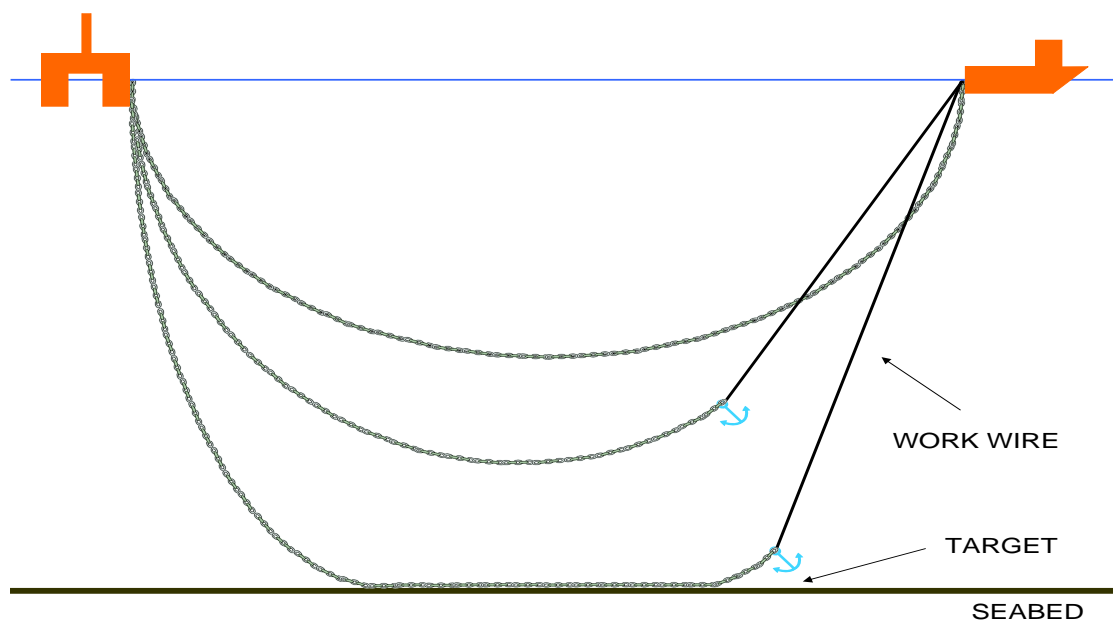
TARGET

SEABED

Figure 2.4. The AHV uses its work wire to deploy the anchor and position it at the anchor target on the seabed.

Phase 3: Chasing back

Upon confirmation of correct mooring line tension, the process of returning the PCP to the OI can begin. First, the PCP must be stripped off the anchor. This is done by the AHV maneuvering itself backwards along the mooring line until a work wire angle of about 50 degrees is obtained, see Figure 2.5. This particular work wire angle allows the PCP to be stripped off the anchor without disturbing its position and attitude. A successful strip off can be observed by a very low work wire tension.
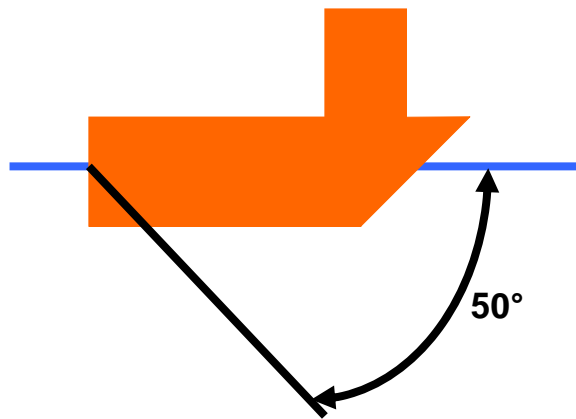
Figure 2.5. Work wire angle for permanent chaser pendant strip off.

The AHV can then tow the PCP back to the rig. Whether the vessel maneuvers bow or stern first is irrelevant, but it is important that the vessel maintains its position above and along the mooring line. During the back-chasing maneuver, the OI should experience a constant winch tension. A reduction of tension most likely means that the chain is being dragged towards the OI.

Phase 4: Passing back the PCP

As the distance between the OI and the AHV reduces, the AHV must maneuver itself to approach the OI with the stern first along the mooring line. As the vertical distance between the AHV and mooring line becomes small, the AHV must clear itself of the cable and maneuver itself towards the PCP pick-up position. The PCP is then passed to the OI by means of the OI crane and the anchor deployment operation is concluded.

2.5.4 Anchor Recovery

A standard anchor recovery operation can be divided into four sequential main phases:

Phase	Description
1	Receiving a PCP
2	Chasing out to the anchor
3	Anchor Recovery
4	Passing back the PCP

Each of these phases are described in the following.

Phase 1: Receiving a PCP

The recovery operation starts by the AHV maneuvering its stern towards the crane of the OI. The PCP is lowered from the crane and the AHV connects its work wire to it. The AHV then maneuvers itself above the mooring line and adjusts its heading to point along the mooring line path.

Phase 2: Chasing out to the anchor

With the PCP connected to the work wire and the AHV in position, the OI applies a torque to its winch to increase the mooring line tension to a specific level[5]. By increasing the mooring line tension to a high level, the AHV is allowed a trouble-free run to the anchor, since there is little slack in the system.

The AHV the starts moving ahead along the mooring line path while paying out work wire from its winch. Power should be reduced and the position of the vessel monitored closely as the AHV approaches the precalculated position of the anchor. The PCP has reached the anchor when the winch on the AHV experiences a large tension increase.

The next step is to break the anchor out of the seabed. Depending on seabed conditions, the anchor itself and the time the anchor has been submerged, the force required to break out the anchor may vary considerably[6]. The AHV begins the process by reducing the length of the work wire to about 1.5 times the water depth while at the same time maintaining power ahead. The OI reduces the tension of the mooring line by paying out chain from its winch. The AHV then increases the power to a specific level and monitors the work wire tension. The anchor is broken out of the seabed when a a clear drop in the work wire tension is observed.

Phase 3: Anchor recovery

After a successful anchor breakout, the AHV can begin to reduce the work wire length. Attention must be given to the angle of the work wire during the recovery process. A

---

[5]The tension is normally set to about 1/2 - 2/3 of the test tension, where the test tension typically is around 1/3 of the break strain for the chain or cable in use.

[6]For a large and deeply buried anchor, a BP of 80 tonnes and winch tension of 200 tonnes sustained over 30 minutes may be required to break the anchor out [22].

vertical lift of the anchor will result in large forces. As the work wire length is reduced, the AHV is positioned such that the anchor is pulled up onto the stern of the vessel.

Phase 4: Passing back the PCP

When the anchor has reached the stern of the AHV, the OI may begin to recover mooring line chain while the AHV moves towards it. As the distance between the OI and AHV is sufficiently close (depending on weather conditions), the OI slows down on the chain recovery speed while the AHV at the same time begins to pay out work wire. Sufficient work wire tension must be maintained to prevent the PCP to slip of the anchor, causing an anchor drop through. The anchor and PCP are then passed on from the AHV to the OI by use of a crane. This concludes the anchor recovery process.

2.5.5   Reduced Procedures for Simulation Purposes

The various stages of anchor handling operations were described in Sections 2.5.3 and 2.5.4. For simulation purposes, it is not necessary to perform all of the stages. Phase 1, 3 and 4 of the anchor deployment procedure and phase 1 and 4 of the anchor recovery procedure may be omitted. This is due to the fact that these phases are not the most critical for the stability of the AHV. It would be necessary to simulate all phases if a training simulator for the vessel crew was to be designed.

Figures 2.2-2.4 illustrates the scenarios that should be part of the reduced anchor deployment simulations. The opposite sequence of the same figures can be used to illustrate how the reduced anchor recovery operation should be simulated, given that all actions are reversed. Note that the figures do not reflect any physical properties of the different elements in the anchor handling operation, but is only to be considered as simple illustrations of the various stages.

2.6   Deep Water Anchor Handling Operations

Deep water anchor handling operations require longer mooring chains than ordinay anchor operations. This increases the forces acting on the AHV. There is no general definition of the water depths required to specify an operation as a deep water operation. The limit is defined as 300 [m] in [19] and 1000 -3000 [m] in [16]. Deep water operations requires some extra precautions. Generally, large vessels with good winch capacity and large bollard pull must be utilized. Using two vessels during the operation could also be necessary. In addition to the main AHV a secondary AHV is used to relieve some of the chain weight held by the main AHV. This is illustrated in Figure 2.6. The secondary vessel uses a hook on the end of its work wire and "fishes" to find the chain.
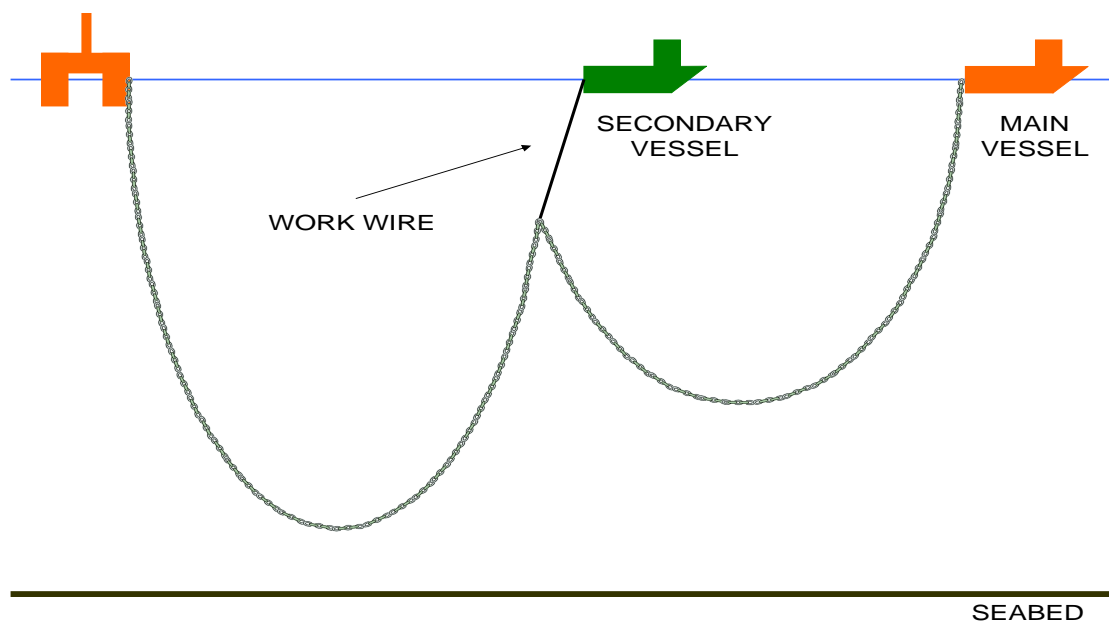
Figure 2.6. The main AHV (orange) is assisted by a secondary AHV (green) during the deep water anchor handling operation. The objective is to reduce the forces acting on the main vessel.

Chapter 3

Cable Modeling

In this chapter an overview of cable modeling approaches is first given, and it is shown why catenary equations are the preferred method for cable modeling. Then the theory of catenary equations is treated. In addition, a catenary model of two cables and a point load is developed based on existing equations in the literature. It is also shown how the solutions of the static catenary equations are converted to polynomials, resulting in a quasi-static approach that can be used in dynamic simulations.

3.1   Cable Modeling Approaches

An important part of any AHV simulator is to incorporate the effects of the various chains and wires into the vessel model. Several methods with different properties exist for this purpose: *Finite Element Methods* (FEM), *Finite Difference Methods* (FDM), *Catenary Equations*, *Lump-Mass-Spring Formulations* (LMS) and *Finite Segment Approaches* (FSA). All these methods are based on a particular and generalized mathematical formulation of the problem. The basic formulation can then be extended to describe different configurations of cables and wires, amongst other mooring cables, towing lines and suspended cables.

FEM methods solve complex elasticity and structural problems. In its most basic form it is a numerical technique for finding approximate solutions of partial differential equations and integral equations. Software packages that solves cable equations using FEM methods exist, and the solutions are accurate. The computational load is however heavy and it is difficult to incorporate such packages into control system designs [30].

Catenary equations provide a static representation of cables [20]. It is easier to gain insight into the mechanisms that govern the solution of the catenary equations than to understand the FEM representation. In addition, they provide a simple representation of the forces acting on the supports where the cable is attached. The equations are

17

solved faster than FEM equations and the result is exact. Catenary equations are normally solved for two dimensions, but three-dimensional approaches also exist [39]. A disadvantage of the catenary approach is that the static solution may become innacurate for deep water applications, because of dynamic interactions between the vessel and the mooring system. If an exact solution is desired for such conditions a FEM method must be utilized.

The LMS formulation has a clear physical interpretation and does not require a large amount of computing. Dynamic analyses of three-dimensional cables based on the LMS approach are discussed in [37]. The method provides a set of ordinary differential equations with boundary conditions that is solved using the FDM method. A general LMS formulation allowing static and dynamic analysis of a variety of slender structures is presented in [5]. The FSA for cable dynamics is discussed in [44]. The cable is modeled as a series of links connected to each other by ball-and-sockets joints. The resulting equations are then solved using standard integration techniques such as Runge-Kutta.

Catenary equations are selected for cable modeling in this thesis. The simple representation of cable forces and tensions is attractive. The basic theory of catenaries is well established and the equations are more suited for implementation in a feedback system than FEM approaches.

3.2   Catenary Equations

The word catenary is derived from the latin word *catena*, referring to the shape of a chain or wire hanging between two points under its own weight. The catenary equation theory is extensively covered in the literature. An overview of general catenary equations is given in [20]. In [40] the theory is extended to apply for submerged cables. The mathematical notation used in the various books and articles differs slightly. The notation used here is based on [20], but some parameters are renamed to give a simpler and more intuitive representation of the equations.

3.2.1   Basic Cable Mechanics

Figure 3.1 shows a cable of length L attached to a point O and a point Q. These points are defined as the cable supports and they are fixed in space. Support O is located at the origin of the coordinate system whereas support Q may be any point with a distance l along the x-axis and h along the z-axis with respect to the origin. The horizontal distance between the end points is defined as the cable span l and the lowest point on the cable is called the cable sag s_d. The cable is only defined in two dimensions, i.e. it is a straight line seen from above.

The catenary equations are derived using a Lagrangian approach [20]. Consider Figure 3.1. Starting from support O and moving along the cable profile, each point on the cable

is described by the Lagrangian coordinate s with respect to the origin. s is defined as the unstretched Lagrangian coordinate. Stretched or strained cables must replace s by the stretched Lagrangian coordinate p. Thus p describes each point on the stretched cable with respect to the origin.
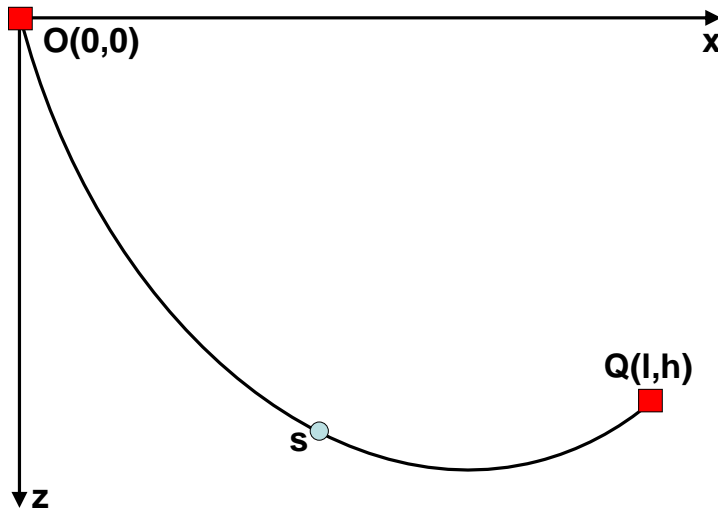
Figure 3.1. A general cable configuration with coordinates for support points.

The cable is assumed to be uniform, meaning that the weight of the cable is distributed equally along its entire length. Bending stiffness is ignored, which is equivalent to having a perfectly flexible cable. A cable may either be modeled as inelastic or elastic. An inelastic cable is assumed to be inextensible while an elastic cable is extensible. Whether an elastic or inelastic model should be used depends on the cable itself and the specific applicaton. Highly tensioned, i.e taut cables requires elastic models. The end point forces of a taut cable are much larger than the forces distributed along its length, and it is therefore natural to assume that the cable can be stretched. For cables suspended above sea level, the distributed forces may comprise both self weight and other elements such as ice on the cable. Since the scope of this report is to model submerged cables, the distributed forces will only be the cable's self weight in water. If the tension of the cable is considered to be low, i.e. the end point forces are low compared to the cable's own weight, an inelastic cable model will suffice. An inelastic model can also be used for a metallic cable with very large elasticity modulus.

Consider a small element of a cable as shown in Figure 3.2. This cable element is subject to three forces [40]: it's own weight W, a hydrostatic force B and a tension T from adjacent segments. The tension T acts along the tangent of the average cable configuration, where the average cable configuration is defined as the smoothest possible profile of the cable. The hydrostatic force, i.e. the buoyancy force B, acts vertically on
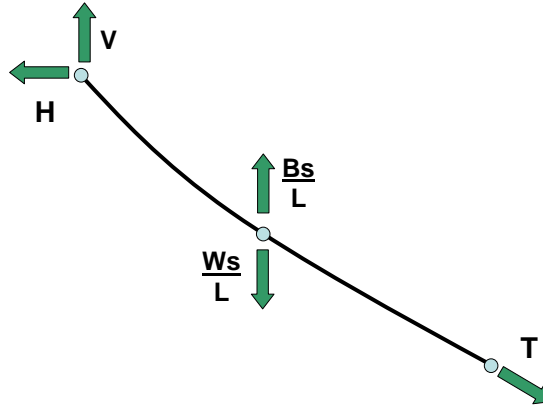
Figure 3.2. Forces acting on a segment of a strained cable profile.

the cable. The buoyancy force per unit length of the cable is

$$B = \rho g A \qquad (3.1)$$

where A is the unstretched cross-sectional area of the cable, g is the acceleration of gravity and ρ the water density. It is assumed that the cable has a constant diameter d along its entire length. The unstretched cross-sectional area of the cable is

$$A = \pi d^2/4 \qquad (3.2)$$

Note that for chains, it is common to calculate the cross-sectional area as two times the area of a wire. Both the cable weight and the buoyancy force act in the vertical direction, but with opposite signs. They can therefore be combined to form the effective weight W_e of the cable as

$$W_e = W - B \qquad (3.3)$$

Since this report only considers cables submerged in water, W will always be considered as the weight of the cable in water, i.e. the effective weight unless otherwise stated.

3.2.2   The General Elastic Catenary

In this section, a detailed procedure for finding the general elastic catenary equations is presented. The procedure is based on [20, 40], but a few elements are added to give a complete description. The reason for rewriting the procedure here is to better understand how the catenary equations in Section 3.2.4 are derived. The procedure starts by balancing the horizontal and vertical forces of a cable segment, as shown in

Figure 3.2, giving

$$T\frac{dx}{dp} = H \tag{3.4}$$

$$T\frac{dz}{dp} = V - W\frac{s}{L} \tag{3.5}$$

where T is the cable tension, H the horizontal end point force and V the vertical end point force of the cable. Equation (3.4) shows that H is constant along the entire cable. The generalized Hooke's law is defined as

$$T = EA\left(\frac{dp}{ds} - 1\right) \tag{3.6}$$

where E is Young's modulus or equivalent the elastic modulus of the cable. The geometric constraint of the cable is

$$\left(\frac{dx}{dp}\right)^2 + \left(\frac{dz}{dp}\right)^2 = 1 \tag{3.7}$$

It is shown in [20] that by squaring and adding (3.4) - (3.5) and substituting them into the geometric constraint (3.7), the cable tension may be written as

$$T(s) = \left\{H^2 + \left(V - W\frac{s}{L}\right)^2\right\}^{1/2} \tag{3.8}$$

which is a function of the unstretched Lagrangian coordinate s. In order to find an expression for $x(s)$ and $z(s)$ it is necessary to find expressions for dx/ds and dz/ds and integrate with respect to s. By writing

$$\frac{dx}{ds} = \frac{dx}{dp}\frac{dp}{ds}$$
$$\frac{dz}{ds} = \frac{dz}{dp}\frac{dp}{ds} \tag{3.9}$$

where dx/dp, dz/dp and dp/ds is found by rearranging (3.4), (3.5) and (3.6), dx/ds and dz/ds becomes

$$\frac{dx}{ds} = \frac{H}{EA} + \frac{H}{[H^2 + \{V - Ws/L\}^2]^{1/2}} \tag{3.10}$$

$$\frac{dz}{ds} = \frac{1}{EA}\left(V - \frac{Ws}{L}\right) + \frac{V - Ws/L}{[H^2 + \{V - Ws/L\}^2]^{1/2}} \tag{3.11}$$

Next, the end conditions of the cable supports is defined as

$$x = 0, \qquad z = 0, \qquad p = 0 \qquad \text{at} \qquad s = 0 \tag{3.12}$$
$$x = l, \qquad z = h, \qquad p = L_s \qquad \text{at} \qquad s = L \tag{3.13}$$

where L_s is the stretched length of the cable. Other end conditions can also be used. This will lead to a modification of the catenary equations used in the literature, where support O normally is placed in the origin of the coordinate system. Consider Figure 3.1 again. Support O is defined to be the cable's attachment point on the offshore installation. Assuming that the OI is fixed in space, i.e. do not exhibit any horizontal or vertical movement, the position of support O can be defined as the origin and the associated end conditions set to zero. Cable support Q will be fixed to the AHV and varies according to the vessel's position and orientation. The general end point conditions are therefore valid. Integrating (3.10) from $s = 0$ to s gives the following solution for x

$$x(s) = \frac{Hs}{EA} + \frac{HL}{W} \left[\text{asinh}\left(\frac{V}{H}\right) - \text{asinh}\left(\frac{V - Ws/L}{H}\right) \right] \qquad (3.14)$$

where $\text{asinh}(x)$ is the inverse hyberbolic sine function of x. Integrating (3.11) from $s = 0$ to s gives the solution for z

$$z(s) = \frac{Ws}{EA}\left(\frac{V}{W} - \frac{s}{2L}\right) + \frac{HL}{W}\left[\left\{1 + \left(\frac{V}{H}\right)^2\right\}^{1/2} - \left\{1 + \left(\frac{V - Ws/L}{H}\right)^2\right\}^{1/2}\right]$$
$$(3.15)$$

The second end condition (3.13) is incorporated into (3.14) and (3.15) in order to find a solution of H and V. This gives

$$l = \frac{HL}{EA} + \frac{HL}{W}\left[\text{asinh}\left(\frac{V}{H}\right) - \text{asinh}\left(\frac{V - W}{H}\right)\right] \qquad (3.16)$$

and

$$h = \frac{WL}{EA}\left(\frac{V}{W} - \frac{1}{2}\right) + \frac{HL}{W}\left[\left\{1 + \left(\frac{V}{H}\right)^2\right\}^{1/2} - \left\{1 + \left(\frac{V - W}{H}\right)^2\right\}^{1/2}\right] \qquad (3.17)$$

The general elastic catenary equations (3.16)-(3.17) must be solved simultaneously to find H and V.

3.2.3   Horizontal Cable Configuration

A horizontal cable configuration is characterized by no bottom attachment and both ends supported at the same horizontal level, as illustrated in Figure 3.3. It can be seen that the profile of the cable is symmetrical about an imaginary vertical line passing through the point C. This implies that it is only necessary to consider half of the cable length in the corresponding catenary equations. Placing the coordinate origin in C, i.e. the lowest point on the cable, with the z-axis pointing upwards and the x-axis to the right gives simplified equations [40].
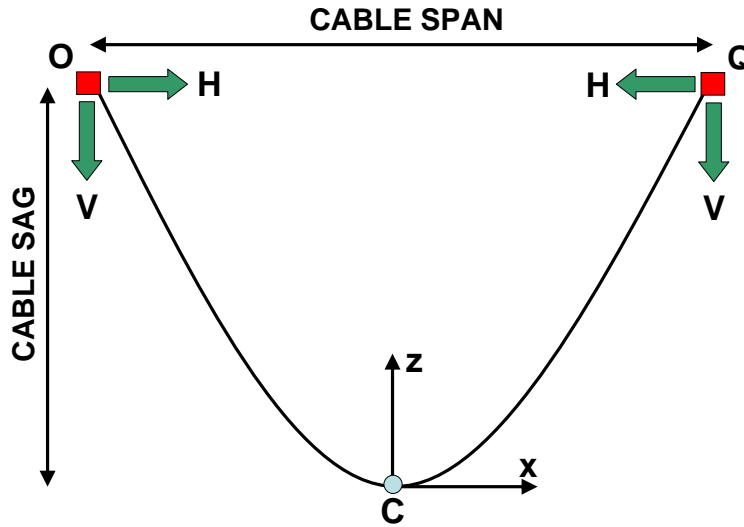
Figure 3.3. Horizontal cable configuration with coordinates system and forces.

By solving Equations (3.16) and (3.17) with $h = 0$ [20], the general elastic catenary equations is reduced to

$$\sinh\left(\frac{Wl}{2HL} - \frac{W}{2EA}\right) = \frac{W}{2H} \tag{3.18}$$

which is called the elastic horizontal catenary equation. The vertical end point force is simply $V = W/2$, i.e the total cable weight dividied by two. This equation is numerically faster to solve than (3.16)-(3.17) since the only unknown variable is the horizontal end point force H. An inelastic version of the elastic horizontal catenary equation is found by setting $E = \infty$ in (3.18).

3.2.4 Double Catenary Configuration with Point Load

In this section the necessary catenary equations to represent two elastic cables connected to each other are developed. In addition, a vertical point load imitating the effect of an anchor is acting at the connection point between the cables. Catenary equations for one cable with concentrated or distributed vertical loads are discussed in [20, 21]. This theory forms the basis for finding the necessary catenary equations.

Figure 3.4 shows the configuration of the two cables and the point load. Cable A is attached to support O, which is defined as the origin, and to cable B in the point P. The point load F_P acts vertically at P. The coordinates of P vary according to the cable properties and the size of the force F_P. Cable B is attached to cable A in the point P

and then to the support Q. In the following, this configuration is referred to as the *double cable configuration*.
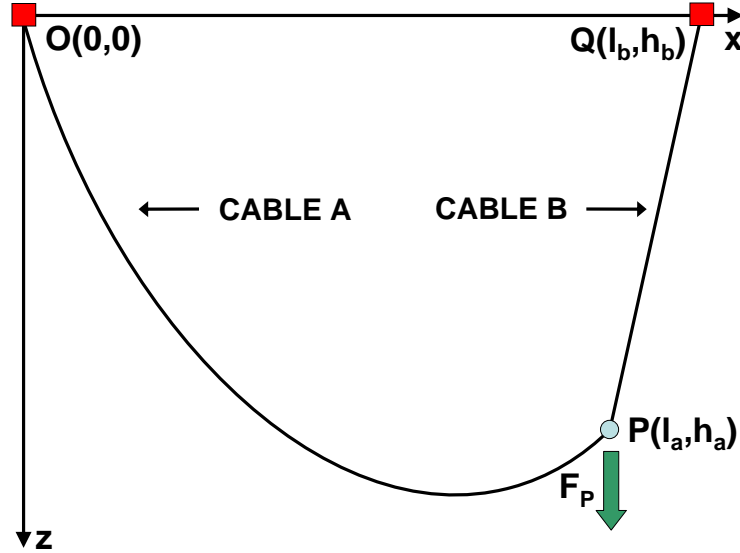
Figure 3.4. Cable configuration with two cables and one point load.

In order to develop the equations, a change of notation is necessary since two cables with different properties are involved. All parameters related to cable A are denoted with subscript A and the parameters related to cable B are denoted with subscript B.

It is necessary to separate the Lagrangian coordinates of the two cables. A cable subject to a single point load requires catenary equations divided into two parts: One part describes the profile left of the point load and the other part describes the profile to the right of the point load. The Lagrangian coordinate of the point where the point load is acting is denoted as s_1. The cable is then divided into the two intervals $0 \leq s < s_1$ and $s_1 \leq s \leq L$. This general expression must be modified since two cables are involved. The total catenary configuration therefore consists of the following intervals:

$$\begin{aligned}
\text{Cable A:} \qquad & 0 \leq s < s_1 \qquad && \text{and} \qquad && s_1 \leq s \leq L_A \\
\text{Cable B:} \qquad & L_A \leq s < s_2 \qquad && \text{and} \qquad && s_2 \leq s \leq L_A + L_B
\end{aligned} \qquad (3.19)$$

The Lagrangian coordinate of cable B is defined relative to cable A. The reason for this is that the complete solution of the catenary equations requires the that the solution of cable A is derived before the solution for cable B can be derived.

The procedure for finding the catenary equations for the double cable configuration is very similar to finding the solution of the general elastic catenary equation. It is shown in [20] that Equation (3.4) remains unchanged. In Equation (3.5) the vertical point load

F_P must be taken into account according to

$$T\frac{dz}{dp} = V - W_i\frac{s}{L_i}, \qquad\qquad 0 \le s < s_1 \qquad \text{and} \qquad s_1 \le s < s_2 \qquad (3.20)$$

$$T\frac{dz}{dp} = V - F_P - W_i\frac{s}{L_i}, \qquad s_1 \le s \le L_A \qquad \text{and} \qquad s_2 \le s \le L_A + L_B \qquad (3.21)$$

where $i \in \{A, B\}$. The end conditions at the cable supports O, P and Q shown in Figure 3.4 are

$$
\begin{array}{llllll}
O: & x = 0, & z = 0, & \text{at} & s = 0 & \\
P: & x = l_A, & z = h_A, & \text{at} & s = L_A & \\
Q: & x = l_B, & z = h_B, & \text{at} & s = L_A + L_B & (3.22)
\end{array}
$$

Note that the end conditions at $s = L_A$ is variable and must therefore be found as a part of the catenary solution. In addition, Hooke's law is violated in this point due the discontinuity created by the point load F_P. It is however possible to maintain continuity by ensuring that

$$
\begin{array}{llllll}
x_A^- = x_A^+, & z_A^- = z_A^+, & p_A^- = p_A^+ & \text{at} & s = s_1 = L_A & \\
x_B^- = x_B^+, & z_B^- = z_B^+, & p_B^- = p_B^+ & \text{at} & s = s_2 = L_A & (3.23)
\end{array}
$$

By applying the same procedure as in Section 3.2.2, the tension T of the cables can be expressed as

$$T(s) = \left\{ H^2 + \left(V - W_i\frac{s}{L_i}\right)^2 \right\}^{1/2}, \qquad 0 \le s < s_1 \quad \text{and} \quad s_1 \le s < s_2, \quad (3.24)$$

$$T(s) = \left\{ H^2 + \left(V - F_P - W_i\frac{s}{L_i}\right)^2 \right\}^{1/2}, \quad s_1 \le s \le L_A \quad \text{and} \quad s_2 \le s \le L_A + L_B$$

$$(3.25)$$

This results in the following expressions for dx/ds and dz/ds

$$\frac{dx}{ds} = \frac{H}{E_i A_i} + \frac{H}{[H^2 + \{V - W_i s/L_i\}^2]^{1/2}},$$

$$0 \leq s < s_1 \text{ and } s_1 \leq s < s_2, \tag{3.26}$$

$$\frac{dx}{ds} = \frac{H}{E_i A_i} + \frac{H}{[H^2 + \{V - F_P - W_i s/L_i\}^2]^{1/2}},$$

$$s_1 \leq s \leq L_A \text{ and } s_2 \leq s \leq L_A + L_B, \tag{3.27}$$

$$\frac{dz}{ds} = \frac{1}{E_i A_i} \left(V - \frac{W_i s}{L_i} \right) + \frac{V - W_i s/L_i}{[H^2 + \{V_i - W_i s/L_i\}^2]^{1/2}},$$

$$0 \leq s < s_1 \text{ and } s_1 \leq s < s_2, \tag{3.28}$$

$$\frac{dz}{ds} = \frac{1}{E_i A_i} \left(V - F_P - \frac{W_i s}{L_i} \right) + \frac{V - F_P - W_i s/L_i}{[H^2 + \{V - F_P - W_i s/L_i\}^2]^{1/2}},$$

$$s_1 \leq s \leq L_A \text{ and } s_2 \leq s \leq L_A + L_B, \tag{3.29}$$

Equations (3.26)-(3.29) must be integrated in a sequential manner. The procedure for finding x is explained in the follwing: First Equation (3.26) is integrated from 0 to s on the right hand side of the equality sign and 0 to x one the left hand side. Equation (3.27) is integrated from s_1 to s one the right hand side and from x_1 to x on the left hand side. x_1 is found by substituting $s = s_1$ into (3.26). This gives the x-solution for cable A. The x-solution for cable B is found using the same procedure, with the exception that the result depends on the solution for cable A. Inserting the correct subscribts and integrating all differential equations leads to the total catenary equations set. The complete solution for x is

$$x(s) = \frac{Hs}{E_A A_A} + \frac{H L_A}{W_A} \left[\sinh^{-1} \left(\frac{V}{H} \right) - \sinh^{-1} \left(\frac{V - W_A s/L_A}{H} \right) \right],$$

$$0 \leq s < s_1,$$

$$x(s) = \frac{Hs}{E_A A_A} + \frac{H L_A}{W_A} \left[sinh^{-1} \left(\frac{V}{H} \right) - \sinh^{-1} \left(\frac{V - F_P - W_A s/L_A}{H} \right) \right. \tag{3.30}$$

$$\left. + \sinh^{-1} \left(\frac{V - F_P - W_A s_1/L_A}{H} \right) - \sinh^{-1} \left(\frac{V - W_A s_1/L_A}{H} \right) \right],$$

$$s_1 \leq s < L_A,$$

$$x(s) = \frac{H(s - s_1)}{E_B A_B} + \frac{H s_1}{E_A A_A}$$
$$+ \frac{H L_B}{W_B} \left[\sinh^{-1}\left(\frac{V - W_B s_1 / L_B}{H}\right) - \sinh^{-1}\left(\frac{V - W_B s / L_B}{H}\right) \right]$$
$$+ \frac{H L_A}{W_A} \left[\sinh^{-1}\left(\frac{V}{H}\right) - \sinh^{-1}\left(\frac{V - W_A s_1 / L_A}{H}\right) \right],$$
$$L_A \leq s < s_2,$$

$$x(s) = \frac{H(s - s_1)}{E_B A_B} + \frac{H s_1}{E_A A_A} + \tag{3.31}$$
$$\frac{H L_B}{W_B} \left[\sinh^{-1}\left(\frac{V - F_P - W_B s_2 / L_B}{H}\right) - \sinh^{-1}\left(\frac{V - F_P - W_B s / L_B}{H}\right) \right.$$
$$\left. + \sinh^{-1}\left(\frac{V - W_B s_1 / L_B}{H}\right) - \sinh^{-1}\left(\frac{V - W_B s_2 / L_B}{H}\right) \right]$$
$$+ \frac{H L_A}{W_A} \left[\sinh^{-1}\left(\frac{V}{H}\right) - \sinh^{-1}\left(\frac{V - W_A s_1 / L_A}{H}\right) \right],$$
$$s_2 \leq s < L_A + L_B.$$

where the relation $\sinh^{-1}(x) = \mathrm{asinh}(x) = \ln\left(x\sqrt{1 + x^2}\right)$ was used. The solution for z is found in a similar manner, resulting in

$$z(s) = \frac{W_A s}{E_A A_A}\left(\frac{V}{W_A} - \frac{s}{2 L_A}\right) + \frac{H L_A}{W_A}\left[\left\{1 + \left(\frac{V}{H}\right)^2\right\}^{1/2} - \left\{1 + \left(\frac{V - W_A s / L_A}{H}\right)^2\right\}^{1/2} \right],$$
$$0 \leq s < s_1,$$

$$z(s) = \frac{W_A s}{E_A A_A}\left(\frac{V}{W_A} - \frac{s}{2 L_A}\right) + \frac{H L_A}{W_A}\left[\left\{1 + \left(\frac{V}{H}\right)^2\right\}^{1/2} - \left\{1 + \left(\frac{V - F_P - W_A s / L_A}{H}\right)^2\right\}^{1/2} \right.$$
$$+ \left\{1 + \left(\frac{V - F_P - W_A s_1 / L_A}{H}\right)^2\right\}^{1/2} - \left\{1 + \left(\frac{V - W_A s_1 / L_A}{H}\right)^2\right\}^{1/2}$$
$$\left. + \frac{F_P}{H}\frac{W_A}{E_A A_A}\left(\frac{s_1}{L_A} - \frac{s}{L_A}\right) \right],$$
$$s_1 \leq s < L_A,$$

$$\tag{3.32}$$

$$z(s) = \frac{W_B s}{E_B A_B}\left(\frac{V}{W_B} - \frac{s}{2L_B}\right) - \frac{W_B s_1}{E_B A_B}\left(\frac{V}{W_B} - \frac{s_1}{2L_B}\right) + \frac{W_A s_1}{E_A A_A}\left(\frac{V}{W_A} - \frac{s_1}{2L_A}\right)$$

$$+ \frac{H L_B}{W_B}\left[\left\{1 + \left(\frac{V - W_B s_1/L_B}{H}\right)^2\right\}^{1/2} - \left\{1 + \left(\frac{V - W_B s/L_B}{H}\right)^2\right\}^{1/2}\right]$$

$$+ \frac{H L_A}{W_A}\left[\left\{1 + \left(\frac{V}{H}\right)^2\right\}^{1/2} - \left\{1 + \left(\frac{V - W_A s_1/L_A}{H}\right)^2\right\}^{1/2}\right],$$

$$L_A \leq s < s_2,$$

$$z(s) = \frac{W_B s}{E_B A_B}\left(\frac{V}{W_B} - \frac{s}{2L_B}\right) - \frac{W_B s_1}{E_B A_B}\left(\frac{V}{W_B} - \frac{s_1}{2L_B}\right) + \frac{W_A s_1}{E_A A_A}\left(\frac{V}{W_A} - \frac{s_1}{2L_A}\right)$$

$$+ \frac{H L_B}{W_B}\left[\left\{1 + \left(\frac{V - F_P - W_B s_2/L_B}{H}\right)^2\right\}^{1/2} - \left\{1 + \left(\frac{V - F_P - W_B s/L_B}{H}\right)^2\right\}^{1/2}\right.$$

$$+ \left\{1 + \left(\frac{V - W_B s_1/L_B}{H}\right)^2\right\}^{1/2} - \left\{1 + \left(\frac{V - W_B s_2/L_B}{H}\right)^2\right\}^{1/2} +$$

$$\left.\frac{F_P}{H}\frac{W_b}{E_B A_B}\left(\frac{s_2}{L_B} - \frac{s}{L_B}\right)\right]$$

$$+ \frac{H L_A}{W_A}\left[\left\{1 + \left(\frac{V}{H}\right)^2\right\}^{1/2} - \left\{1 + \left(\frac{V - W_A s_1/L_A}{H}\right)^2\right\}^{1/2}\right],$$

$$s_2 \leq s < L_A + L_B.$$

$$\tag{3.33}$$

Equations (3.30)-(3.33) describe the double cable configuration shown in Figure 3.4 completely. The equations have four unknowns; The horizontal force H, the vertical force V, the horizontal point load position l_A and the vertical point load position h_A. H and V are found by inserting $s = L_A + L_B$ into the second parts of (3.31) and(3.33) and using a numerical scheme to solve the equations. l_A and l_B are found by inserting H and V in the second parts of (3.30) and (3.32). The properties of the cables do not depend on each other except for one case. An unresolved problem requires that $m_A \leq m_B$. In practice this means that the mooring chain must be implemented as cable B and the work-wire as cable A. This does not create a problem since it is just a matter of defining the cable properties correctly in the implementation of the equations.

3.2.5 Inclined Elastic Catenary with Stretching

The inclined elastic catenary is a special case of Equations (3.14)-(3.15). Consider Figure 3.5 where support point P is on the seabed and support point Q is at the stern of the vessel. The new end conditions for the catenary equation are

$$x = x_0, \qquad z = z_0, \qquad p = 0 \qquad \text{at} \qquad s = 0 \qquad (3.34)$$
$$x = l, \qquad z = h, \qquad p = L_s \qquad \text{at} \qquad s = L \qquad (3.35)$$
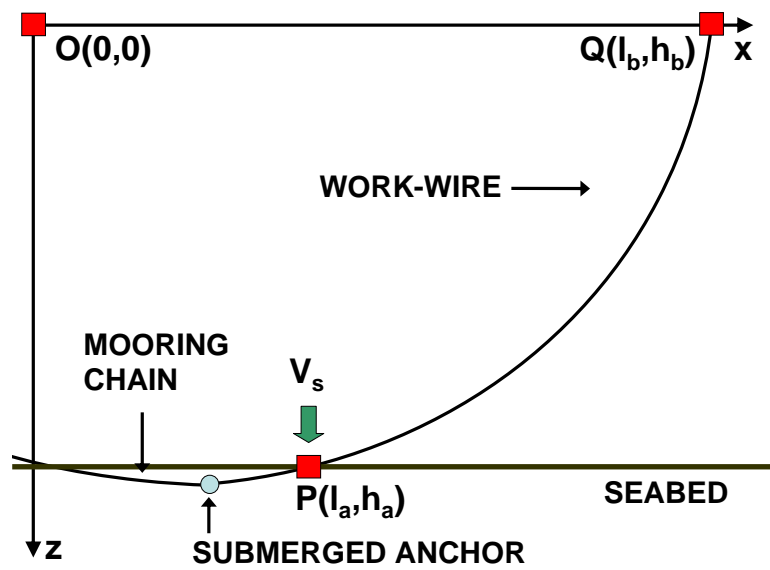
Figure 3.5. Inclined cable configuration with coordinates system and forces.

By applying the same approach as in Section 3.2.2, the solution of the inclined elastic catenary becomes

$$x(s) = \frac{Hs}{EA_0} + \frac{HL}{W} \left[\operatorname{asinh}\left(\frac{V}{H}\right) - \operatorname{asinh}\left(\frac{V - Ws/L}{H}\right) \right] + x_0 \qquad (3.36)$$

$$z(s) = \frac{Ws}{EA_0}\left(\frac{V}{W} - \frac{s}{2L}\right) + \frac{HL}{W}\left[\left\{ 1 + \left(\frac{V}{H}\right)^2 \right\}^{1/2} - \left\{ 1 + \left(\frac{V - Ws/L}{H}\right)^2 \right\}^{1/2} \right] + z_0 \qquad (3.37)$$

The tension of the cable can get very high during anchor breakout. It is therefore necessary to account for cable stretching. The relation between the stretched Lagrangian

coordinate p and the unstretched Lagrangian coordinate s is [40]

$$p = s + \frac{1}{2EAW_s} + \left[(V_s + W_s s)(H^2 + (V_s + W_s s)^2)^{1/2} \right.$$
$$\left. + H^2 \text{ln}\left(\frac{V_s + W_s s}{H} + \frac{(H^2 + (V_s + W_s s)^2)^{1/2}}{H} \right) \right] \qquad (3.38)$$

where W_s is the specific cable weight, i.e cable weight per meter and V_s is the vertical end point force at the seabed

$$V_s = V - W_s L \qquad (3.39)$$

Inserting $s = L$ into Equation (3.38) gives the solution of the stretched cable length $p = L_s$

$$L_s = L + \frac{1}{2EAW_s}\left[V(H^2 + V^2)^{1/2} + H^2 \text{ln}\left\{ \frac{V}{H} + \left(1 + \left(\frac{V}{H}\right)^2 \right\}^{1/2} \right) \right] \qquad (3.40)$$

By inserting $L = L_s$, $s = p$, $x = l$ and $z = h$ into Equations (3.36)-(3.37) a solution of the inclined elastic catenary equation with stretching is found.

3.3   Quasi-Static Polynomial Approach

3.3.1   Implementation Issues

The catenary equations are static equations, i.e. only a single cable configuration is described by the equations for a given set of parameters. In order to incorporate the catenary equations into a dynamic simulation of an anchor handling vessel, a quasi-static approach must be adopted. The quasi-static approach consists of solving the catenary equations with respect to the horizontal and vertical end point forces H and V off-line. In the following, it is shown how the polynomials are created and used together with look-up tables and cable span segmentation.

3.3.2   Two-Dimensional Polynomial Creation

As stated in Section 3.3.1, it is necessary to find polynomials for the horizontal and vertical end point forces H and V. The general elastic catenary model and the inclined elastic catenary model have to variables, i.e. the cable span l and cable length L. A two-dimensional polynomial approach can therefore be adopted, and the forces H and

V are then expressed as a function of both the cable length L and the cable span l. The MATLAB-function polyfitweighted2 is used to generate the two-dimensional polynomials in a least-squares sense [31]. General polynomials of first, second and third order can be written as

$$P_1(\alpha, \beta) = a_{00} + a_{10}\alpha + a_{01}\beta \tag{3.41}$$
$$P_2(\alpha, \beta) = a_{00} + a_{10}\alpha + a_{01}\beta + a_{20}\alpha^2 + a_{11}\alpha\beta + a_{02}\beta^2$$
$$P_3(\alpha, \beta) = a_{00} + a_{10}\alpha + a_{01}\beta + a_{20}\alpha^2 + a_{11}\alpha\beta + a_{02}\beta^2$$
$$+ a_{30}\alpha^3 + a_{21}\alpha^2\beta + a_{12}\alpha\beta^2 + a_{03}\beta^3$$

where a_{ii}, $i \in \{1, 3\}$ are the coefficients in ascending powers and α, β are the variables in which the polynomial is evaluated. If n_p is the order of the polynomial, the number of coefficients $N(n_p)$ used to describe it is calculated as

$$N(n) = \frac{(n_p + 1)(n_p + 2)}{2} \tag{3.42}$$

A scaling and centering procedure is also used to improve the numerical properties of the polynomials. This involves a change of variables, substituting α by

$$\hat{\alpha} = \frac{\alpha - \mu_\alpha}{\sigma_\alpha^2} \tag{3.43}$$

where μ_α is the mean value of α and σ_α^2 the standard deviation. The same scaling and centering procedure is also used for β. The scaling and centering procedure is necessary since the data sets will contain many equal datapoints. By setting $\alpha = L$ and $\beta = l$, an example polynomial of third order for H and V becomes

$$H(L, l) = h_{00} + h_{10}L + h_{01}l + h_{20}L^2 + h_{11}Ll + h_{02}l^2 \tag{3.44}$$
$$+ h_{30}L^3 + h_{21}L^2l + h_{12}Ll^2 + h_{03}l^3$$
$$V(L, l) = v_{00} + v_{10}L + v_{01}l + v_{20}L^2 + v_{11}Ll + v_{02}l^2$$
$$+ v_{30}L^3 + v_{21}L^2l + v_{12}Ll^2 + v_{03}l^3$$

where h_{ii}, v_{ii}, $i \in \{1, 3\}$ are the coefficients of the respective polynomials. Finally, the polynomials can be evaluated in specific datapoints using the MATLAB-function polyval2 [31].

3.3.3   Look-Up Tables and Cable Span Segmentation

The double cable configuration derived in Section 3.2.4 has three parameters that can
be varied; the cable span l, the length of cable A and the length of cable B. A two-
dimensional polynomial is therefore not sufficient in order to be able to control all three
variables during simulations. Lets assume that the length of cable B and the cable span
are the primary variables, i.e $\alpha = L_A$ and $\beta = l$ in(3.41). The length of cable B is then
the secondary variable. A series of polynomials can then be created for different values
of the secondary variable, resulting in a look-up table as shown in Table 3.1.

L_B	Horizontal Force	Vertical Force
50	$H_{50}(L_A, l)$	$V_{50}(L_B, l)$
60	$H_{60}(L_B, l)$	$V_{60}(L_B, l)$
70	$H_{70}(L_B, l)$	$V_{70}(L_B, l)$
...	...	...
...	...	...
990	$H_{990}(L_B, l)$	$V_{990}(L_B, l)$
1000	$H_{1000}(L_B, l)$	$V_{1000}(L_B, l)$

Table 3.1. Example of a look-up table for two-dimensional polynomials.

The minimum and maximum values of L_B as well as the interval between the length
values are a design criterion. A trade-off between accuracy and amount of stored data
must be made. If the intervals between the seconday variable values are large, a jump in
force values will be experienced when changing the index values in the look-up table. A
low-pass filter must therefore be implemented to smooth out the force profile. The time
constant of the low-pass filter must be tuned to match the look-up table setup.

The choice of primary and secondary variables is free, and does not influence the overall
results. Since the secondary variable does not cover all possible values, a rounding
function is necessary in order to find the correct row in the look-up table. The rounding
function is implemented to find the closest whole integer in the look-up table. This
approach restrics the vessel movement. The vessel can only move within the area specified
by the minimum and maximum values of the secondary variable.

Another issue concerning the quasi-static polynomial approach is that a polynomial for
different cable lengths and cable span must be matched. Consider a case where the cable
span is varied between 100 and 1000 [m]. This forces the minimum cable length to be
approximately 1000 [m]. It is therefore impossible to use that polynomial if the desired
span is 200 [m] and the desired cable length is less than 1000 [m]. The problem is solved
using cable span segmentation. An example of a cable span segmentation for the double
cable configuration is given in Table 3.2, where cable A is the mooring chain and cable
B the work wire. The table divides the span into intervals and states the allowed cable
lengths for each of the given intervals.

Span	1500-1750	1750-2000	2000-2250	2250-2500	2750 - 3000
Chain	1850-3000	2100-3000	2350-3000	2350-3000	2350 - 3000
Work wire	10-1500	10-1500	10-1500	250-1500	750 -1500

Table 3.2. Example of cable span segmentation.

3.3.4   Parameter Selection and Polynomial Generation

The different phases of an anchor handling operations requires that different catenary models are used. An overview of anchor deployment and anchor recovery operations was given in Section 2.5. Figures 2.2 and 2.3 illustrate phases where only the mooring chain of the OI is deployed. For this purpose the the general elastic catenary configuration given by Equations (3.16)-(3.17) will be used. Figure 2.4 shows a phase of the operation where both the mooring chain, work wire and anchor is deployed. For this purpose the double cable configuration given by Equations (3.30) and (3.33) will be used. When the anchor is submerged in the seabed or lies on the top of the seabed the inclined elastic catenary model given by Equations (3.36)-(3.37) is used.

The parameter values of the work wire and mooring chain are matched close to the values used in [29], but the exact values are taken from the *International Mooring Systems* product specification manual [18]. The resulting parameter set is listed in Table 3.3.

| Cable Type	m [kg/m]	m_s [kg/m]	d [mm]	A [m^2]
Work Wire	24.7	20.83	77	0.0047
Mooring wire	29	24.46	83	0.0054
Mooring chain	155	130.7	84	0.0111

Table 3.3. Parameters values of the various cables.

When offshore installations are moored, a combination of mooring chain and wire is used to reduce the total weight of the cable. In the simulations, a mean value of the mooring wire and mooring chain parameter values will be used. The submerged mass of the mooring chain[1] will therefore be approximately 80 [kg/m]. The point load value F_P is set to match an anchor that weighs 18000 [kg].

The general elastic catenary configuration and the double cable configuration are selected to illustrate the generation of two-dimensional polynomials. Figure 3.6 shows the results for the general elastic catenary configuration. The vertical and horizontal force polynomials are created for cable lengths 1100-1600 [m] and cable spans 100-1000 [m]. It can be observed that the vertical end point force does not depend on the cable span, but only on the cable weight. It is therefore sufficient with a polynomial of order 1 to describe

---

[1]The term mooring chain will be used through the rest of the paper even though the mooring cable is made up of a chain part and a wire part.

the force surface. The horizontal force surface is more complex. When the length of the cable span and the cable itself has approximately the same value, the horizontal force will have an extremely high value that tends to infinity. It is therefore difficult to find a low-order polynomial that describes the force surface with sufficient accuracy. Figure 3.6(b) shows the horizontal error induced by a polynomial of order 15.
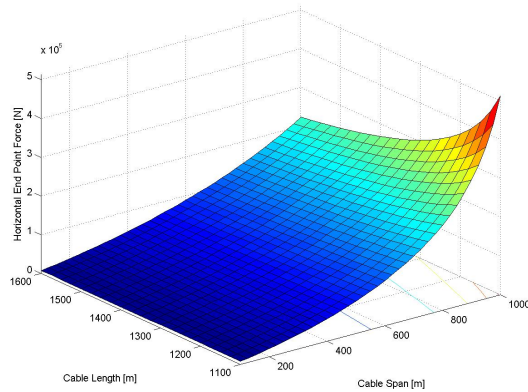
(a) Horizontal end point force.
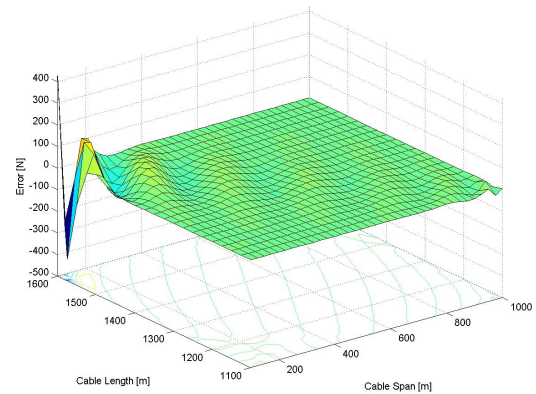
(b) Horizontal force error induced by polynomial of order 15.
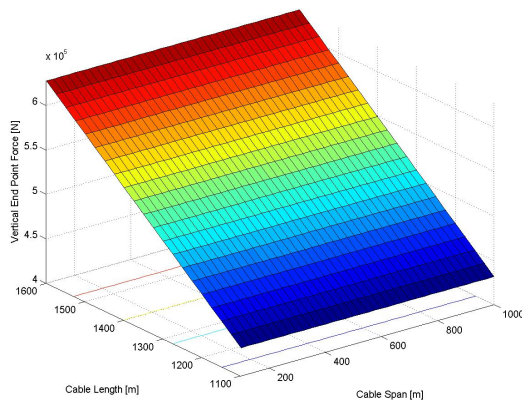
(c) Vertical end point force.

(d) Vertical force error induced by polynomial of order 1.

Figure 3.6. Two-dimensional force surfaces and corresponding errors induced by polynomials for the general elastic catenary model.

Figure 3.7 shows the results for the double cable configuration. The polynomials were created with mooring chain length $L_B = 1100$ [m], work wire lengths $L_A = 10 - 500$ [m] and cable spans $100 - 1000$ [m]. The value of the point load is $F_P = 176.5$ [kN]. It can be observed that the vertical force surface is more complex in this case, since it depends on the values of the point load and the two different cable masses. Polynomials of order 15 is sufficient to keep the horizontal and vertical error surfaces sufficiently small.
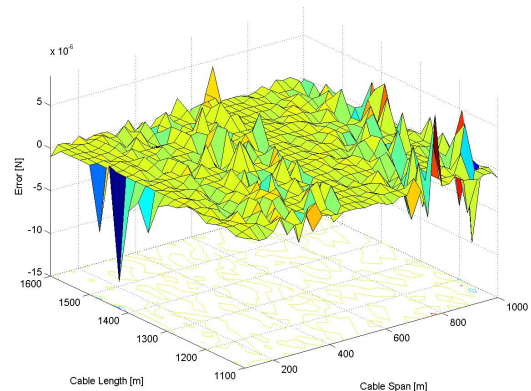

(a) Horizontal end point force.

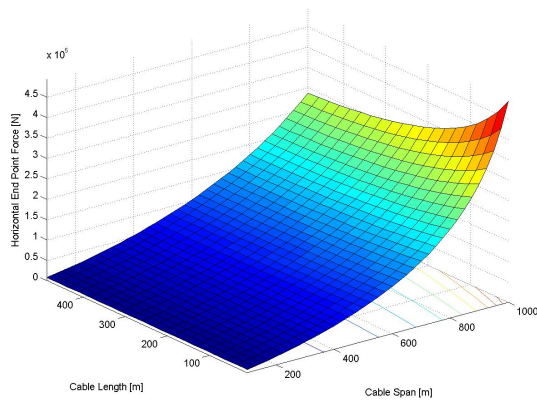(b) Horizontal force error induced by polynomial of order 15.
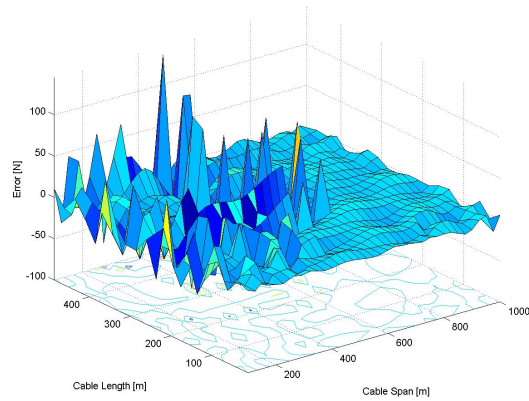

(c) Vertical end point force.
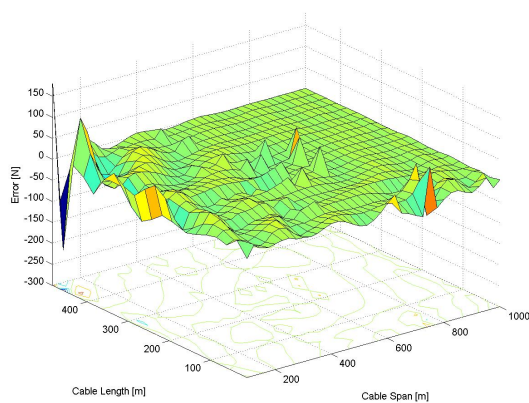
(d) Vertical force error induced by polynomial of order 15.

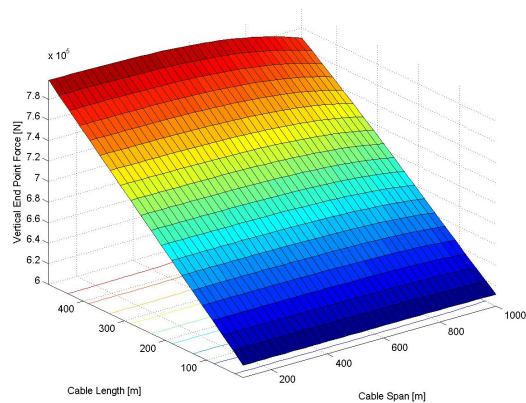Figure 3.7. Two-dimensional force surfaces and corresponding errors induced by polynomials for the double catenary configuration with point load.

Chapter 4

Seabed and Anchor Interaction

4.1 Anchor Types and Their Use

Anchors used in the offshore industry are normally one of the following types [8, 42]:

- Drag embedment anchors
- Vertically loaded anchors
- Drag-in plate anchors
- Pile anchors
- Suction anchors
- Gravity or dead weight anchors

Note that some name variations exist in the literature. The performance of a specific anchor type depends on several parameters related to it [42], amongst other:

- Fluke area and design
- Shank design
- Soil conditions
- Load conditions
- Mooring line type

The type of mooring line selected for a particular offshore installation is often related to the water depth, and this relates directly to anchor type requirements. For deepwater applications a taut leg mooring system with synthetic ropes is favourable [35]. For a taut leg mooring system vertically loaded anchors is the best choice for end termination of the mooring cable [7], since vertical loaded anchors can withstand both large horizontal and vertical forces. For shallow waters the most normal mooring line configuration is the classic catenary mooring with either chain, wire ropes or a combination of the two cable types, which also is the modeling scope in this report. This mooring configuration requires that a part of the chain or wire rope is laying on the seabed. This gives rise

to load situations where the anchor is required to withstand large horizontal forces and small vertical forces. Drag embedment anchors are ideal for this purpose.

4.2   The Breakout Phenomenon

The breakout phenomenon refers to the process of removing an object that is either partially or completely embedded into the seafloor soil [32, 36]. The force required to remove the object is called the breakout force F_b and the resistance imposed by the object embedded into the seafloor is called the breakout resistance R_b. The force needed to break out an object embedded in the seafloor is greater than the submerged weight of the object itself. This is described by the simple relationship

$$F_b = F - W \geq R_b \tag{4.1}$$

where W is the weight of the object and F is the resultant force required to break out the object. The duration of the applied breakout force is equally important as the magnitude. For a large and deeply buried anchor, a bollard pull of 80 tonnes and winch tension of 200 tons sustained over 30 minutes may be required to break out the anchor [22]. The breakout time is denoted t_b.

The breakout phenomenon can be divided into two main categories: Breakout of completely submerged objects and partially submerged objects. The first complete breakout solution of a partially submerged object is presented in [45], whereas a FEM analysis of the problem is presented in [23]. The kinematics of drag embedment anchors in sand is treated in [25], but focus is directed towards the embedment phase of the anchor. Literature on breakout of completely submerged anchors is scarce.

The solutions suggested in the mentioned papers lacks generality. Some of the models are just valid for given phases of the breakout process and some is only valid for a certain type of seabed soil, whereas other methods are not well suited for implementaion in a control system design. Another approach to the breakout problem is therefore adopted, using friction models from the robotics literature, which is the topic of the next section.

4.3   Dynamic Friction Model

An overview of static and dynamics friction models is given in [10]. Static friction models calculates the friction force as a function of velocity. The main disadvantage of the static models is that they are dependent on detecting zero velocity and using a different model for this purpose. In addition they are not capable of describing pre-sliding displacement, varying break-away force and frictional lags, which all are dynamic effects. Two well known dynamics friction model exist: The Dahl model and the LuGre model. Both models have potential for drifting in the sticking region. The LuGre model is in essence

a generalization of the Dahl model and it is in addition more accurate. The LuGre model is therefore selected for implementation. The LuGre dynamic friction model is given by [4]

$$\dot{z} = v - \sigma_0 \frac{|v|}{g(v)} z \tag{4.2}$$

where z is the average bristle deflection between two surfaces, σ_0 is the bristle stiffness constant and v is the speed of item subject to friction. The function $g(v)$ is a representation of the Stribeck effect and it is written as

$$\sigma_0 g(v) = F_c + (F_s - F_c) e^{-(v/v_s)^2} \tag{4.3}$$

where F_c is the Coloumb friction level, F_s the stiction force level and v_s the Stribeck velocity. Finally, the friction force F_f is given by

$$F_f = \sigma_0 z + \sigma_1 \dot{z} + \sigma_2 v \tag{4.4}$$

where σ_1 is the bristle damping constant and σ_2 the viscous friction constant. The anchor and seabed interaction is modeled as a mass and a damper

$$m_a \dot{v} + d_a v = T - F_f \tag{4.5}$$

where m_a is the mass of the anchor, d_a is a damping constant imitating the damping effect of the surrounding masses of the anchor, T is the cable tension used to break out the anchor and F_f the friction force given by the LuGre friction model.

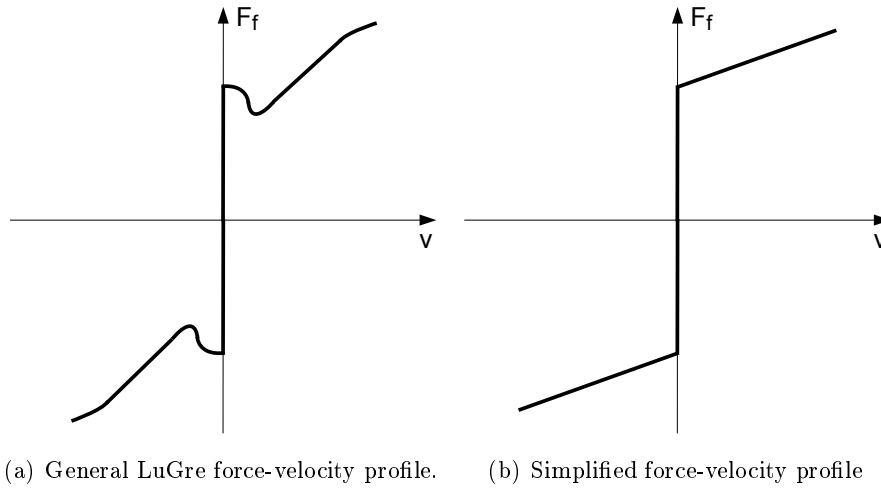(a) General LuGre force-velocity profile.   (b) Simplified force-velocity profile

Figure 4.1. Friction force as a function of velocity for different parameter sets of the LuGre model.

An illustration of how the friction force develops as a function of the velocity is given in Figure 4.1(a) and a simplification of the profile is illustrated in Figure 4.1(b). The friction force affecting the anchor will be adapted to the latter profile. The anchor will not move until the cable tension reaches a certain value, and as the tension increases further the velocity of the ancher increases linearly. The reason for making this simplification is the lack of empirical and experimental data that describes the velocity profile of the anchor as a function of the forces affecting it during breakout.

Onshore breakout tests of scaled down drag-in-plate anchors are performed in [7]. The velocities and pullout resistances were recorded for different anchors types in clay. The tests indicated that the pullout speeds varied between 0.1 and 0.4 [m/min] and the pullout resistances varied between 80 and 210 [kN] for anchors that were scaled down to 30-40 % of normal size. This data setis used as the basis for selecting the variables of the LuGre friction model. In later simulations, an anchor of 18000 [kg] is used. Assuming a high value for the pullout resistance of a 33 percent scaled down anchor, i.e 200 [kN], results in a stiction force level $F_s = 600$ [kN]. The rest of the parameters used to obtain the force-velocity relationship in Figure 4.1(b) are listed in Table 4.1.

m_a	d_a	F_s	F_c	v_s	σ_0	σ_1	σ_2
18000	20000	$6 \cdot 10^5$	$6 \cdot 10^5$	0.1	$5 \cdot 10^7$	$1 \cdot 10^4$	$4 \cdot 10^6$

Table 4.1. Simulation parameters for the LuGre dynamic friction model.

Finally, the position of the anchor is defined relative to the cable position as the seabed. No means of calculating the trajectory of the anchor during breakout is implemented. It is assumed that the anchor is broken out of the seabed in the same direction as the cable points towards the seabed.

Chapter 5

Vessel Model

In this section the model of the anchor handling vessel and a simplified representation of the offshore installation are presented. In addition the thrust limitations of the AHV are discussed. The coordinates of the cable attachment point on the vessel are derived and the end point forces provided by the catenary equations are decomposed into six degrees of freedom (DOF) to give realistic force and moment interaction with the vessel.

5.1 Zero Speed DP Model with Fluid Memory Effects

A vessel model from the *Marine Systems Simulator* (MSS) [24] is used in this thesis. MSS is a MATLAB/Simulink-library for marine systems. The library contains amongst other Simulink template models for various ships. A zero-speed DP force RAO model with fluid memory effects in 6 DOF is selected as the basis for simulations. All equations use the standard SNAME-notation, see Table 5.3. The complete vessel model is written as

$$\dot{\boldsymbol{\eta}} = \mathbf{J}(\boldsymbol{\eta})\boldsymbol{\nu} \tag{5.1}$$

$$\mathbf{M}\dot{\boldsymbol{\nu}} + \mathbf{D}\boldsymbol{\nu}_r + \mathbf{d}(\boldsymbol{\nu}_r) + \mathbf{G}\boldsymbol{\eta} + \boldsymbol{\mu} = \boldsymbol{\tau}_{waves} + \boldsymbol{\tau}_I + \boldsymbol{\tau}_P \tag{5.2}$$

$$\dot{\boldsymbol{\chi}} = \mathbf{A}_r\boldsymbol{\chi} + \mathbf{B}_r\boldsymbol{\chi} \tag{5.3}$$

$$\boldsymbol{\mu} = \mathbf{C}_r\boldsymbol{\chi} \tag{5.4}$$

Equation (5.1) accounts for the kinematics and Equation (5.2) for the kinetics of the vessel dynamics. Equations (5.3)-(5.4) are a linear reduced-order state space model that approximates the fluid memory effects. The states in χ express the changes in future fluid forces as a function of the change of fluid momentum due to vessel movement. Table 5.4 contains a list of all the elements in Equations (5.1)-(5.4) and explains their meaning as well as dimensions. More information about the MSS vessel model can be found in [38] and general information about vessel modeling is discussed in [13, 15].

Note that there is no coriolis-centripental matrix $\mathbf{C}(\nu_r)$ in the model. For low-speed applications the quadratic term given by $\mathbf{C}(\boldsymbol{\nu_r})\boldsymbol{\nu_r}$ is negligible. The nonlinear damping term $\mathbf{D}(\boldsymbol{\nu_r})$ is reduced to a linear damping matrix $\mathbf{D}$ for the same reason.

A parameter set for a supply vessel ship supplied by the MSS library is used in the simulations. The main particulars of the supply vessel are listed in Appendix C.1. The elements of the kinematic transformation matrix $\mathbf{J}(\boldsymbol{\eta})$, the position vector $\boldsymbol{\eta}$ and velocity vector $\boldsymbol{\nu}$ are given in Appendix A, together with an explanation of the relative velocity vector $\boldsymbol{\nu}_r$.

5.2   Thrust Limitations

In order to give the vessel model realistic thrust characteristics, the main particulars of the supply ship model supplied by the MSS library was compared against real anchor handling vessel. The best match was found to be the AHTS *Far Sapphire* by Farstad [12], see Figure 2.1. The propulsion setup of *Far Sapphire* is explained in Table 5.1.

Propulsion Unit	Power [kW]	Number	Total Power [kW]	Force [kN]
Main propeller	6000	2	12000	2000
Bow tunnel thruster	883	2	1766	234
Aft tunnel thruster	1500	1	1500	193
Bow azimuth thruster	1800	1	1800	320
Aft azimuth thruster	1800	1	1800	320

Table 5.1. Propulsion setup of *Far Sapphire*. The available propulsion power is converted to forces by courtesy of *Marine Cybernetics*.

It is assumed that only the main propellers are used in surge, whereas the tunnel and azimuth thrusters are used in sway and yaw. The moment lever arm in yaw is assumed to be 18 [m]. The final thruster characteristics implemented in the simulator is presented in Table 5.2. The thruster characteristics correspond to the most powerful class of new generation anchor handling vessels [6]. Note that the saturation and rate limit implementation does not capture the effect of reduced bollard pull when using tunnel and azimuth thrusters to control the heading of the vessel.

DOF	Min	Max	T [s]	Rate
Surge	-2000 [kN]	2000 [kN]	12	167 [kN/s]
Sway	-1000 [kN]	1000 [kN]	8	125 [kN/s]
Yaw	-20000 [kNm]	20000 [kNm]	8	2500 [kNm/s]

Table 5.2. Saturation and rate limits for simulator thrust setup. The time constant T describes the necessary time to output maximum power.

DOF	Motion	Axis	Forces and moments	Linear and angular velocites	Positions and Euler angles
1) Surge	Translation	x	X	u	x
2) Sway	Translation	y	Y	v	y
3) Heave	Translation	z	Z	w	z
4) Roll	Rotation	x	K	p	ϕ
5) Pitch	Rotation	y	M	q	θ
6) Yaw	Rotation	z	N	r	ψ

Table 5.3. The notation of SNAME for marine vessels [13].

Symbol	Dimension	Explanation
$\boldsymbol{\eta}$	$\mathbb{R}^6$	Position and orientation vector
$\boldsymbol{\nu}$	$\mathbb{R}^6$	Linear and angular velocity vector
$\boldsymbol{\nu_r}$	$\mathbb{R}^6$	Relative velocity vector
$\mathbf{J}(\boldsymbol{\eta})$	$\mathbb{R}^{6\times6}$	Kinematic transformation matrix between n- and b-frame
$\mathbf{M}$	$\mathbb{R}^{6\times6}$	System inertia matrix ($\mathbf{M} = \mathbf{M}_A + \mathbf{M}_{RB}$)
$\mathbf{M}_A$	$\mathbb{R}^{6\times6}$	Added mass matrix
$\mathbf{M}_{RB}$	$\mathbb{R}^{6\times6}$	Rigid body inertia matrix
$\mathbf{C}(\nu_r)$	$\mathbb{R}^{6\times6}$	Coriolis-centripental matrix
$\mathbf{D}$	$\mathbb{R}^{6\times6}$	Linear damping matrix
$\mathbf{G}$	$\mathbb{R}^{6\times6}$	Linear spring stiffness matrix
$\mathbf{d}(\boldsymbol{\nu_r})$	$\mathbb{R}^6$	Nonlinear damping in b-frame due to current forces
$\boldsymbol{\mu}$	$\mathbb{R}^6$	Viscous and potential damping
$\boldsymbol{\tau}_P$	$\mathbb{R}^6$	Vector of control inputs
$\boldsymbol{\tau}_{waves}$	$\mathbb{R}^6$	Vector of wave drift forces and first order wave loads, i.e Froude-Krylov diffraction forces
$\boldsymbol{\tau}_I$	$\mathbb{R}^6$	External forces from interacting systems
$\boldsymbol{\chi}$	$\mathbb{R}^6$	Fluid memory effect state vector
$\mathbf{A}_r, \mathbf{B}_r, \mathbf{C}_r$	$\mathbb{R}^6$	Fluid memory state-space matrices

Table 5.4. Explanation of parameters, variables and other elements related to the vessel model.

5.3   Offshore Installation Model

The offshore installation is not of primary interest in this thesis. It is therefore unnecessary to use a realistic model of it in simulations: only its position is of interest. Let the n-frame position of the OI be defined as

$$\mathbf{p}_{oi}^n = \begin{bmatrix} x_{oi}^n & y_{oi}^n & z_{oi}^n \end{bmatrix}^\top \tag{5.5}$$

The position of the OI would normally fluctuate due to the effects of wind, waves and currents. It is however assumed that the horizontal position, i.e. x_{oi}^n and y_{oi}^n are constant. The vertical component z_{oi}^n is modeled another way to achieve an attractive simplification. z_{oi}^n is assumed to be equal to the vertical coordinate of the cable attachment point on the vessel. Thus

$$z_{oi}^n = z_c^n \tag{5.6}$$

where z_c^n is given by Equation (5.12) in Section 5.4.1. This assumption simplifies the preprocessing of the catenary equations, since the height difference of the two cable support points can be neglected.

5.4   Cable Forces and Moments on the Vessel

5.4.1   Cable Attachment Points

The solution of a catenary equation provides a horizontal and a vertical force acting on the vessel. The point of attachment is defined relative to the vessel's coordinate origin (CO). The CO is located on the still waterplane at a distance $L_{pp}/2$ from the aft perpendicular [14]. L_{pp} is defined as the length between the perpendiculars.

Consider Figure 5.1. The cable is fixed in two points. The first support is on the OI and the other at the stern of the AHV. Seen from above the cable is a straight line. It is not affected by currents and cannot assume a curved shape in the horizontal plane. The b-frame cable position $\mathbf{p}_c^b$ at the stern of the vessel is defined as

$$\mathbf{p}_c^b = \begin{bmatrix} x_c^b & y_c^b & z_c^b \end{bmatrix}^\top \tag{5.7}$$

The position of the vessel itself is gived by the n-frame coordinates

$$\mathbf{p}^n = \begin{bmatrix} n & e & d \end{bmatrix}^\top \tag{5.8}$$

The b-frame coordinates $\mathbf{p}_c^b$ of the cable attachment point is transformed into n-frame coordinates $\mathbf{p}_c^n$ using geometrical relations. This results in

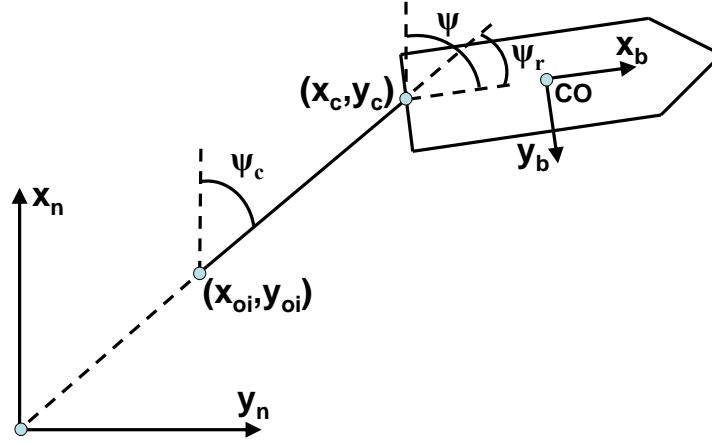$$\mathbf{p}_c^n = \begin{bmatrix} x_c^n & y_c^n & z_c^n \end{bmatrix}^\top \tag{5.9}$$

Figure 5.1. Coordinate systems and angles which are used to compute the n-frame coordinates of the cable attachment point on the vessel.

where the elements of Equation (5.9) are

$$x_c^n = n + x_c^b \cos(\psi) - y_c^b \cos(\psi - \pi/2) \tag{5.10}$$

$$y_c^n = e + x_c^b \sin(\psi) - y_c^b \sin(\psi - \pi/2) \tag{5.11}$$

$$z_c^n = d + x_c^b \sin(\psi) \tag{5.12}$$

The other attachment point of the cable is on the OI and is given directly by its n-frame position

$$\mathbf{p}_{oi}^n = \begin{bmatrix} x_{oi}^n & y_{oi}^n & z_{oi}^n \end{bmatrix}^\top \tag{5.13}$$

The cable span l can then be calculated as

$$l = \sqrt{(x_c^n - x_{oi}^n)^2 + (y_c^n - y_{oi}^n)^2} \tag{5.14}$$

5.4.2 Decomposing the Catenary Forces

The horizontal and vertical end point forces H and V provided by the catenary equations are always assumed to act in the point $\mathbf{p}_c^n$ defined by Equation (5.9). The horizontal force vector H will always remain parallell to the xy-plane and the vertical force vector

V will remain parallell to the yz-plane. Let the cable angle ψ_c be defined as

$$\psi_c = \operatorname{atan}\left(\frac{y_c^n - y_{oi}^n}{x_c^n - x_{oi}^n}\right) \tag{5.15}$$

The relative cable angle ψ_r, see Figure 5.1, is defined as the difference between the vessel heading ψ and the cable angle ψ_c according to

$$\psi_r = \psi - \psi_c \tag{5.16}$$

The nature of which the forces H and V affect the vessel depends on the vessel's orientation $\boldsymbol{\Theta} = \begin{bmatrix} \phi & \theta & \psi \end{bmatrix}^\top$. H and V are decomposed into the 3 DOF force vector $\mathbf{f}_c$ with elements

$$\mathbf{f}_c = \begin{bmatrix} X_c & Y_c & Z_c \end{bmatrix}^\top \tag{5.17}$$

$\mathbf{f}_c$ will always act on the vessel in the point $\mathbf{p}_c^n$. The elements of $\mathbf{f}_c$ are found by considering geometric relations between H, V, the relative cable angle ψ_r and the vessel states ϕ and θ. This results in

$$\mathbf{f}_c = \begin{bmatrix} X_c \\ Y_c \\ Z_c \end{bmatrix} = \begin{bmatrix} -(H\cos\theta + V\sin\theta)\cos\psi_r \\ (H\cos\theta + V\sin\theta)\sin\psi_r\cos\phi - (H\sin\theta - V\cos\theta)\sin\phi \\ -(H\cos\theta + V\sin\theta)\sin\psi_r\sin\phi - (H\sin\theta - V\cos\theta)\cos\phi \end{bmatrix} \tag{5.18}$$

Proof: Equation (5.18) was initially found by geometric considerations. Another way of producing the same result is by means of rotation matrices. Let the end-point force vector be

$$\mathbf{f}_{cat} = \begin{bmatrix} -H & 0 & V \end{bmatrix}^\top \tag{5.19}$$

Three rotations are necessary to decompose (5.19) into (5.18). The corresponding rotation matrices are

$$\mathbf{R}_x(\phi) = \begin{bmatrix} 1 & 0 & 0 \\ 0 & \cos(\phi) & -\sin(\phi) \\ 0 & \sin(\phi) & \cos(\phi) \end{bmatrix} \tag{5.20}$$

$$\mathbf{R}_y(\theta) = \begin{bmatrix} \cos(\theta) & 0 & \sin(\theta) \\ 0 & 1 & 0 \\ -\sin(\theta) & 0 & \cos(\theta) \end{bmatrix} \tag{5.21}$$

$$\mathbf{R}_z(\psi_r) = \begin{bmatrix} \cos(\psi_r) & -\sin(\psi_r) & 0 \\ \sin(\psi_r) & \cos(\psi_r) & 0 \\ 0 & 0 & 1 \end{bmatrix} \tag{5.22}$$

where $\mathbf{R}_x(\phi)$ corresponds to a rotation of ϕ [rad] around the x-axis, $\mathbf{R}_y(\theta)$ to a rotation of θ [rad] around the y-axis and $\mathbf{R}_z(\psi_r)$ to a rotation of ψ_r [rad] around the z-axis The rotations are carried out as follows

$$\mathbf{R} = \mathbf{R}_x(\phi)^\top \mathbf{R}_z(\psi_r)^\top \mathbf{R}_y(\theta)^\top \tag{5.23}$$

The force vector is then calculated as $\mathbf{f}_c = \mathbf{R}\mathbf{f}_{cat}$ resulting in Equation (5.18) which concludes the proof. $\qquad\square$

The force vector $\mathbf{f}_c$ will also give rise to a moment vector $\mathbf{m}_c$ since $\mathbf{p}_c^b$ does not coincide with the vessel's CO. The moment vector $\mathbf{m}_c$ is found by calculating the crossproduct between the cable force vector and end point cable position

$$\begin{aligned}
\mathbf{m}_c &= \mathbf{p}_c^b \times \mathbf{f}_c \\
&= \begin{bmatrix} x_c^b \\ y_c^b \\ z_c^b \end{bmatrix} \times \begin{bmatrix} X_c \\ Y_c \\ Z_c \end{bmatrix} \\
&= \begin{bmatrix} K_c \\ M_c \\ N_c \end{bmatrix}
\end{aligned} \tag{5.24}$$

resulting in

$$\mathbf{m}_c = \begin{bmatrix} K_c \\ M_c \\ N_c \end{bmatrix} = \begin{bmatrix} -F_{cs}(z_c^b\cos\phi + y_c^b\sin\phi)\sin\psi_r & +F_{sc}(z_c^b\sin\phi - y_c^b\cos\phi) \\ F_{cs}(x_c^b\sin\psi_r\sin\phi - z_c^b\cos\psi_r) & +F_{sc}x_c^b\cos\phi \\ F_{cs}(x_c^b\sin\psi_r\cos\phi + y_c^b\cos\psi_r) & -F_{sc}x_c^b\sin\phi \end{bmatrix} \tag{5.25}$$

where

$$F_{cs} = H\cos\theta + V\sin\theta \tag{5.26}$$
$$F_{sc} = H\sin\theta - V\cos\theta \tag{5.27}$$

is used for notational convenience. Finally, the generalized force and moment vector $\boldsymbol{\tau}_c$ acting from the cable on the vessel is written as

$$\begin{aligned}
\boldsymbol{\tau}_c &= \begin{bmatrix} \mathbf{f}_c^\top & \mathbf{m}_c^\top \end{bmatrix}^\top \\
&= \begin{bmatrix} X_c & Y_c & Z_c & K_c & M_c & N_c \end{bmatrix}^\top
\end{aligned} \tag{5.28}$$

where the elements of (5.28) are given by Equations (5.18) and (5.25)

Chapter 6

Deck Equipment

This chapter contains the mathematical models for the deck equipment on the anchor handling vessel. Two systems are considered: the winch and the guidepin system. The winch contains the vessel's work wire which is restricted on the stern by the guide pins. An illustration of the setup is given in Figure 6.1.
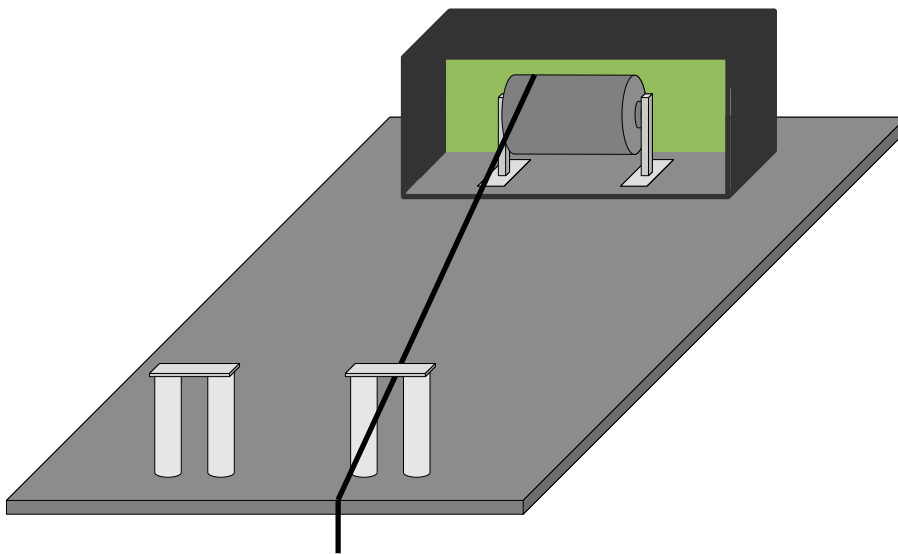

Figure 6.1. Overview and setup of the vessel's after deck equipment.

6.1 Winch System

The implemented winch system includes a motor, a gear and a winch. The motor may either be hydraulic, electric or diesel driven. For simulation purposes, a general motor

will be implemented. A PID-controller is used to control the angular velocity of the winch. Figure 6.2 gives an overview of the components in the system.
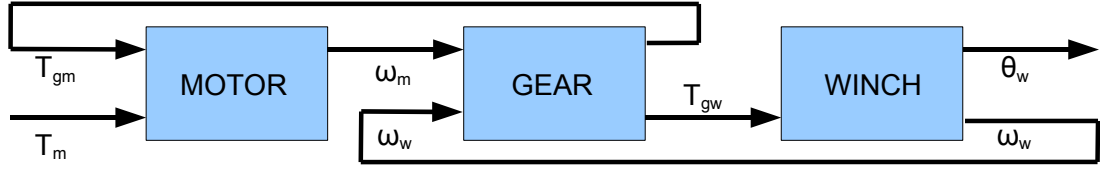

Figure 6.2. Block diagram of the winch system consisting of a motor, a gear and the winch itself.

6.1.1   Motor Model

A general motor can be modeled as a rotating shaft driven by an input torque and driving a load. The equation of motion for the motor shaft is [10]

$$\dot{\theta}_m = \omega_m \tag{6.1}$$

$$J_m \dot{\omega}_m = T_m - T_{gm} \tag{6.2}$$

where θ_m is the angular position of the shaft, ω_m is the angular velocity of the shaft, J_m is the motor inertia, T_m is the motor torque and T_{gm} is the gear torque on the motor side.

6.1.2   Gear Model

The gear is connected to the motor on one side and to the winch on the other side, as illustrated in Figure 6.2. The main purpose of the gear is to adjust the speed of the load to the speed of the motor. This is accomplished by a reduction gear, which also gives a higher load torque. In the following, a model of an elastic gear with deadzone is described. Let the gear ratio be denoted n_g. The angular speed and torque relation between the input port and output port, as illustrated in Figure 6.3, can then be written as [10]

$$\omega_w = n_g \omega_m \tag{6.3}$$

$$T_{gw} = \frac{1}{n_g} T_{gm} \tag{6.4}$$

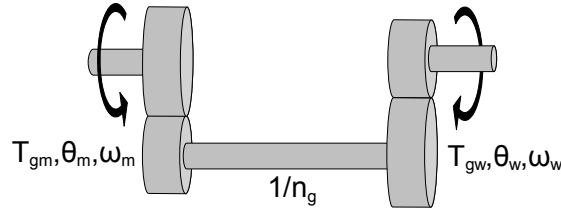where ω_w is the angular winch velocity and T_{gw} is the gear torque on the winch side.

Figure 6.3. Reduction gear.

The gear is modelled as a spring and a damper with torque defined as

$$T_{gm}(\phi_g) = K_g(\phi_g) + D_g\dot{\phi}_g \tag{6.5}$$

where D_g is the gear damping and K_g the spring stiffness. The elastic deformation of the gear referenced to the motor side, i.e the gear deflection ϕ_g between the motor and the load is

$$\phi_g = \theta_m - \frac{1}{n_g}\theta_w \tag{6.6}$$

where θ_w is the angular position of the winch shaft. The gear torque T_{gm} is dependent on the gear deflection ϕ_g resulting in

$$T_{gm}(\phi) = \begin{cases} K(\phi_g + \delta_g), & \phi_g \leq -\delta_g \\ 0, & -\delta_g \leq \phi_g \leq \delta_g \\ K(\phi_g - \delta_g), & \delta_g \leq \phi_g \end{cases} \tag{6.7}$$

where δ_g is the deadzone of the gear. The interconnection of the gear and winch is given by the relation

$$T_{gw}(\phi_g) = \frac{1}{n_g}T_{gm}(\phi_g) \tag{6.8}$$

6.1.3 Winch Model

A general winch can be modeled as a rotating shaft with a large inertia that is subject to torques from wire pulling and the gear. A winch drum model suggested in [17] yields

$$\dot{\theta}_w = \omega_w \tag{6.9}$$

$$J_w\dot{\omega}_w = -d_w\omega_w + T_{wd} + T_{gw} \tag{6.10}$$

where J_m is the inertia of the winch drum, d_w is a linear damping term mainly due to friction and T_{wd} is the wire torque on the drum. The winch represents a transition from rotating motion and vice versa, see Figure 6.4.
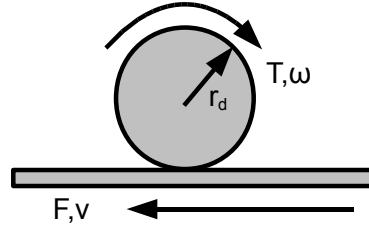
Figure 6.4. Rotation to translation.

The translating motion corresponds to the deployment or recovery of cable on the winch. This transition is described by

$$\omega_w = \frac{1}{r_d} v_w \tag{6.11}$$

$$T_{wd} = H r_d \tag{6.12}$$

where H is the horizontal catenary force, r_d is the winch drum radius and v_w is the linear cable speed.

6.1.4   Winch System Simulations

The angular winch velocity is controlled using a PID-controller on the form

$$T_m = K_d \dot{\omega}_w + K_p(\omega_d - \omega_w) + K_i \int_0^t (\omega_d - \omega_w)dt \tag{6.13}$$

where ω_d is the desired winch velocity and T_m the motor torque input. In reality, the winch speed set-point is given as the linear cable speed v_w, which is the cable length in meters deployed or recovered per minute.

The winch system and controller parameters are selected to give a stable behaviour for cable feedrates of 0-35 [m/min], which approximates the characteristics of the winch systems onboard *Far Sapphire* [12]. The resulting parameter set for the motor, gear, winch and controller is listed in Table 6.1.

Motor	Gear				Winch			Controller		
J_m	n_g	K_g	D_g	δ_g	J_w	d_w	r_d	K_p	K_d	K_i
15000	10	10	5000	0.2	3000	3000	0.98	$3.9 \cdot 10^5$	$4.9 \cdot 10^5$	$4 \cdot 10^5$

Table 6.1. Winch system simulation parameters.

The system is simulated for two different winch loads. The results are shown in Figure 6.5. The winch is able to follow the reference signal, but a transient period with an underdamped behaviour is observed after changes in the set-point. There is no notable behaviour difference for the two load conditions.
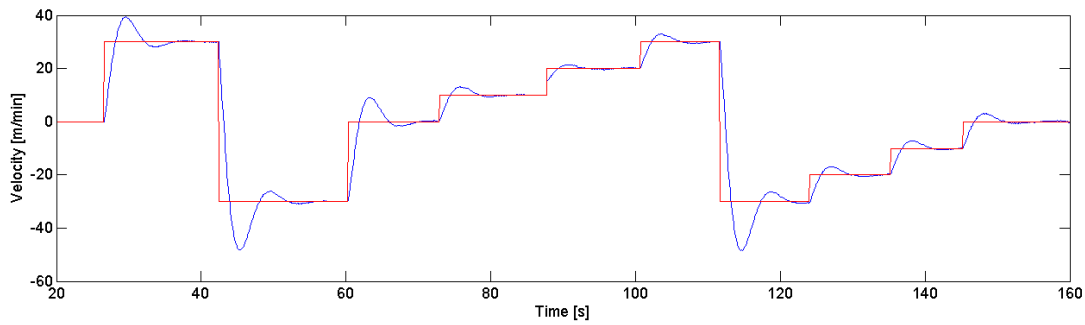
(a) Simulations with constant winch load $T_{wd} = 0.5 \cdot 10^6$ [N].
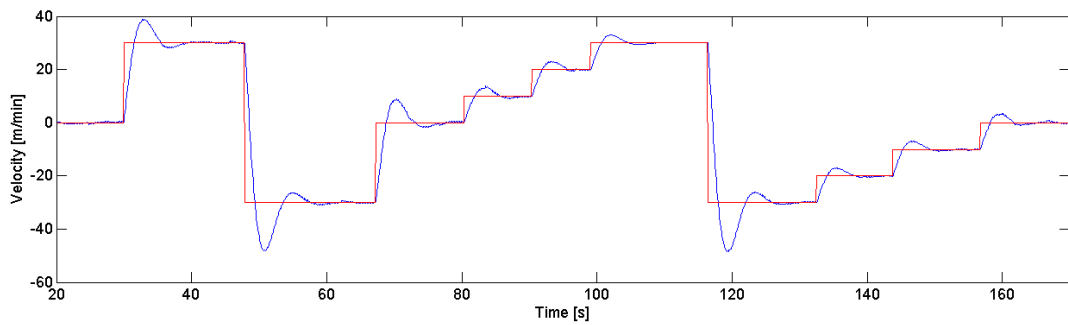
(b) Simulations with constant winch load $T_{wd} = 1 \cdot 10^6$ [N]

Figure 6.5. Comparison of winch velocity (blue) and set-point (red) for two different winch load conditions. The winch velocity is given as the linear cable speed in meters per minute.

6.2 Guide Pins

The basic functionality of a guide pin is to contain the work wire or mooring chain within a restricted area at the stern of the vessel. Guide pins are always used in pairs, i.e it is necessary to use two guide pins for lateral restriction. Figure 6.6 illustrates step-by-step how a guide pin pair is raised.

(a) Lowered   (b) Raised   (c) Raised and rotated   (d) Completely raised
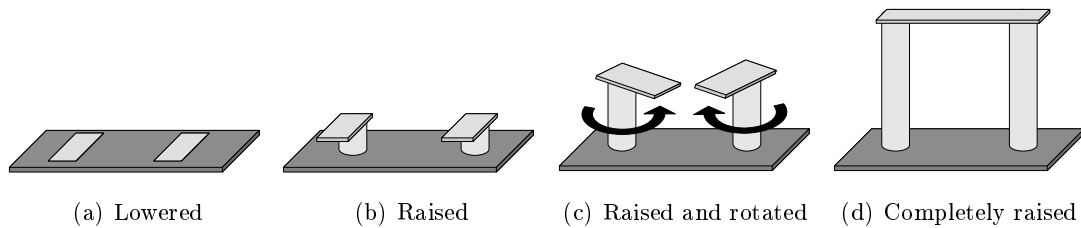
Figure 6.6. Illustration of how guide pins are raised.

Figure 6.6(a) shows that the lowered guide pins impose no restrictions. However, as illustrated in Figure 6.6(d), a raised guide pin pair will restrict both the horizontal and vertical motion of the cable. Each guidepin is rotated 90 degrees during lowering and raising, as shown in Figure 6.6(c), creating the vertical restriction.

6.2.1 Assumptions

No literature exists on guide pin modeling. A model will therefore be developed based on descriptions of their properties and functionalities in [16, 22].

Assumption 6.1. *The complete model consists of four guidepins.*

Assumption 6.2. *Each guide pin is modeled as a logical object with input and output values between zero and one. A raised guide pin outputs a value of one and a lowered guide pin outputs a value of zero. The transition between the two extremeties is carried out with a constant rate. A broken guide pin outputs zero immediately.*

Assumption 6.3. *The guide pins are not rotated during raising or lowering. The vertical restriction is implemented by letting the vertical coordinate of the cable be equal to the vertical level of the guide pin base.*

Assumption 6.4. *Each guide pin has a fixed but configurable position at the stern of the vessel. The position is defined relative to the CO of the vessel in the b-frame coordinate system.*

Assumption 6.5. *A three-parted solution is necessary to simulate the complete guide pin system: 1) One logical model for each guide pin. 2) Determination of the active guide pin set. 3) Calculation of the cable position at the stern of the vessel.*

6.2.2 Logical Guide Pin Model

The total number of guide pins on the vessel is denoted n_{gp}. The model for an individual guide pin can be written as

$$g = \text{SR}(u) \cdot \overline{e} \tag{6.14}$$

where u [0/1] is the input signal indicating whether the guide pin is to be raised or lowered, e [0/1] indicates whether the guide pin is broken or functioning and g the output signal indicating if the guidepin is raised or not. The input signal u is subject to a rate limitation defined as

$$\text{SR}(u) = \begin{cases} \Delta t \cdot R + \text{SR}(u-1), & g = 1 \\ \Delta t \cdot F + \text{SR}(u-1), & g = 0 \end{cases} \tag{6.15}$$

where R is the rising slewrate and F is the falling slew rate of the signal. Note that g can assume any value between zero and one. Since u is subject to a linear rate limitation, the value of g can be interpreted as the percentage the guide pin is raised. Also notice that $e = 1$ indicates a broken guide pin. The position on the vessel is defined relative to the CO in the body-fixed reference frame yielding

$$\mathbf{p}_g^b = \begin{bmatrix} x_g^b & y_g^b & z_g^b \end{bmatrix}^\top \tag{6.16}$$

Both the position and the logical model are used to determine the active guide pins in the next section.

6.2.3 Active Guide Pin Algorithm

The logical guide pin model described in the previous section only considers the state of each individual guide pin. It is therefore necessary to use an algorithm to determine which two guide pins that actually restricts the cable motion at the stern of the vessel. These guide pins are called the *active guide pins*.

Definition: Active Guide Pins. *From the set of guide pins that are raised, the active guide pins are defined as the two guide pins that restricts the cable motion at the stern of the vessel.*

For instance, in Figure 6.1 the starboard guide pin pair functions as the active guide pins. The position of the small cable segment trapped between the guide pins on the stern of the vessel is crucial to determine the active guide pin set. That position is defined as

$$\mathbf{p}_c^b = \begin{bmatrix} x_c^b & y_c^b & z_c^b \end{bmatrix}^\top \tag{6.17}$$

with respect to the vessel's CO in the body-fixed reference frame.

Algorithm 1 determines the active guide pin set. The result of the algorithm is the set $\mathcal{S}$ containing the number of the two active guide pins on the vessel. The algorithm uses the lateral cable position y_c^b in addition og the y-coordinate of the guide pins to determine the active set. A set of four guide pins are used, implying that $n_{gp} = 4$. The algorithm can however easily be adjusted to account for a different number guide pins. The guide pins are numbered sequentially from port side to starboard side.

Algorithm 1 Active Guide Pin Algorithm

Require: $g_1 = 1$ and $g_4 = 1$
1: **if** $g_2 = 0$ and $g_3 = 0$ **then**
2:         $\mathcal{S} \leftarrow \{1, 4\}$
3: **else if** $g_2 > 0$ and $g_3 = 0$ **then**
4:         **if** $y_c > y_2$ **then**
5:              $\mathcal{S} \leftarrow \{2, 4\}$
6:         **else**
7:              $\mathcal{S} \leftarrow \{1, 2\}$
8:         **end if**
9: **else if** $g_2 = 0$ and $g_3 > 0$ **then**
10:         **if** $y_c > y_3$ **then**
11:              $\mathcal{S} \leftarrow \{3, 4\}$
12:         **else**
13:              $\mathcal{S} \leftarrow \{1, 3\}$
14:         **end if**
15: **else if** $g_2 > 0$ and $g_3 > 0$ **then**
16:         **if** $y_c > y_3$ **then**
17:              $\mathcal{S} \leftarrow \{3, 4\}$
18:         **else if** $y_c < y_2$ **then**
19:              $\mathcal{S} \leftarrow \{1, 2\}$
20:         **else if** $y_c > y_2$ and $y_c < y_3$ **then**
21:              $\mathcal{S} \leftarrow \{2, 3\}$
22:         **end if**
23: **end if**
24: **return** $\mathcal{S}$

6.2.4   End-Point Cable Position

Only the lateral cable position y_c^b was used to determine the active guide pin set. The other two coordinates are considered to be fixed and equal to the corresponding guide pin coordinates according to

$$x_c^b = x_i^b$$
$$z_c^b = z_i^b$$

where $i \in \{1, ..., n_{gp}\}$ is the guide pin number. The x and z-coordinates of all guidepins on the vessel are normally identical, whereas the y-coordinate is variable. The lateral cable position y_c^b is thus restricted by the y-coordinate of the active guide pins. The cable moves between the guide pins as a consequence of

- the end point forces H and V provided by the solution of the catenary equations
- the heading ψ of the vessel
- the roll ϕ of the vessel
- the relative cable angle ψ_r

It is difficult to incorporate all of the elements listed above into an algorithm that calculates the lateral cable position y_c^b. An attractive simplification to the problem is given in Assumption 6.6.

Assumption 6.6. *The lateral cable position y_c^b is only affected by the vessel's roll condition. The roll condition of the vessel is defined as $C_\phi = sign(\phi)$. $C_\phi = 1$ indicates a positive roll value whereas $C_\phi = -1$ indicates a negative roll value.*

Algorithm 2 is used to calculate the lateral cable position y_c^b based on the active guide pin set $\mathcal{S}(1)$ and the vessel's roll condition C_ϕ. In essence the algorithm states that if the roll condition is negative then the cable moves towards port until it is stopped by a guidepin. If the roll condition is positive then the cable moves towards starboard until it is stopped by a guide pin.

Algorithm 2 End-Point Cable Position Algorithm

Require: $i \leftarrow 1$
  1: **if** $C_\phi < 0$ **then**
  2:              $i \leftarrow \mathcal{S}(1)$
  3: **else**
  4:              $i \leftarrow \mathcal{S}(2)$
  5: **end if**
  6: $y_c^b \leftarrow \text{SR}(y_i)$
  7: **return** y_c^b

The result of Algorithm 2 is a numerical value of y_c^b. The lateral position coordinate does not change instantly, but with a constant rate calculated as

$$\text{SR}(y_i^b) = \left\{ \begin{array}{ll} \Delta t \cdot R + \text{SR}(y_i^b - 1), & y_i^b > y_c^b \\ \Delta t \cdot F + \text{SR}(y_i^b - 1), & y_i^b < y_c^b \end{array} \right. \tag{6.18}$$

where R is the rising slew rate, F the falling slew rate and i the guide pin number. Finally, the cable position in the body-fixed reference frame can be written as

$$\mathbf{p}_c^b = \left[\begin{array}{ccc} x_{gp}^b & y_c^b & z_{gp}^b \end{array} \right]^\top \tag{6.19}$$

where it is assumed that $x_{gp}^b = x_i^b$ and $z_{gp}^b = z_i^b$ for all $i \in \{1, 4\}$. Note that (6.19) is the implementation of (5.7) which is used in Section 5.4.2 to decompose the catenary forces H and V into a 6 DOF vector of forces and moments acting from the cable on the vessel.

A simulation is carried out demonstrate the guide pin model. The position of each guide pin is listed in Table 6.2. The rising and falling slewrates are for demonstration purposes set to $R = 2$ and $F = -2$. Under normal operation conditions with a cable under tension, it is reasonable to assume that the slewrates tends to infinity and that the cable will have a snap-like motion between the guide pins.

Guide Pin Number	x_g^b	y_g^b	z_g^b
1	-41.4	-2.5	0
2	-41.4	-2	0
3	-41.4	2	0
4	-41.4	2.5	0

Table 6.2. Position of the guide pins used in simulations.

Figure 6.7 shows the results of the simulation. Guide pins 1 and 4 are always completely raised, whereas guide pins 2 and 3 are lowered and raised as shown in Figure 6.7(b). The vessel is floating freely and is affected by waves. The roll amplitudes are illustrated in Figure 6.7(a). The resulting lateral motion of the cable is shown in Figure 6.7(c). The figure illustrates how the cable moves between the guide pins as a function of the roll angle and how it is restriced by the lateral positions of the active guide pins.
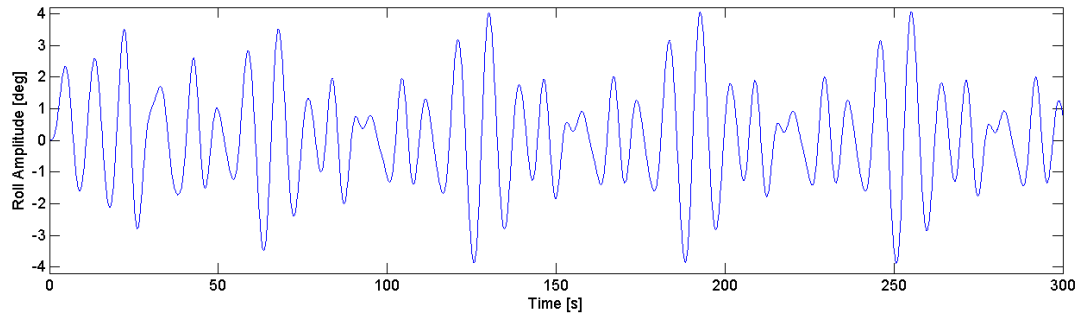
(a) Roll amplitude of the vessel.
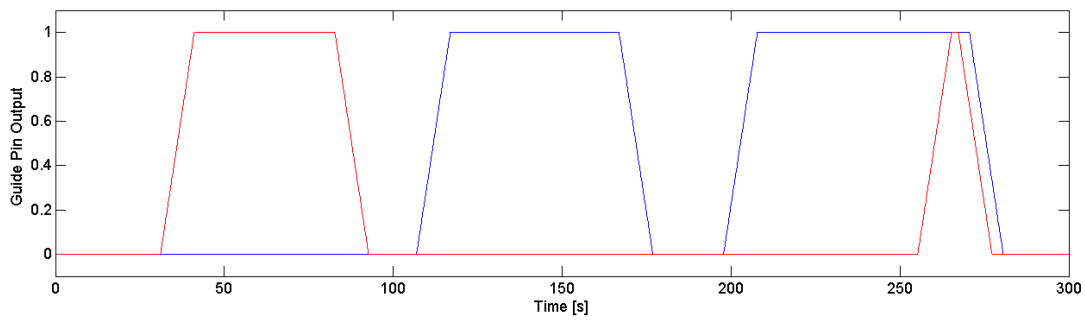
(b) Output g of guide pin 2 (blue) and 3 (red). The output of guidepin 1 and 4 is always 1.
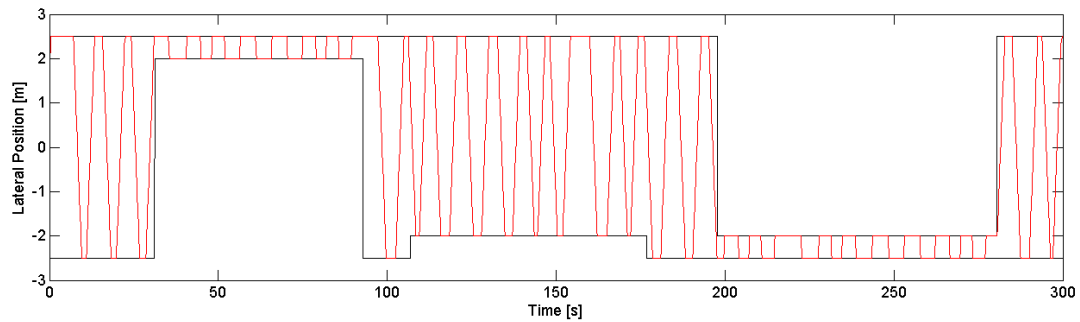
(c) Lateral cable position y_c^b and y-coordinates of the active guide pins (black).

Figure 6.7. Illustration of how the lateral cable movement at the stern of the vessel is restricted by the guide pins and affected by the roll motion of the vessel.

Chapter 7

Ballast and Anti-Roll Tank System

This chapter contains the mathematics used to model ballast and anti-roll tanks on vessels. The subjects are treated separately, and at the end of each subject simulations are performed to show how the vessel is affected by the inclusion of the tanks.

7.1 Ballast Tank System

7.1.1 Ballast Tank Properties

Ballast tanks are manufactured in various shapes and sizes. The volume V_b of a general tank is [15]

$$V_b(h_b) = \int_0^{h_b} A_b(h)dh \tag{7.1}$$

where $A_b(h)$ is the area of the tank at height h. For simplicity, it is assumed that the vessel has n_b rectangular ballast tanks. Figure 7.1 illustrates a ballast tank with area $A_b = l_b b_b$ where l_b is the length and is b_b is the width of the tank. The height of the tank is h_b whereas the height of the water column within the tank is h_w.
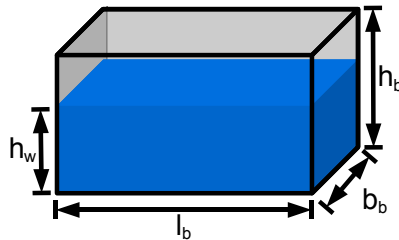

Figure 7.1. Rectangular ballast tank with height h_b [m], width b_b [m], length l_b [m] and water column height h_w [m].

The maximum volume of the tank is

$$V_{b,\max} = A_b h_b \tag{7.2}$$

and the effective volume of the water column

$$V_b = A_b h_w \tag{7.3}$$

The location of each ballast tank is given relative to the vessel's CO in the body-fixed reference frame and to the geometric center of the tank itself. The position vector is defined as

$$\mathbf{r}_b = \begin{bmatrix} x_b & y_b & z_b \end{bmatrix}^\top \tag{7.4}$$

An illustration of four ballast tank and their relative positions is presented in Figure 7.2. Note that the tanks are numbered in sequence starting from forward starboard and following the clock. A similar tank setup will be used later in simulations.
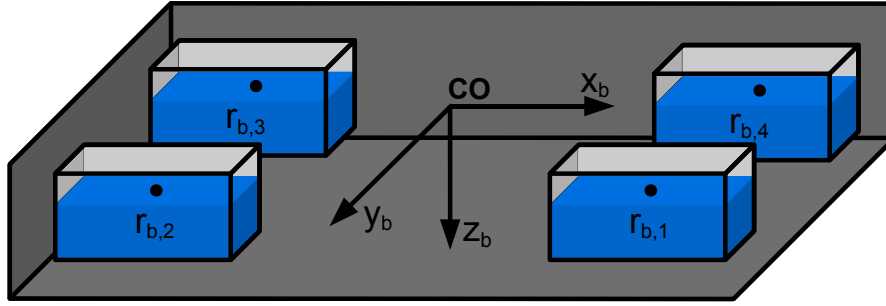

Figure 7.2. Illustration of four ballast tanks and their position relative to the vessel's coordinate origin.

7.1.2   Ballast Forces and Moments

The ballast tanks introduce a ballast vector $\mathbf{g}_0$ in the vessel model. Equation (5.2) then takes the new form

$$\mathbf{M}\dot{\boldsymbol{\nu}} + \mathbf{D}\boldsymbol{\nu}_r + \mathbf{d}(\boldsymbol{\nu}_r) + \mathbf{G}\boldsymbol{\eta} + \mathbf{g}_0 + \boldsymbol{\mu} = \boldsymbol{\tau}_{waves} + \boldsymbol{\tau}_I + \boldsymbol{\tau}_P \tag{7.5}$$

The procedure for finding an expression for $\mathbf{g}_0$ is given in [15] and repeated here for convenience. The gravitational force W_b by a ballast tank in heave is

$$W_b = \rho g V_b \tag{7.6}$$

where ρ is the water density and g is the acceleration of gravity. The cross product of the heave force and the location of the tank is used to calculate the moment vecetor $\mathbf{m}_b = \mathbf{r}_b \times \mathbf{f}_b$, resulting in

$$\mathbf{m}_b = \begin{bmatrix} x_b \\ y_b \\ z_b \end{bmatrix} \times \begin{bmatrix} 0 \\ 0 \\ Z_b \end{bmatrix} = \begin{bmatrix} y_b Z_b \\ -x_b Z_b \\ 0 \end{bmatrix} \tag{7.7}$$

Summing up the gravitational forces and moments for all ballast tanks gives

$$Z_b = \rho g \sum_{i=1}^{n_b} V_{b,i} \tag{7.8}$$

$$K_b = \rho g \sum_{i=1}^{n_b} V_{b,i} y_{b,i} \tag{7.9}$$

$$M_b = -\rho g \sum_{i=1}^{n_b} V_{b,i} x_{b,i} \tag{7.10}$$

where $i \in \{1, ..., n_b\}$, Z_b is the total heave force, K_b the total roll moment and M_b the total pitch moment of the complete ballast tank system. The ballast vector $\mathbf{g}_o$ can then be written as

$$\mathbf{g}_o = \begin{bmatrix} 0 \\ 0 \\ Z_b \\ K_b \\ M_b \\ 0 \end{bmatrix} = \begin{bmatrix} 0 \\ 0 \\ \rho g \sum_{i=1}^{n_b} V_{b,i} \\ \rho g \sum_{i=1}^{n_b} V_{b,i} y_{b,i} \\ -\rho g \sum_{i=1}^{n_b} V_{b,i} x_{b,i} \\ 0 \end{bmatrix} \tag{7.11}$$

7.1.3 Water Pump Dynamics

It is convenient to be capable of controlling the water level in each ballast tank separately. For simplicity, it is assumed that each ballast tank has a separate water pump. The dynamics of a single water pump are [15]

$$\dot{V}_b = p_p$$
$$T_p \dot{p}_p + p_p = \text{sat}(p_d) \tag{7.12}$$

where T_p is the time constant of the pump, p_p is the volumentric flow rate, p_d is the pump set-point and V_b is the tank volume. The pump is also subject to saturation, meaning that the water flow in each direction is limited. This is expressed through the pump set-point p_d as

$$\text{sat}(p_d) = \begin{cases} p_{p,\max}^+ & p_d > p_{p,\max}^+ \\ p_d & p_{p,\max}^- \leq p_d \leq p_{p,\max}^+ \\ p_{p,\max}^- & p_d < p_{p,\max}^- \end{cases} \tag{7.13}$$

where $+$ indicates a positive flow direction and $-$ a negative flow direction. The water level in each ballast tank is controlled by introducing a PID-controller on the form

$$p_d(t) = K_d \dot{h}_w + K_p(h_d - h_w) + K_i \int_0^t (h_d - h_w)dt \tag{7.14}$$

where h_d is the desired water height of the ballast tank and K_p, K_d and K_i are the controller gains. An illustration of relation between a single ballast tank, a water pump and a controller is given in Figure 7.3.
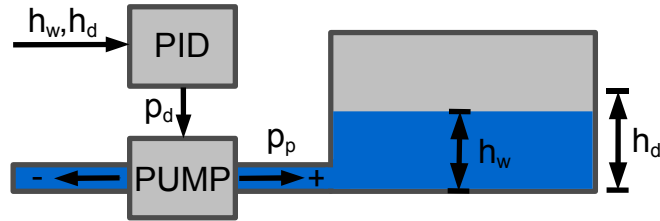

Figure 7.3. Illustration of relations between water pump, ballast tank and PID-controller.

7.1.4 Ballast Tank System Simulations

A simulation is performed using four ballast tanks and a separate water pump for each tank to control the water levels within them. The pump controller gains are $K_p = 25$, $K_p = 100$ and $K_i = 0$ for all of the four water pumps. The parameters of the water pumps and ballast tanks used in the simulation is listed in Table tab:ballast-system-parameters.

Ballast Tanks					Water Pumps			
Tank Number	A_b	x_b	y_b	z_b	Pump Number	T_p	$p_{p,min}$	$p_{p,max}$
1	36	30	5	5	1	7	-2	2
2	36	-30	5	5	2	7	-2	2
3	36	-30	-5	5	3	7	-2	2
4	36	30	-5	5	4	7	-2	2

Table 7.1. Parameters used for ballast tank system simulation.

The results of the simulation are shown in Figures 7.4 and 7.5. Each ballast tank is filled with $h_w = 2.5$ [m] water in a sequential manner starting with tank number 1 and ending with tank number 4. Then the tanks are emptied in the same sequence. It can be observed that vessel's roll motion is most affected by the inclusion of the tanks. The asymmetrical pitch amplitude is due to the filling sequence of the tanks. The heave amplitude does not change remarkably, since the total mass of the ballast tanks is small compared to the total vessel weight.
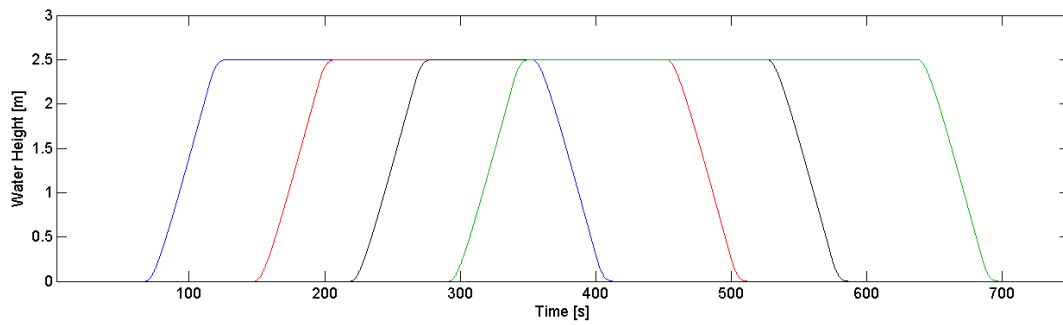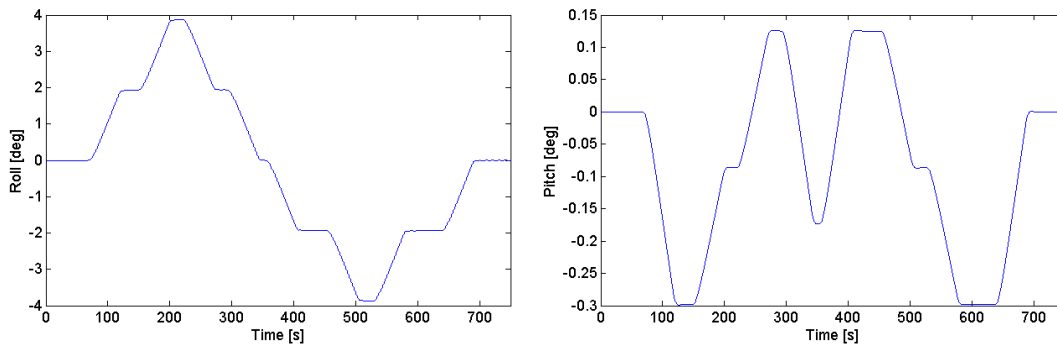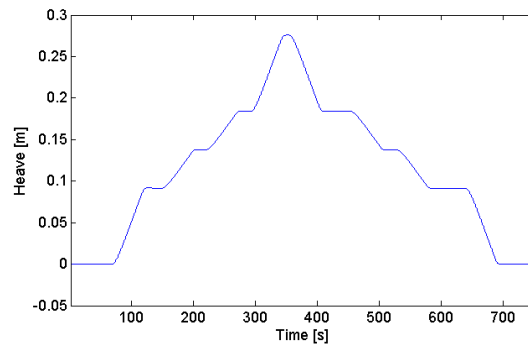
Figure 7.4. Height h_w of water column in ballast tank 1 (blue), 2 (red), 3 (black) and 4 (green).

(a) Vessel roll amplitude [deg].

(b) Vessel pitch amplitude [deg].

(c) Vessel heave [m].

Figure 7.5. Heave, pitch and roll amplitudes for varying water column heights h_w in ballast tanks.

7.2   Anti-Roll System

7.2.1   Roll Reduction Fundamentals

The roll motion of a ship is typically the largest amplitude of all the degrees of freedom [34]. For many ships the natural period in roll coincides with the wave energy spectrum and causes an amplification of the roll amplitude. The most extreme roll motion occurs at resonance, which is known as synchronous rolling [1]. The best way to reduce the amplitude of the roll motion is by increasing the roll damping. This can be achieved by performing hull modifications, installing bilge keels or by the use of anti-roll tanks. These methods are known to be passive solutions to the problem. Active roll damping is obtained by using fin stabilizers or rudder-roll damping systems [13]. No matter which method or combination of methods that is chosen for a particular ship, damping can only reduce the roll motion, never eliminate it.

Anchor handling vessels are known to use anti-roll tanks to obtain roll reduction. The main advantage of using such tanks on AHVs is that the tank performace is independent of the vessel speed. Their performance is in the medium to high range, being able to reduce the roll motion 20-70 %. On the other hand these tanks require much space within the hull and the stability properties of the vessel can be compromized due to a reduction of the metacentric height caused by the free surface effect (FSE) [41].

Anti-roll tanks comes in different types of sizes and shapes. Free-surface tanks and U-tube tanks are the most common, but free-flooding tanks and other variations also exist [34]. In the following, focus is placed on the use of free-surface tanks to reduce the roll motion of AHVs.

Free-surface tanks are uniform cross-sectional tanks that are partially filled with water. Figure 7.6 illustrates such a tank with height h_f, width b_f, length l_f and water column height h_w.
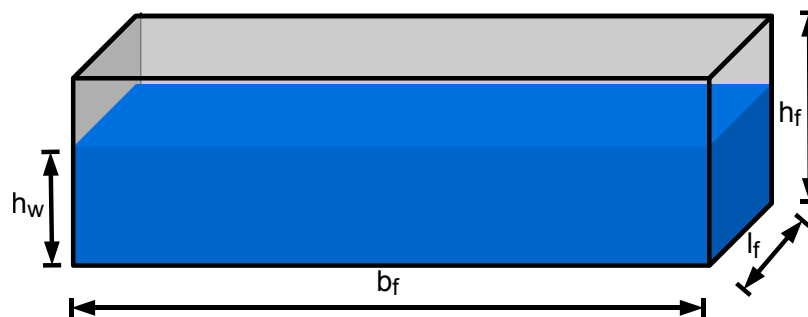

Figure 7.6. Free surface tank with height h_f [m], width b_f [m], length l_f [m] and water column height h_w [m].

The tanks are generally placed above the ship's center of gravity and at right angles to the centerline of the ship. The condition of these tanks are modified by changing the water level h_w within the tank itself. Since the water is running freely, the tank may cause the vessel to become unstable in rough weather. Some control can be achieved by installing restrictions or baffles inside the tanks, but such restrictions are not considered in this thesis. Normally each vessel only contains one free-surface tank, but if the vessel operates with a wide range of metacentric heights, an additional tank can be used [11].

7.2.2 Roll Dynamics

A separate model for the roll motion of the vessel is necessary to explore the roll properties. Extracting the roll components from Equation (5.2) gives the following equation of motion in roll

$$[I_x + A_{44}(\omega_4)]\,\ddot{\phi} + [B_{44}(\omega_4) + B_{44v}(\omega_4)]\,\dot{\phi} + C_{44}\phi = F_4 \tag{7.15}$$

where I_x is the moment of inertia in roll, ω_4 the undamped resonance frequency in roll, $A_{44}(\omega_4)$ the added mass, $B_{44}(\omega_4)$ the linear damping, $B_{44v}(\omega_4)$ the viscous damping and C_{44} the roll restoring moment coefficient. The wave exitation moment F_4 in roll is

$$F_4 = A_4 cos\sigma_4 t \tag{7.16}$$

where σ_4 is the wave encounter frequency and A_4 is the amplitude of the exitation roll moment.

7.2.3 Free Surface Correction

A partially filled ballast or anti-roll tank on a ship is known as a slack tank. The liquids in these tanks reduce the transverse metacentric height $\overline{GM}_T$ of the ship. This reduction of metacentric height is known as the free-surface effect (FSE). The effective metacentric height of the ship, when corrected for slack tanks filled with water is [15]

$$\overline{GM}_{T,eff} = \overline{GM}_T - FSC \tag{7.17}$$

The free-surface correction (FSC) is defined as

$$FSC = \sum_{r=1}^{n_f} \frac{\rho}{m} i_r \tag{7.18}$$

where ρ is the water density, i_r is the moment of inertia of the water surface, m is mass of the vessel and n_f is the number of free surface tanks. Note that the mass of the liquid

or the location of the tank is irrelevant. The moment of inertia of the surface depends on the tank design. For a rectangular tank the moment of inertia of the surface about an axis through the centroid is

$$i_r = \frac{l_f b_f^3}{12} \tag{7.19}$$

The restoring coefficient C_{44} in roll is calculated as

$$C_{44} = \rho g \nabla \overline{GM}_T \tag{7.20}$$

where ∇ is the displacement volume of the vessel. By replacing $\overline{GM}_T$ with $\overline{GM}_{T,eff}$ in (7.20) such that

$$C_{44} = \rho g \nabla \overline{GM}_{T,eff} \tag{7.21}$$

the free surface correction is incorporated into the roll motion of equation (7.15).

7.2.4 Roll Damping

In addition to reducing the transverse metacentric height of the vessel, the anti-roll tank will also contribute to damping of the roll motion. The wave excitation moment F_4 will result in a tank roll moment [11]

$$F_t = K_{ta} sin(\sigma_4 t + \epsilon_t) \tag{7.22}$$

Writing F_t as a function of F_4 yields [11]

$$\begin{aligned}
F_t &= K_{ta} \sin(\sigma_4 t + \epsilon_t) \\
&= K_{ta} \sin(\sigma_4 t) \cos(\epsilon_t) + K_{ta} \cos(\sigma_4 t) \sin(\epsilon_t) \\
&= \frac{K_{ta}}{A_4} cos(\epsilon_t) \phi + \frac{K_{ta}}{\sigma_4 A_4} sin(\epsilon_t) \dot{\phi}
\end{aligned} \tag{7.23}$$

Adding (7.23) to the right hand side of (7.15) results in the following equation of motion with anti-roll tanks included

$$A\ddot{\phi} + B\dot{\phi} + C\phi = F_4 \tag{7.24}$$

where

$$A = [I_x + A_{44}(\omega_4)] \tag{7.25}$$

$$B = \left[B_{44}(\omega_4) + B_{44v}(\omega_4) - \frac{K_{ta}}{\sigma_w A_4} sin(\epsilon_t) \right] \tag{7.26}$$

$$C = \left[C_{44} + C_t - \frac{K_{ta}}{A_4} cos(\epsilon_t) \right] \tag{7.27}$$

Note that the damping contribution from the free-surface tank is given by

$$B_t = -\frac{K_{ta}}{\sigma_w A_4} sin(\epsilon_t) \tag{7.28}$$

7.2.5 Free-Surface Tank Tuning Procedure

A free-surface tank will normally have a free-surface correction ratio of

$$R_{FSC} = \frac{FSC}{\overline{GM}_T} \tag{7.29}$$

between 0.15 and 0.30 [11]. This fact can be used to design the desired free-surface correction as

$$FSC = \overline{GM}_T R_{FSC} \tag{7.30}$$

The width of the tank should extend over the most part of the vessel breadth and b_f is therefor a design parameter. The length of the tank can then be found as

$$l_f = \frac{12m}{\rho b_f^3} FSC \tag{7.31}$$

and the desired water height in the tank as [11]

$$h_w = \left(\frac{b_f}{\pi}\right)^2 \frac{\rho \nabla}{I_x + A_{44}} GM_T \tag{7.32}$$

This follows from assuming that the natural frequency in roll is equal to the lowest natural sloshing frequency $\sigma_w = \omega_4$. The relative damping coefficient of the equation of motion in roll (7.15) is

$$\zeta_4 = \frac{1}{2\omega_4} \frac{B_{44}(\omega_4) + B_{44}(\omega_4 v) + B_t}{I_x + A_{44}(\omega_4)} \tag{7.33}$$

A roll amplitude reduction of $40-60\,\%$ at the roll resonance frequency ω_4 can be obtained by tuning B_t such that ζ_4 is within the interval 0.4 - 0.6. The damping contribution from B_{44} is approximately 0.05 - 0.10. K_{ta} and ϵ_t are normally found experimentally by doing forced harmonic oscillation tests of the tank [11]. However, by choosing $\epsilon_t = -90$ [deg] then

$$\frac{K_{ta}}{A_4} cos(\epsilon_t) = 0 \tag{7.34}$$

in Equation (7.27) and

$$\frac{K_{ta}}{\sigma_w A_4} sin(\epsilon_t) = \frac{K_{ta}}{\sigma_w A_4} \tag{7.35}$$

in Equation (7.26). The relation K_{ta}/A_4 is then selected to give the desired value of the relative damping coefficient ζ_4.

7.2.6   Anti-Roll System Simulations

The vessel is simulated together with one anti-roll tank of dimensions $l_f = 6.28$ [m], $b_f = 17.2$ [m] and $h_w = 1.02$ [m] resulting in a free surface correction of $FSC = 0.4288$. A Torsethaugen wave spectrum, included in the MSS Toolbox, with significant wave heights $H_s = 4$ and 6 [m] is utilized. The other wave spectrum parameters is listed in Appendix C.2.

The results of the simulations are shown in Figure 7.7. It can be observed that an increase of the relative damping coefficient effectively reduces the roll amplitude, whereas the roll period remains almost unchanged. A reduction of the metacentric height will normally result in a larger roll period, but for vessels of large dimensions a significant change in the metacentric height is required to change the roll period substantially.
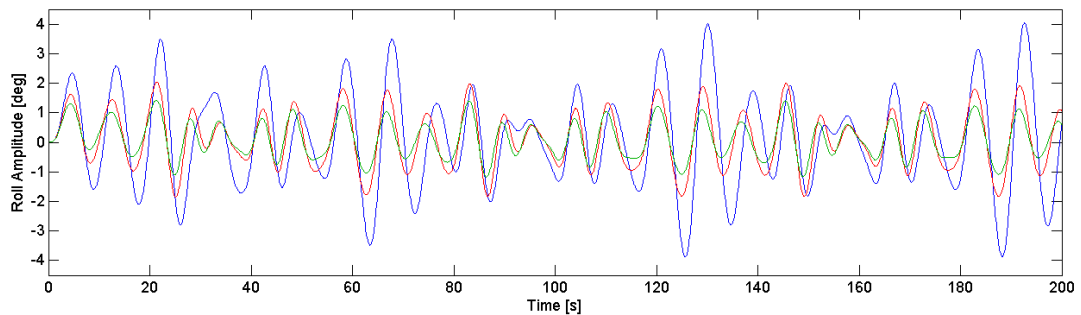
(a) Roll amplitude for significant wave height $H_s = 4$ [m]
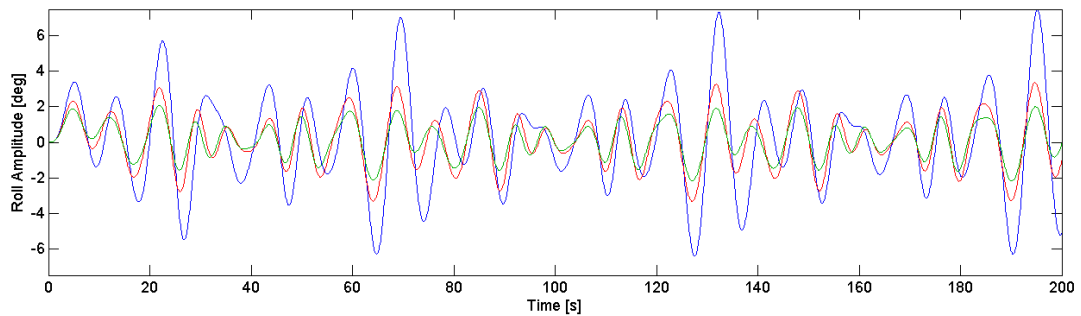
(b) Roll amplitude for significant wave height $H_s = 6$ [m]

Figure 7.7. Comparison of roll characteristics with $\zeta_4 = 0.2374$ (red),$\zeta_4 = 0.4976$ (green) and no anti-roll tank (blue) for different significant wave heights.

Chapter 8

Simulations and Results

Time-domain simulations of the complete anchor handling vessel simulator are presented in this chapter. Anchor handling operations normally last for many hours and presenting results for such time aspects is not suitable within a report. A set of case studies has therefore been designed, allowing specific situations and scenarios that occurs during anchor handling operations to be evaluated and discussed. The case studies have two main purposes: to verify the simulator itself and to gain insight into the vessel performance during anchor handling operations. The results of each case study are briefly commented in this chapter and discussed further in Chapter 9.

8.1 Anchor Handling Vessel Simulator

8.1.1 Simulator Implementation

A conceptual block diagram of the anchor handling vessel simulator is presented in Figure 8.1, resembling the final Simulink model used to perform the simulations. None of the actual Simulink diagrams are provided in the report due to their size. They are however available in a digital format as described in Appendix D. Further descriptions of the most important simulator modules in Figure 8.1 are presented in Appendix B, together with a description of the preprocessing of cable data. Appendix C.5 contains a list of all parameters values used in the case study simulations.

8.1.2 DP Controller and Wave Filtering

A nonlinear PID DP controller from the MSS-library [24] is used for set-point regulation in surge, sway and yaw. The desired heading and position of the vessel is set in the manual control module. A passive DP wave filter from the MSS-library is [24] is used to filter out the 1st-order wave induced disturbances from the measurements of the vessel
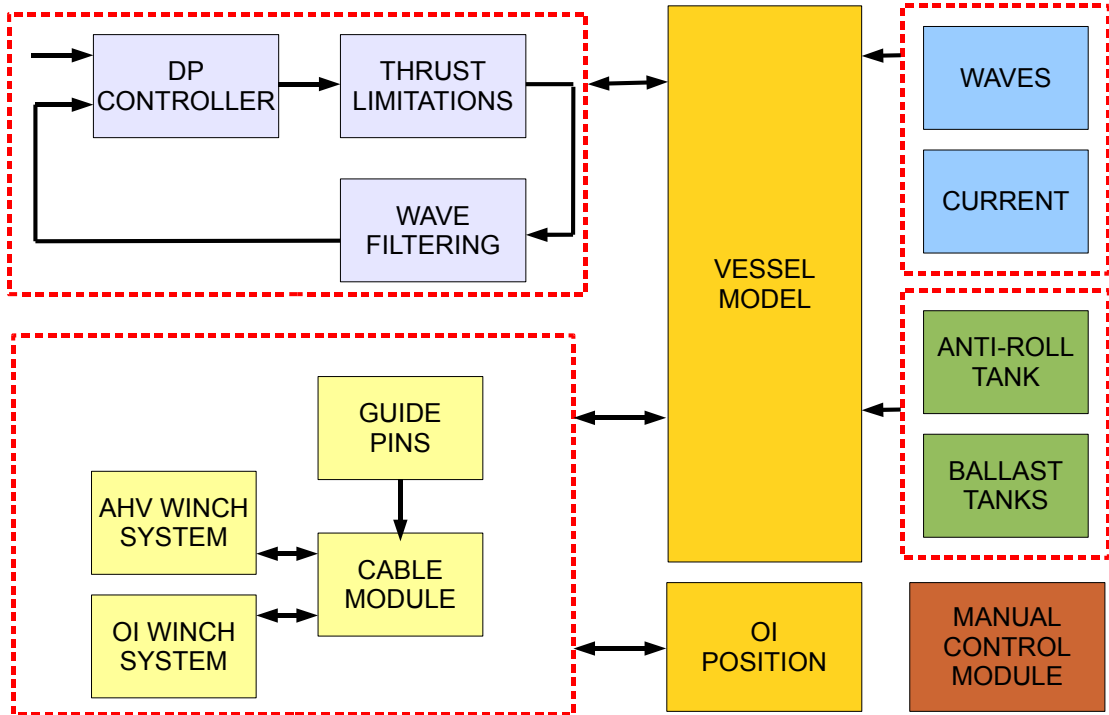
Figure 8.1. Conceptual block diagram of the anchor handling vessel simulator used for simulations.

states. The wave filter is a 3 DOF model-based observer which separates the position and heading measurements in a low frequency and wave-frequency position and heading part [13]. Only the slowly-varying disturbances in $\boldsymbol{\eta}$ and $\boldsymbol{\nu}$ are counteracted by the PID-controller to avoid wear and tear of the propulsion units. The wave-filter parameters are listed in Appendix C.3 and the parameters of the DP controller are listed in Appendix C.4.

8.1.3   Current and Waves

A Torsethaugen wave spectrum is used to simulate the effect of wave forces on the vessel. The wave module is included in the MSS-library [24]. The parameter values used in the simulations are listed in Appendix C.2.

A two-dimensional irrotational current model included in the MSS-library is used to simulate the effect of current forces on the vessel. A brief description of the current model is given in Appendix A.1. All case studies that include the current effect use a sideslip angle value of $\beta_c = 135$ [deg] and current velocity $V_c = 0.4$ [m/s].

8.2 Case Studies

8.2.1 Anchor Deployment in Ideal Conditions

Case Study 1 Purpose

The purpose of this case study is to evaluate the vessel performance during anchor deployment in ideal weather conditions.

Simulation Outline

No waves or current are present, and the ballast and anti-roll tanks are not used. The starboard guide pin pair is used to restrict the cable at the stern of the vessel

The AHV is initially located 1550 [m] west of the OI. 2100 [m] of mooring chain is already deployed. The goal of the operation is to land the anchor approximately 2200 [m] west of the OI at a seabed depth of 700 [m]. To achieve this the AHV must maneuver itself to its target position 3250 [m] west of the OI and deploy about 1200 [m] of work wire. The mooring chain length must at the same time be increased to 2450 [m].

First the OI deploys all its mooring chain until the desired length is reached. The anchor is launched from the AHV when a position 1650 [m] west of the OI is reached. The AHV then starts to pay out work-wire. The deployment speed is adjusted according to the vessel position. After the anchor reaches its target and lands on the seabed the AHV continues to pay out work-wire until the cable force is sufficiently low for the vessel to maneuver freely, which marks the end of the simulation.

Comments on Results

The results of the simulation are presented in Figures 8.2-8.5. The movement and heading of the AHV and the corresponding cable profiles are shown in Figure 8.2. The AHV was able to reach its target position and maintain its desired heading. Note that Figure 8.2(b) shows that at some points during the simulations a part of the mooring chain is below the seabed indicated by the blue line. This is a consequence of the fact that the cable equations does not take seabed interactions into account. Only the vertical anchor position is used to determine when the anchor lands on the seabed. Figure 8.3 illustrates how the vertical and horizontal catenary forces develops as a function of the mooring chain length, work wire length and cable span. The catenary forces reaches their highest values just before the anchor touchdown, and a sudden decrease is then observed. Figure 8.5 compares the end point cable forces acting on the vessel in surge, sway and yaw to the corresponding thrust forces of the vessel. The DP controller is able to counteract the effect of the external cable forces. Note that required surge force tends towards the maximum available thrust force in surge, see Table 5.2. The maximum roll and pitch amplitudes are approximately 1.5 and 0.5 [deg]. Both the roll, pitch and heave amplitudes increase with increasing cable forces, as illustrated in Figure 8.4.
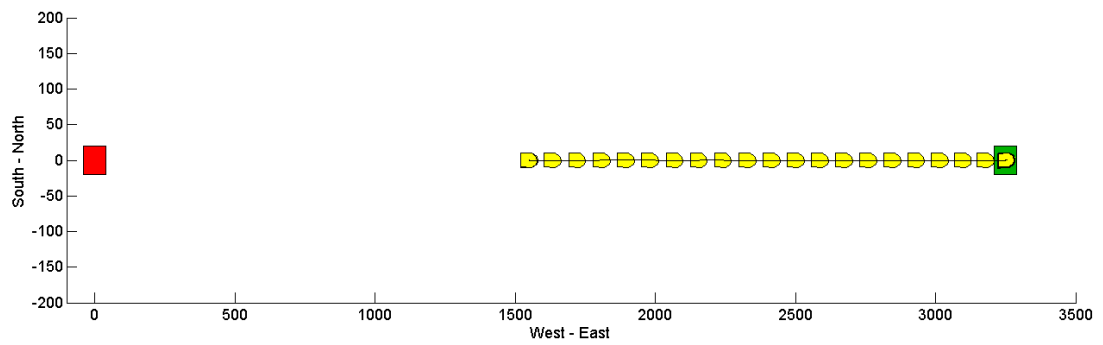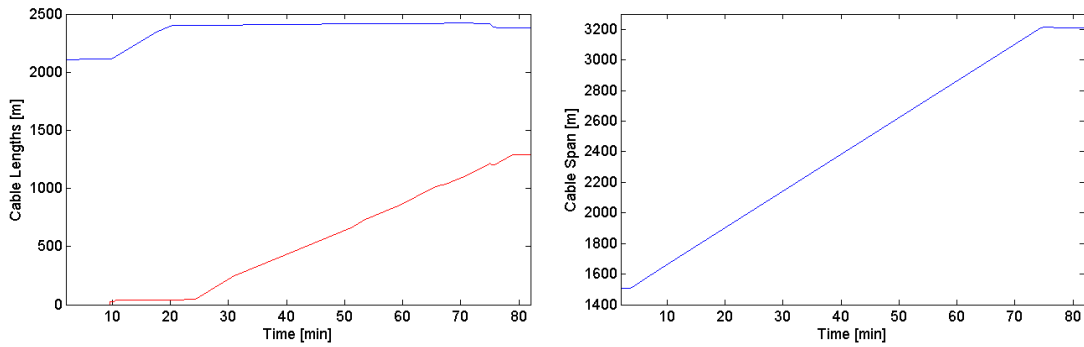
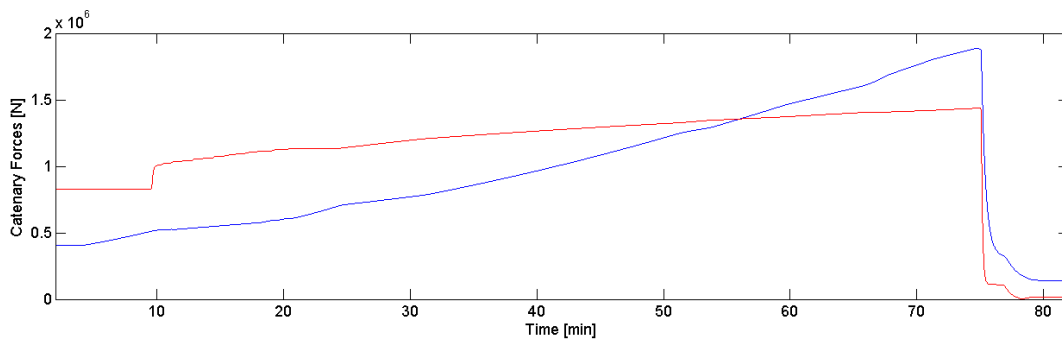(a) AHV (yellow), AHV target (green) and OI (red).
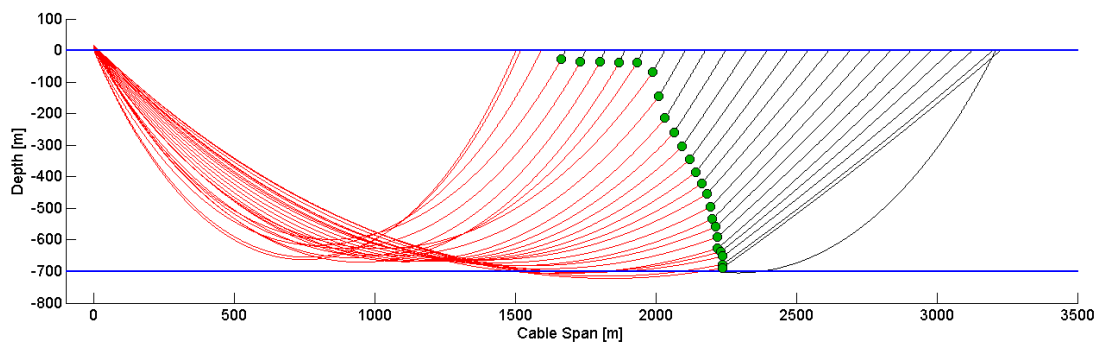
(b) Mooring chain (red), work wire (black), anchor (green) and surface and seabed (blue)

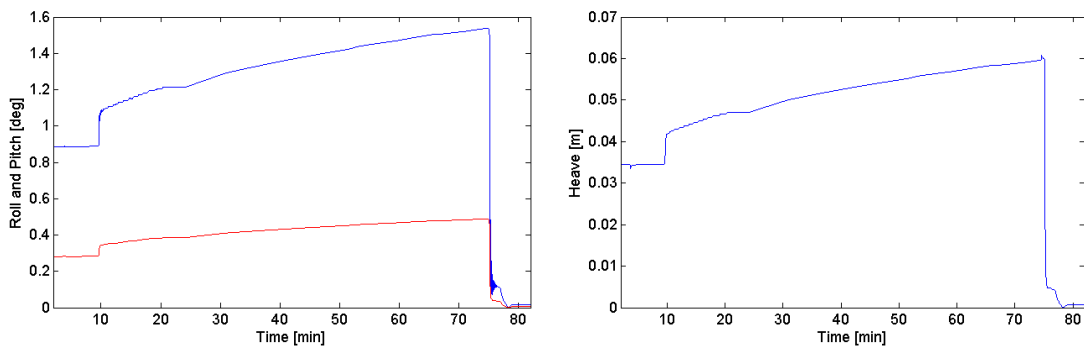Figure 8.2. Illustration of vessel movement and cable profiles.

(a) Work wire (red) and mooring chain length (blue).

(b) Cable span.

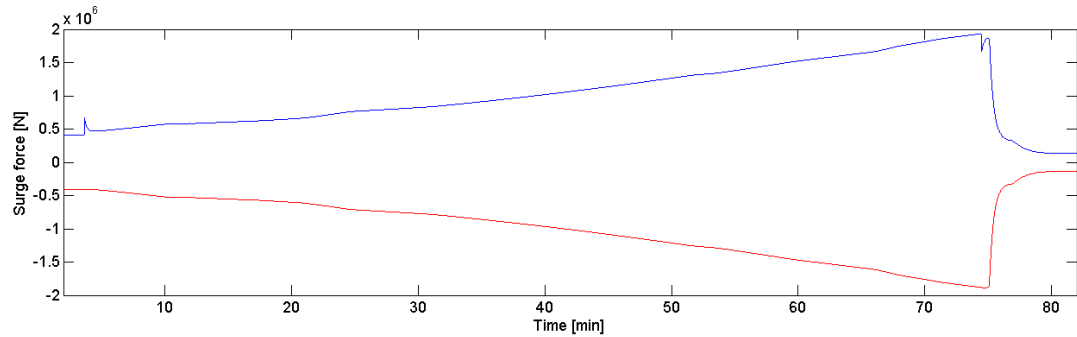(c) Vertical (red) and horizontal (blue) catenary forces.

Figure 8.3. Illustration of catenary forces as a function of cable span, work wire length and mooring chain length.
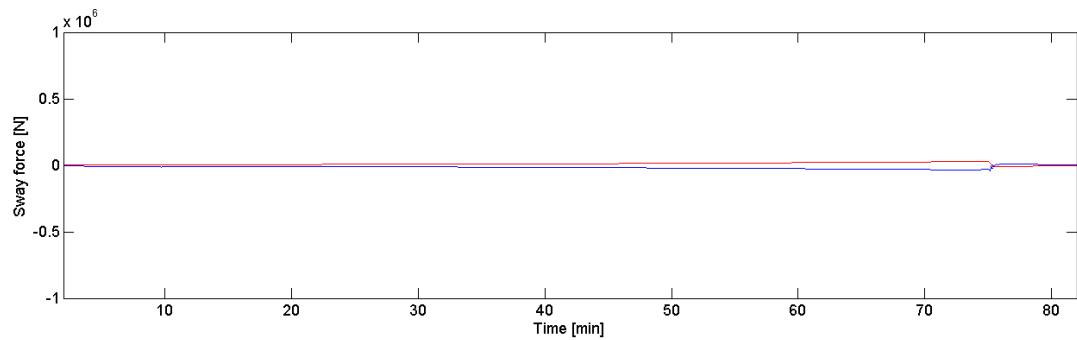

(a) Roll (blue) and pitch (red) amplitudes.
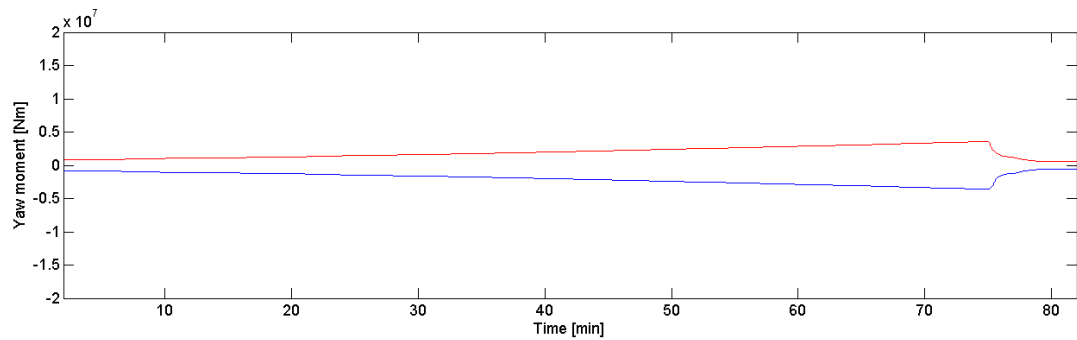

(b) Heave amplitude.

Figure 8.4. Roll, pitch and heave amplitudes for the vessel.

(a) Vessel thrust force (blue) and end-point cable force (red) in surge.

(b) Vessel thrust force (blue) and end-point cable force (red) in sway.

(c) Vessel thrust moment (blue) and end-point cable moment (red) in yaw.

Figure 8.5. Comparison of end point cable and vessel thrust forces and moment in surge, sway and yaw.

8.2.2   Anchor Deployment in Rough Weather Conditions

Case Study 2 Purpose

The purpose of this case study is to evaluate the vessel performance during anchor deployment in rough weather conditions with proper use of guide pins, ballast tanks and the anti-roll tank.

Simulation Outline

The simulation outline from Case Study 1 is repeated, but waves and currents are also present. Both the anti-roll tank and ballast tanks are used. The starboard guide pin pair is used to restrict the cable motion at the stern of the vessel.

Initially ballast tanks 1, 3 and 4 are filled with respectively 3.4, 2.4 and 2.4 [m] of water to counteract the maximum roll and pitch angles experienced in Case Study 1. After the anchor has landed on the seabed, they are emptied.

Comments on Results

The results of the simulation are presented in Figures 8.6-8.8. The movement and heading of the AHV and the corresponding cable profiles are shown in Figure 8.6. The AHV was able to reach its target position and maintain its desired heading. The anchor was successfully deployed at the desired location. Note that the path of the vessel deviates a little bit from the ideal path, and the heading has a small deviation. This is due to the effect of the current and waves.

Figure 8.3 illustrates how the vertical and horizontal catenary forces develops as a function of the mooring chain length, work wire length and cable span. The catenary forces reaches their highest values just before the anchor touchdown, and a sudden decrease is then observed. In Figure 8.8 it can be observed that the AHV must use maximum force in surge just before anchor touchdown. Also note the AHV uses approximately 75 % of the available power in sway to counteract the effect of the current. The force required to maintain the heading is small due to the small relative cable angle and the mean directions of the waves and current.

In Figure 8.9 it can be observed that the vessel is subject to large heave amplitudes. The roll and pitch amplitudes are within acceptable limits. Note that the roll has an initial offset of about 1 [deg]. When the ballast tanks are filled, the offset changes to approximately -0.6 [deg]. The offset then decreases as the cable forces increase. Finally, a sudden change in the roll offset is observed as the anchor lands on the seabed and the cable forces decrease. The offset is corrected by emptying all ballast tanks at the end of the simulation.
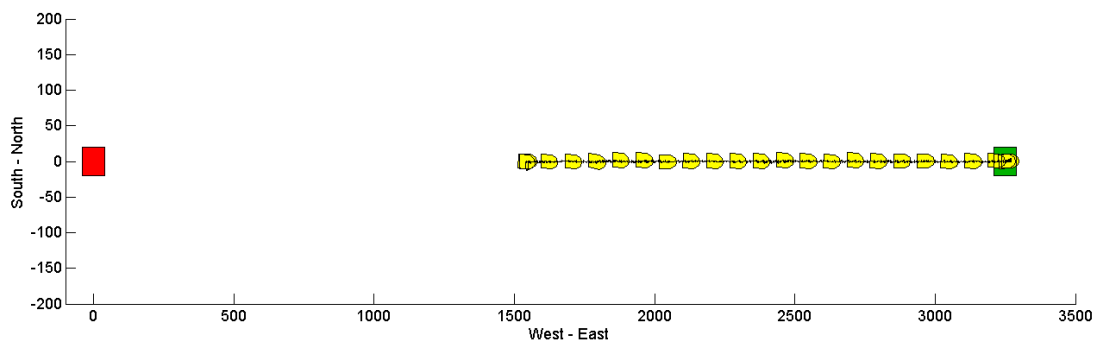
(a) AHV (yellow), AHV target (green) and OI (red).
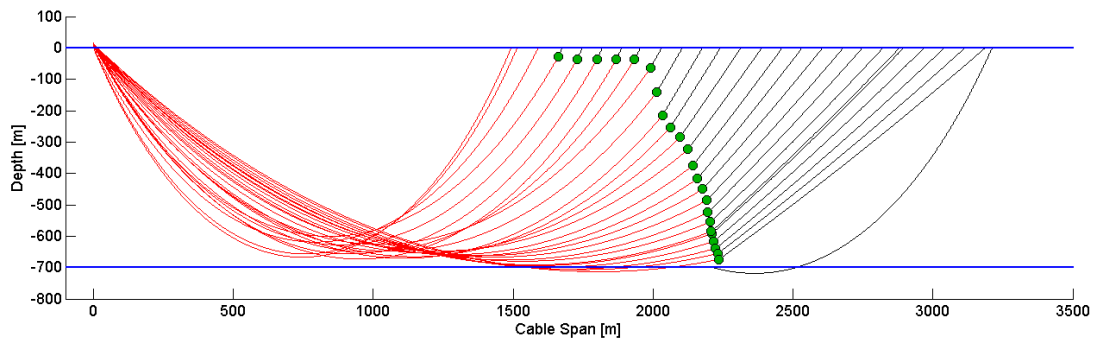
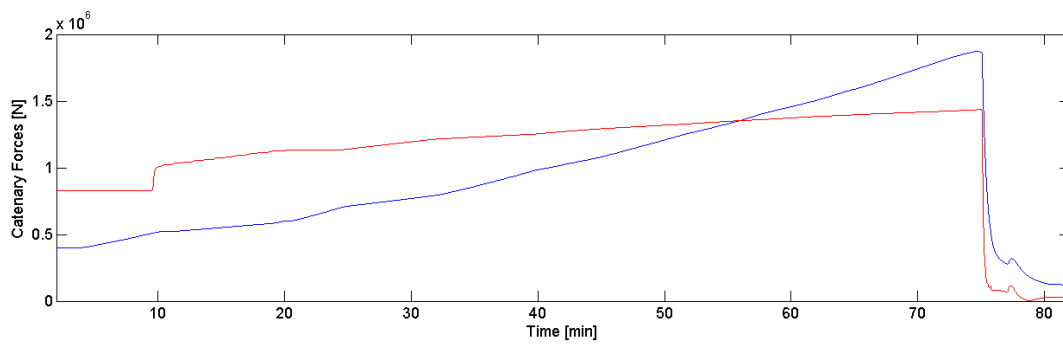(b) Mooring chain (red), work wire (black), anchor (green) and surface and seabed (blue).

Figure 8.6. Illustration of vessel movement and cable profiles.
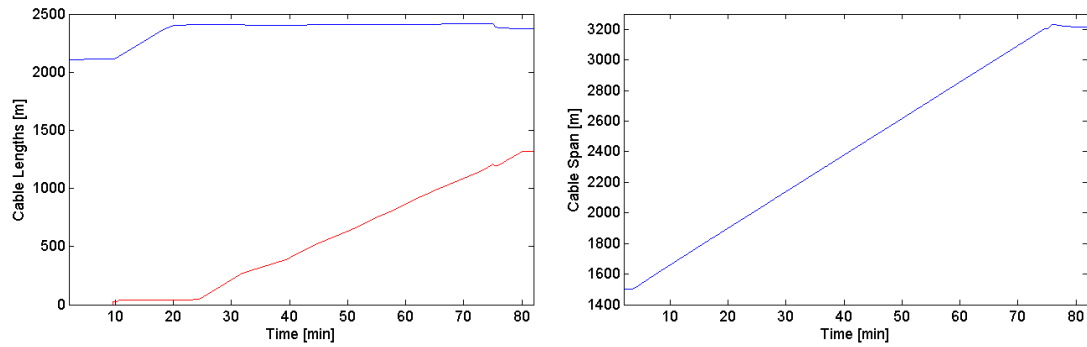
(a) Work wire (red) and mooring chain length (blue).

(b) Cable span.

(c) Vertical (red) and horizontal (blue) catenary forces.

Figure 8.7. Illustration of catenary forces as a function of cable span, work wire length and mooring chain length.
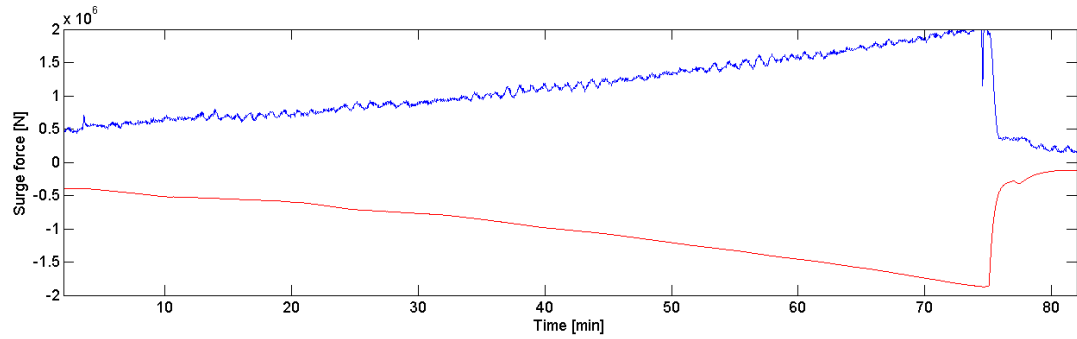
(a) Vessel thrust force (blue) and end-point cable force (red) in surge.
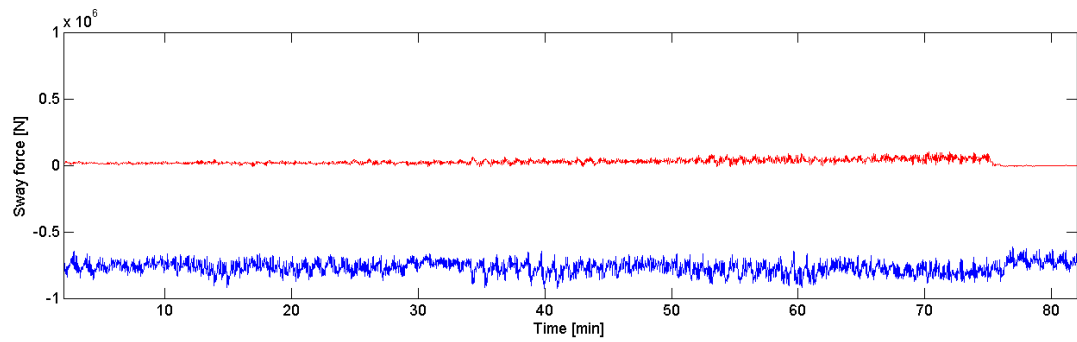
(b) Vessel thrust force (blue) and end-point cable force (red) in sway.
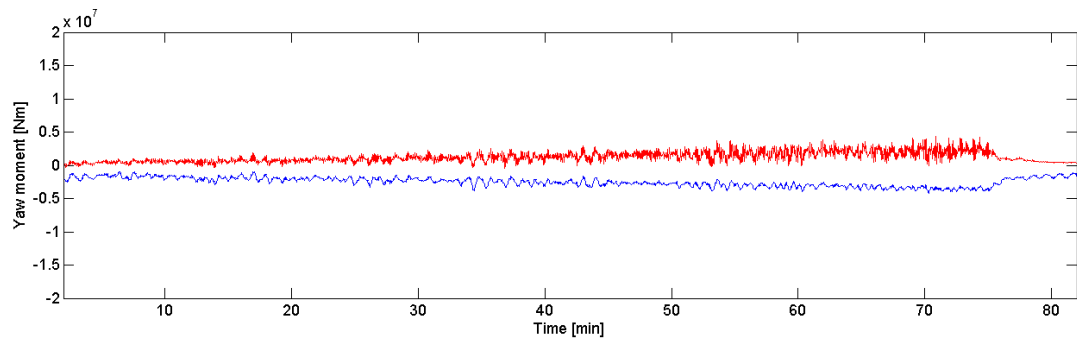
(c) Vessel thrust moment (blue) and end-point cable moment (red) in yaw.

Figure 8.8. Comparison of end point cable and vessel thrust forces and moment in surge, sway and yaw.
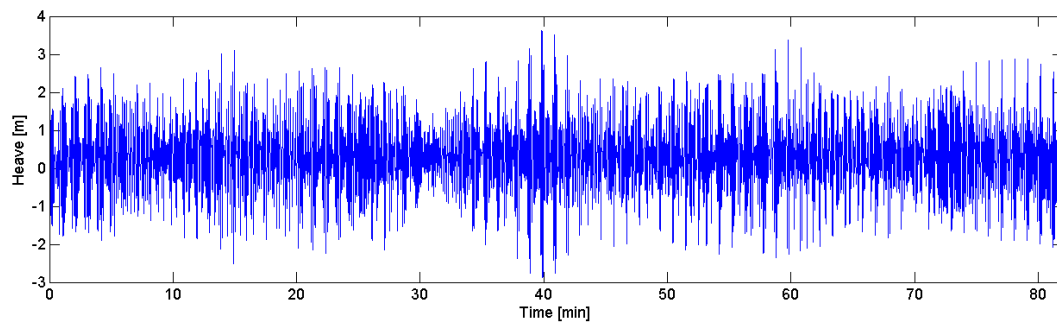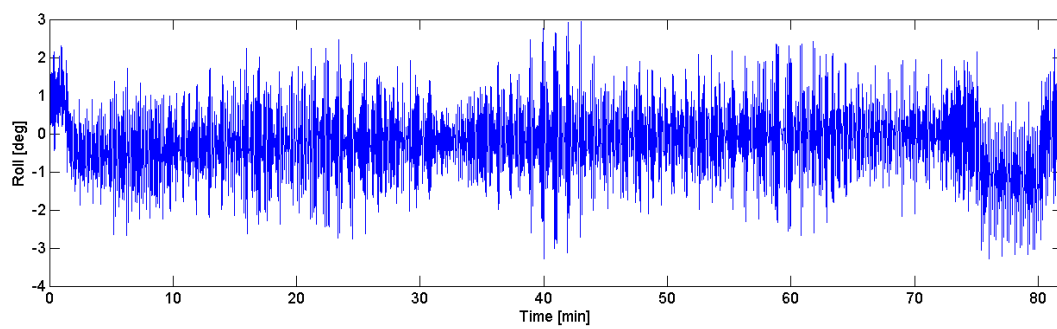
(a) Heave amplitude.
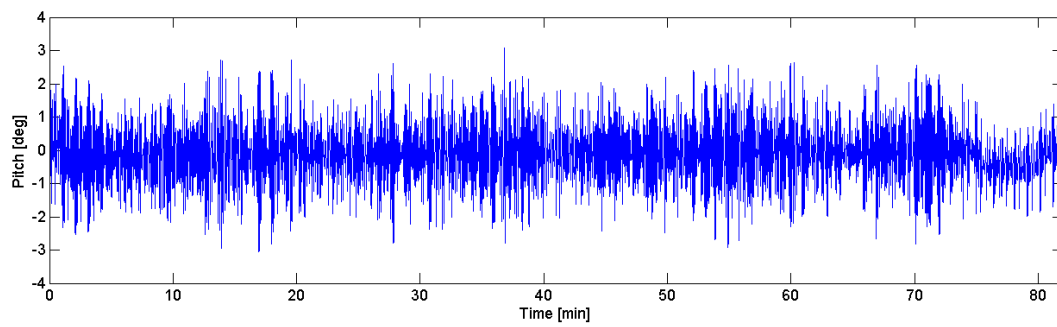
(b) Roll amplitude.

(c) Pitch amplitude.

Figure 8.9. Roll, pitch and heave amplitudes for the vessel.

8.2.3   Anchor Deployment in Rough Weather with System Failures

Case Study 3 Purpose

The purpose of this case study is to evaluate the vessel performance during anchor deployment in rough weather conditions with system and equipment failures on the vessel.

Simulation Outline

The simulation outline from Case Study 1 is repeated, but waves and currents are also present. The ballast tanks are used, but not the anti-roll tank.

Initially ballast tanks 1, 3 and 4 are filled with respectively 3.4, 2.4 and 2.4 [m] of water to counteract the maximum roll and pitch angles experienced in Case Study 1. However, instead of using the starboard guide pin pair as in Case Study 2, the port side guide pin pair is used to illustrate the effect of wrong guide pin and ballast tank configuration.

As the AHV reaches a position 2200 [m] west of the OI, a 50 % loss of thrust force in sway and yaw comes into effect, meant to illustrate reduced thrust power due to engine related failures on the vessel. The inner port guide pin will also break at some time during the simulation.

Comments on Results

The results of the simulation are presented in Figures 8.10-8.12. The movement and heading of the AHV and the corresponding cable profiles are shown in Figure 8.6. It can be observed that the AHV not was able to reach its target position and deploy the anchor. When the AHV is positioned approximately 2200 [m] west of the OI, the thruster failure in sway and yaw comes into effect. The available thrust force in sway is then less than the required force to counteract the effect of the current. This is illustrated in Figure 8.12, where it can be seen that the thrust in sway immediately saturates. As a result of this, the vessel starts to drift off its original path.

The inner port side guide pin breaks approximately 45 [min] into the simulation, causing the cable to move freely between the outer port and outer starboard guide pins. The end point cable forces acting on the vessel in surge, sway and yaw will therefore oscillate as the roll amplitude of the vessel varies. This is illustrated in Figure 8.12.

The vessel has drifted approximately 150 [m] off the desired path 53 [min] into the simulation. At this point the heading reference is changed from 90 to 60 [deg] in order to try and reach the target position. It can be observed in Figure 8.12 that this causes the thrust forces in surge, sway and yaw to saturate immediately. The vessel is not able to maneuver freely and reach the target. The simulation was therefore stopped.

In Figure 8.9 it can be observed that the vessel is subject to large heave amplitudes. The pitch amplitude is within acceptable limits. Note that the roll has an initial offset of about 1 [deg]. When the ballast tanks are filled and the cable is secured by the port side guide pin pair, the AHV develops an roll offset of about −3 [deg]. This is illustrated

in Figure 8.13. The relative large offset is due to the wrong ballast tank and guide pin combination. Both systems forces the vessel to roll towards port. Also note that the maximum and minimum roll amplitudes are respectively 7.5 and 13.5 [deg]. The large roll amplitudes are a a direct result of an empty anti-roll tank.
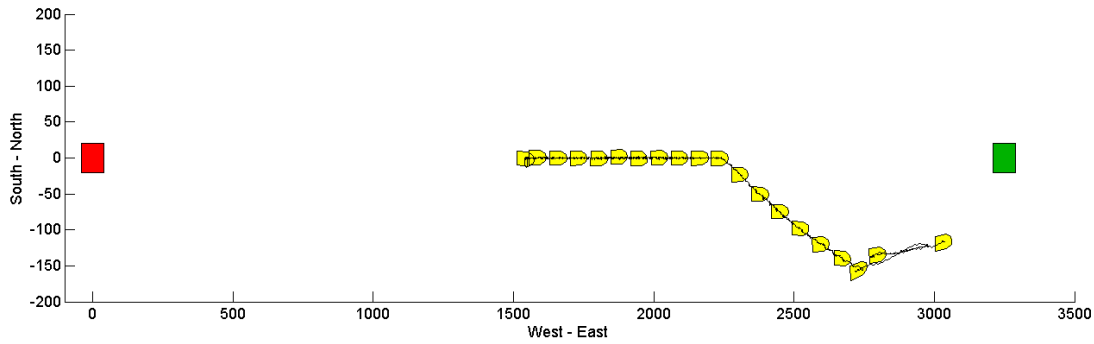
(a) AHV (yellow), AHV target (green) and OI (red).
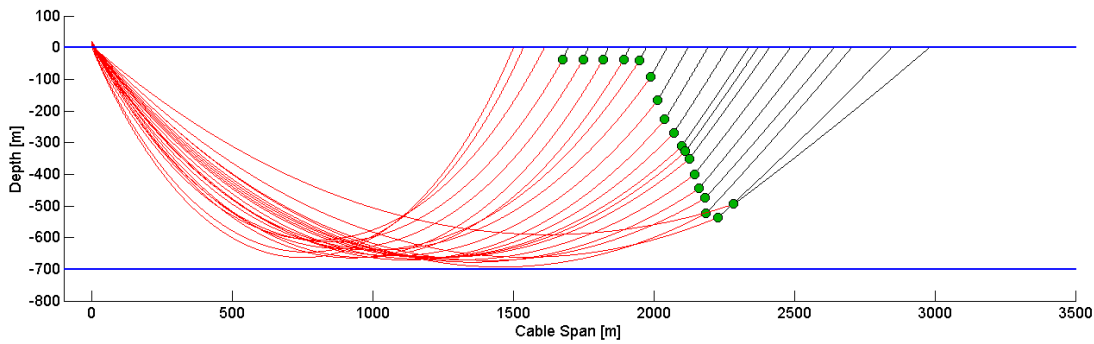
(b) Mooring chain (red), work wire (black), anchor (green) and surface and seabed (blue).

Figure 8.10. Illustration of vessel movement and cable profiles.
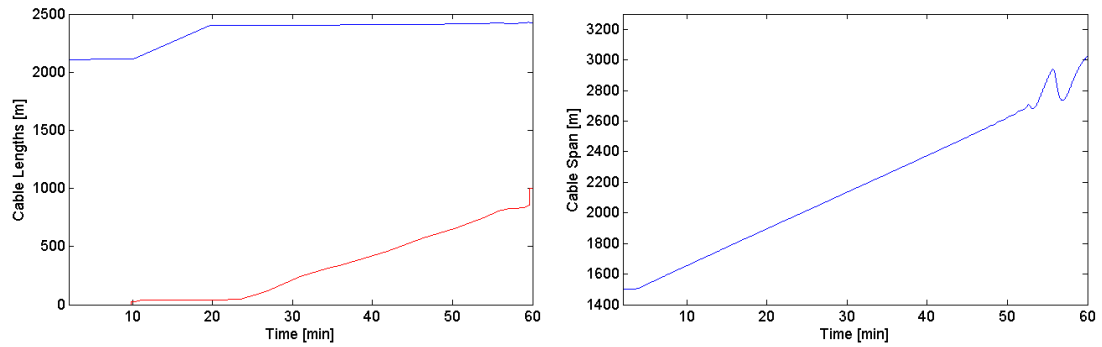
(a) Work wire (red) and mooring chain length (blue).
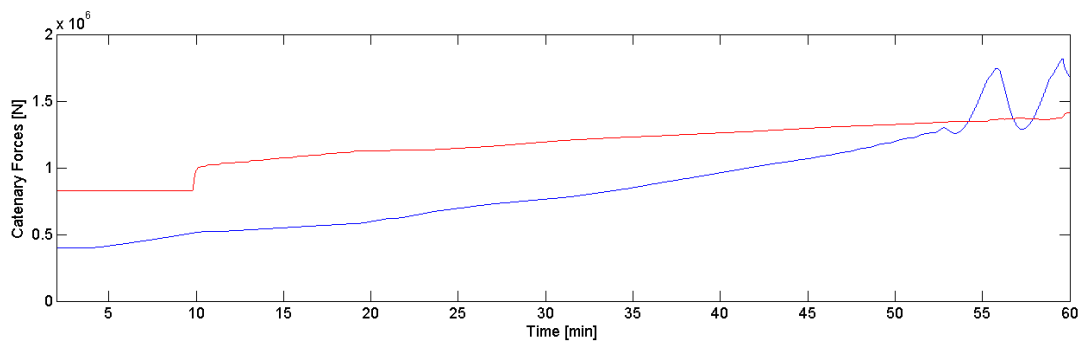
(b) Cable span.

(c) Vertical (red) and horizontal (blue) catenary force.

Figure 8.11. Illustration of catenary forces as a function of cable span, work wire length and mooring chain length.
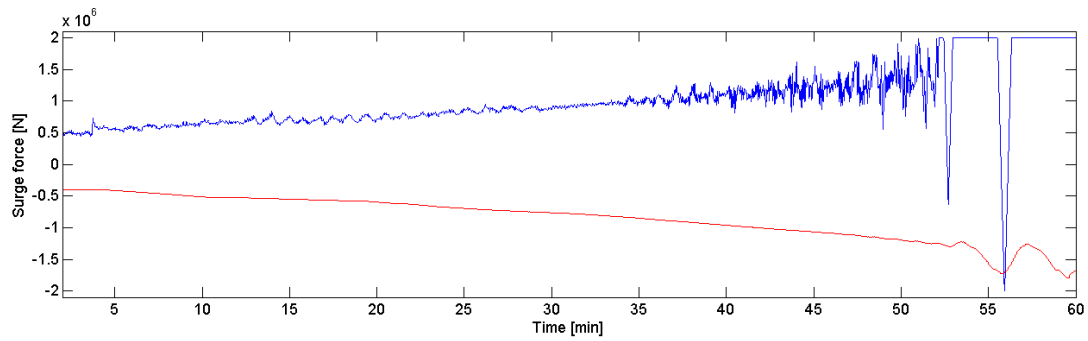
(a) Vessel thrust force (blue) and end-point cable force (red) in surge.
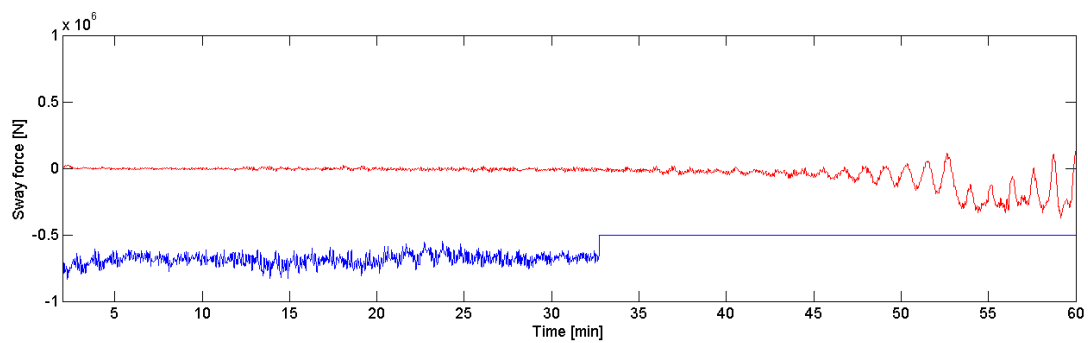
(b) Vessel thrust force (blue) and end-point cable force (red) in sway.
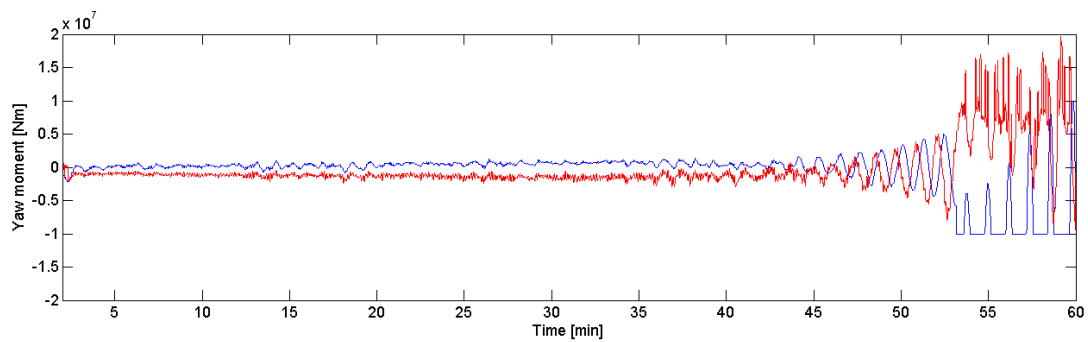
(c) Vessel thrust moment (blue) and end-point cable moment (red) in yaw.

Figure 8.12. Comparison of end point cable and vessel thrust forces and moment in surge, sway and yaw.
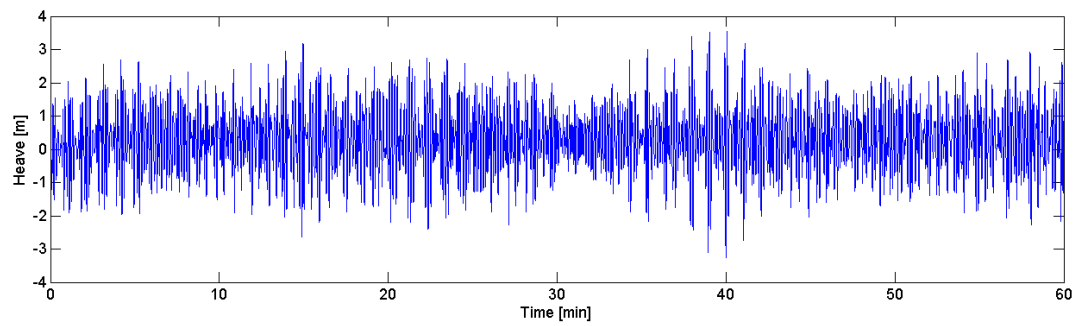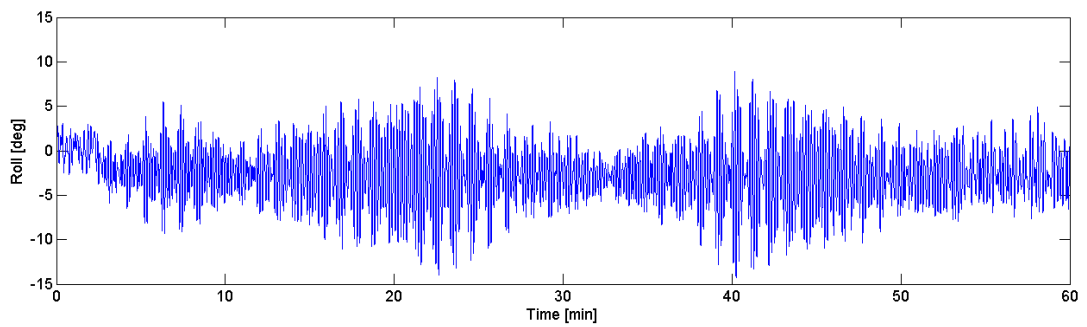
(a) Heave amplitude.
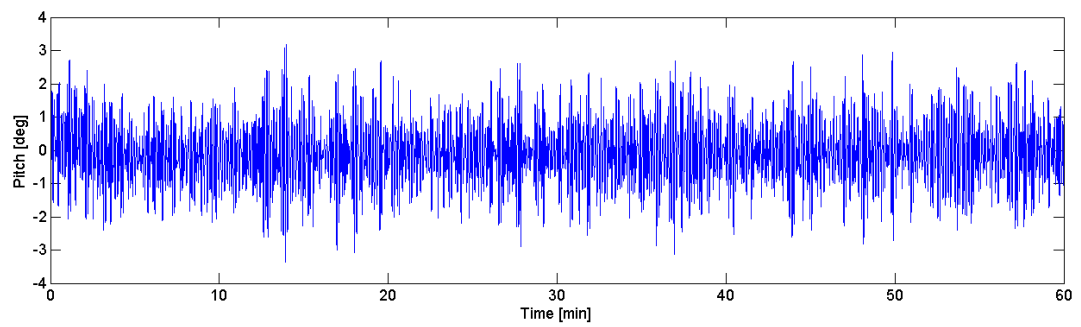
(b) Roll amplitude.

(c) Pitch amplitude

Figure 8.13. Roll, pitch and heave amplitudes for the vessel.

8.2.4 Anchor Retrieval in Ideal Weather Conditions

Case Study 4 Purpose

The purpose of this case study is to evaluate the anchor and seabed friction interaction during anchor recovery in ideal weather conditions.

Simulation Outline

No waves or current are present, and the ballast and anti-roll tanks are not used. The starboard guide pin pair is used to restrict the cable at the stern of the vessel

The anchor is located 2200 [m] west of the OI and 4 [m] under the seabed. The seabed depth is 700 [m]. The AHV is initially located 2600 [m] west of the OI with 840 [m] of work wire deployed and connected to the mooring chain near the anchor. The goal of the operation is to break the anchor out of the seabed. This requires that the AHV posititions itself at the target posisition 3400 [m] west of the OI, while at the same time deploying work wire to keep sufficient cable slack. When the target position is reached, the AHV reduces the work wire length in order to increase the cable tension. The simulation ends when the anchor is broken out of the seabed.

Comments on Results

The results of the simulation are presented in Figures 8.14-8.19. The movement and heading of the AHV and the corresponding cable profiles are shown in Figure 8.6.

Figure 8.15 illustrates how the vertical and horizontal catenary forces develops as a function of the work wire length and the cable span. The catenary forces increase slowly as the AHV moves towards the target position, since the work wire is kept sufficiently long to avoid large forces in the positioning phase. When the AHV has reached the target position, the length of the work wire is reduced, causing an rapid increase in the catenary forces. The forces are constant until the anchor is broken out and the length of the work wire is increased to allow the vessel to maneuver freely. The resulting roll, pitch and heave amplitudes, illustrated in Figure 8.16, are small.

Figure 8.17 shows how the cable tension and the friction force develop during the anchor breakout. Both have the same behaviour as the catenary forces, but with different magnitudes. The velocity of the anchor is shown as a function of the friction force in Figure 8.19. The anchor starts to move when the cable tension exceeds 600 [kN], and the resulting velocity and force profile is linear. The linear relationship is due to the simplifications that were discussed in Section 4.3. Finally the anchor velocity and position are illustrated in Figure 8.18 as a function of time. A constant anchor velocity just above 0.3 [m/min] is observed, and it takes about 13 minutes to break the anchor out of the seabed.
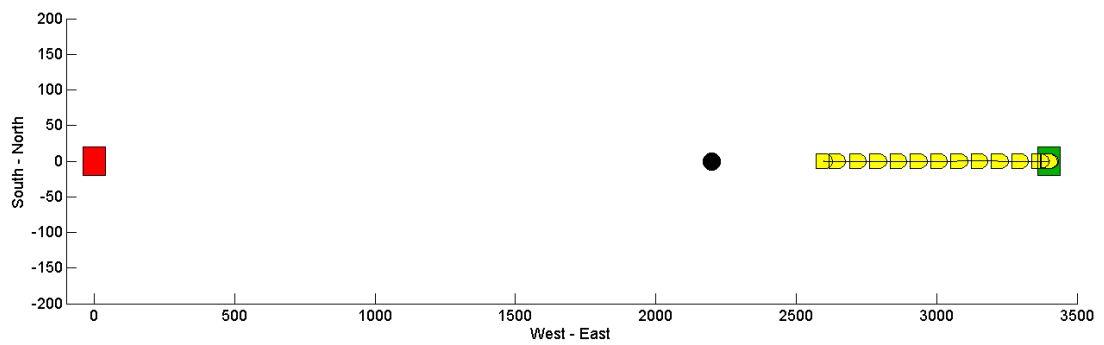
(a) AHV (yellow), AHV target (green), OI (red) and anchor target position (black).
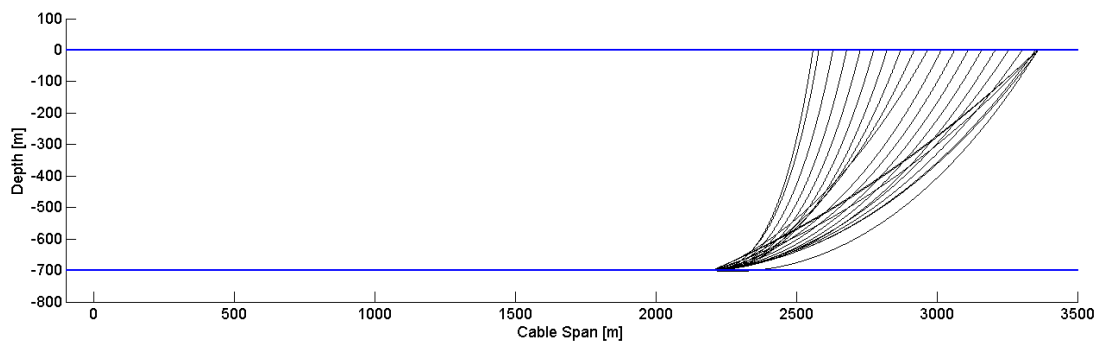

(b) Work wire (black) and surface and seabed (blue).

Figure 8.14. Illustration of vessel movement and cable profiles.

(a) Work wire length.

(b) Cable span.

(c) Vertical (red) and horizontal (blue) catenary forces.
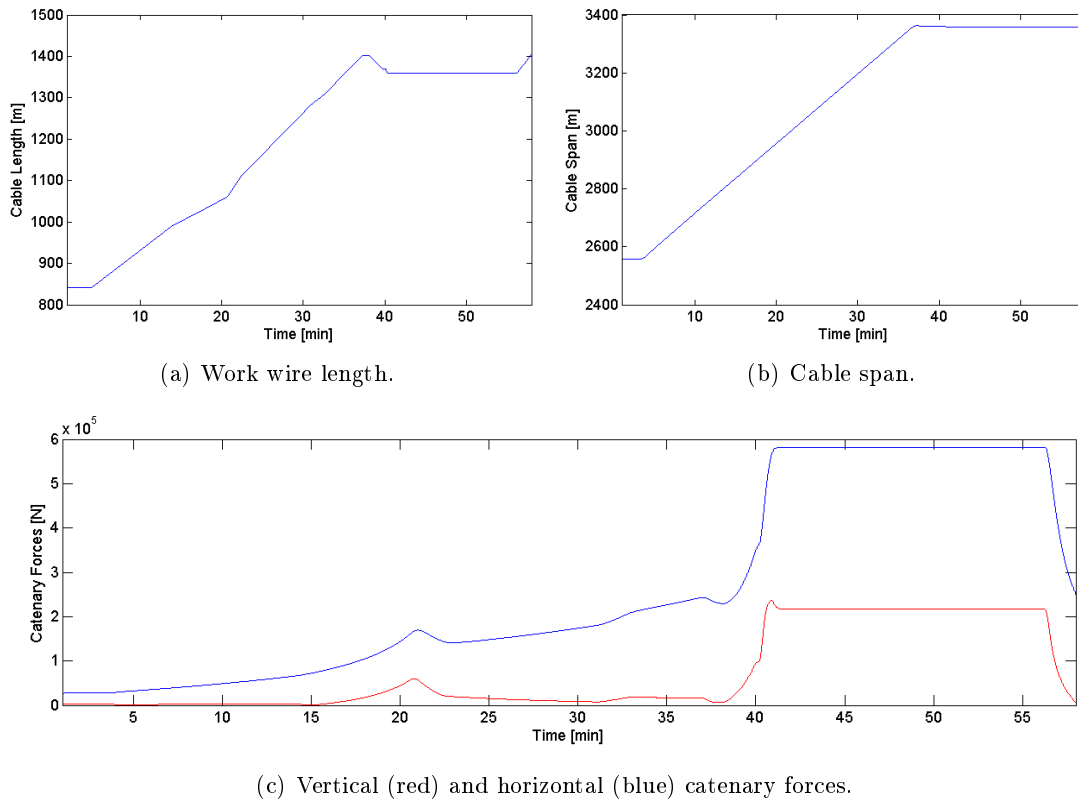
Figure 8.15. Illustration of catenary forces as a function of cable span and work wire length.

(a) Roll (blue) and pitch (red).
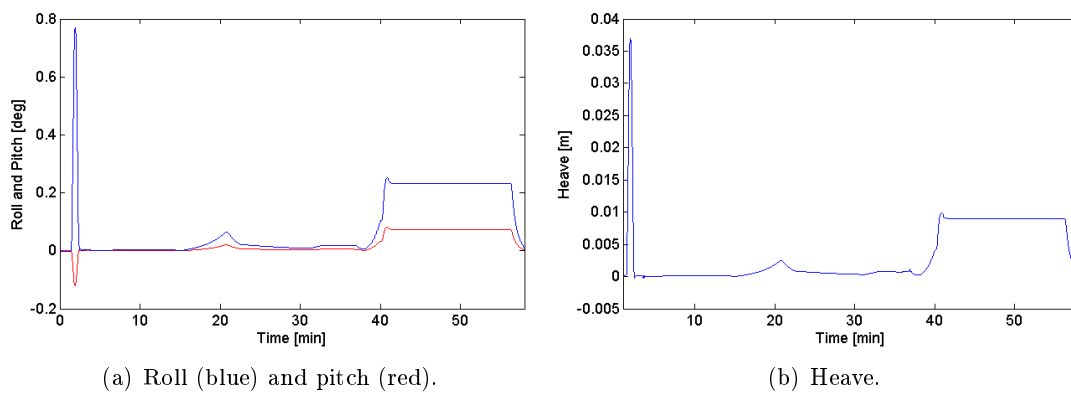
(b) Heave.

Figure 8.16. Roll, pitch and heave amplitudes for the vessel.

(a) Cable Tension.   (b) Friction Force.
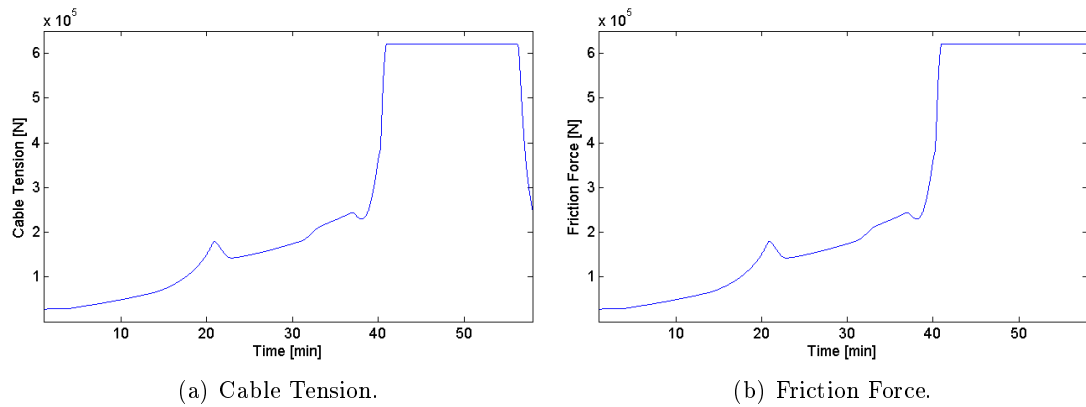
Figure 8.17. Cable Tension and Friction Force

(a) Anchor Velocity.   (b) Anchor Position.
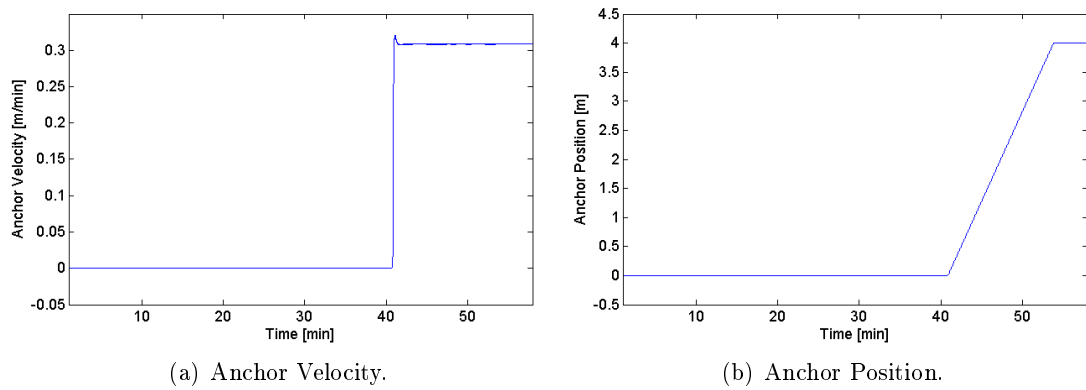
Figure 8.18. Anchor velocity and position during breakout.
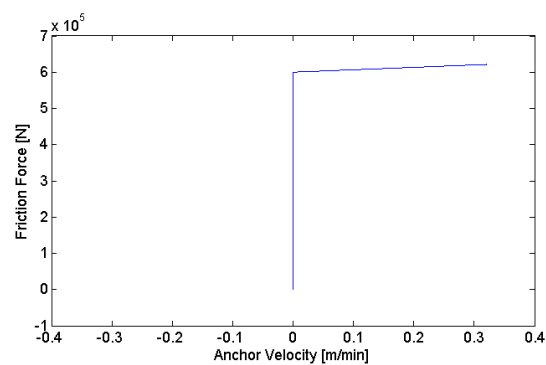
Figure 8.19. Friction force vs anchor velocity

Chapter 9

Discussion

9.1 The Use of Guide Pins and Ballast Tanks

Guide pins and ballast tanks are the two means anchor handling vessels have to manipulate their roll and pitch amplitudes during anchor handling operations. The guide pins restrict the cable movement at the stern of vessel, with the purpose of controlling the attack point of the cable forces and moments.

In *Case Study 1* the starboard guide pin par was used to restrict the cable motion. The ideal weather conditions made it possible to assess the roll and pitch angles as a function of the cable forces. The maximum roll and pitch amplitudes were approximately 1.5 and 0.5 [deg]. In *Case Study 2* the ballast system was used to compensate for the expected roll and pitch values experienced in *Case Study 1*. The ballast tanks effectively corrected the equilibrium point of the vessel during maximum cable load. However, for smaller cable loads, the ballast tanks caused an offset in the roll and pitch values of the vessel. Having full ballast tanks for small cable loads is however better than having empty tanks for large cable loads, since the cable forces are more difficult to predict than the ballast tank loads. For instance, if the ballast tanks of the vessel are filled to counteract an expected cable load, but the cable load is somewhat larger than the expectations, the resulting roll and pitch amplitudes will probably be smaller than the roll and pitch amplitudes of the vessel during the inital phase of the operation.

In *Case Study 4* the portside guide pin par was used to restrict the cable motion. The port side ballast tanks were in addition filled. This means that both the ballast tanks and the cables contributed to a roll moment towards port. The maximum roll amplitude was about 4 [deg]. In the same case study, the inner starboard guide pin broke. The cable could then move freely between the outer starboard and outer port side guide pin, resulting in almost no control of the cable force attack point on the vessel. For operations with heavier and longer cables, such misuse and failures can lead to decreased and critical vessel stability properties.

Guide pins and ballast tanks should always be used together as one system to counteract the effect of the cable forces. The ideal situation would be that the ballast tanks were filled and emptied continuously during the operations based on cable force estimates. It is however difficult to estimate the cable forces. The anchor handling vessels should therefore fill their ballast tanks based on estimates of the maximum cable forces prior to the operation. This should be done in accordance with the selected guide pin configuration. The importance of using ballasts tanks correctly increases with increasing cable weights and seabed depths.

9.2   Roll Reduction

The primary objective of using anti-roll tanks on anchor handling vessels is to create a safe and stable working environment onboard the vessel during rough weather conditions. Free-surface tanks were implemented in the simulator in this thesis.

In *Case Study 2* the free-surface tank was tuned at the vessel's natural frequency in roll. The tank was successful in reducing the roll amplitude of the vessel due to the wave effects. The maximum roll amplitude was approximately 3 [deg], which is within acceptable operating limits. In *Case Study 3* the vessel was subject to the same environmental forces, but the free-surface tank was not used. This resulted in a maximum and minimum roll amplitude of respectively 7.5 and 13.5 [deg], with an offset of about 3 [deg] caused by the ballast tanks and cable forces. Performing anchor handling operations under such working conditions is not an ideal situation.

One of the main limitations of the anchor handling vessel simulator developed in this thesis is the linear restoring moment in roll. The linear restoring moment makes the vessel model valid only for small roll amplitudes. The roll motion result of *Case Study 3*, where large roll amplitudes were experienced, does therefore not reflect reality. The result can however be used as an indication of the large roll amplitudes anchor handling vessel will experience in rough weather conditions.

9.3   Quasi-Static Polynomials and Implementation Issues

Catenary equations were used for cable modeling in this thesis, and a quasi-static polynomial approach with look-up tables was adopted for inclusion of the cable forces in the simulator. The different cable configurations require different catenary models. Finding a polynomial order that results in an acceptable low polynomial error is a design criterion. It depends on the properties of the catenary model and the interval of the cable lengths and cable spans. If a polynomial contains data points with cable spans and cable lengths of similar values, a high polynomial order is required to obtain small errors since the horizontal force will tend towards infinity. It is difficult to determine exactly which polynomial order that is required in any given situation. In this thesis the

polynomial orders were selected based on trial and error, and by considering force error plots induced by the polynomials. A method that automatically evaluates the induced errors and adjusts the polynomial order accordingly should be implemented, but this was not performed since it primarily is a task of commercial and not academic interest.

Look-up tables were used for the double cable configuration since it was necessary to control three variables. The use of look-up tables has some disadvantages. It requires the generation of many polynomials. The amount of polynomials required is primarily determined by the secondary variable interval. A small interval leads to a large amount of polynomial data and much time will be required to generate it. The advantage of using a small interval is that only small jumps in the horizontal and vertical catenary forces will be experienced when the table index is changed. Increasing the secondary interval value results in increasing force jumps. A low-pass filter, which was implemented in the simulator, can however be used to smooth the polynomial outputs. Finding a suitable value for the time constant of the filter is again a design issue depending on the secondary variable interval, the maximum angular winch speed and the vessel speed, since all these elements affect how fast the table index changes.

Cable span segmentation was used to differentiate between the allowable cable lengths for certain cable spans. The segmentation does not add much more complexity to the overall system, but increases the amount of data that must be generated and thus the necessary computing time increases.

The quasi-static approach was successfully implemented in the simulator, using polynomials, look-up tables and cable span segmentation. The implemented scripts generated all cable data automatically for each cable span segmentation, with the desired cable lengths as input. However, much more effort should be put into architectural design of the data generation procedures in order to make the system perfectly flexible for any given simulation scenario. The ideal case would be a system where all cable data is generated based on the seabed depth and the maximum allowable cable span.

9.4 Seabed Interactions

The simulator does not include an explicit model of the seabed. There are two specific situations where seabed interactions are of particular interest. The first is during anchor deployment operations. When the anchor is lowered, some of the mooring chain will land on the seabed before the anchor itself, resulting in a reduction of the cable forces. The simulator implemented in this thesis only used a concept of a virtual seabed, where the vertical anchor coordinate was used to determine when the anchor touchdown occured. This could be observed in the case study cable profile plots, where some of the chain was below the seabed indication line. As a result of this, the cable forces might have been higher during the end phase of the simulations than what would be experienced in real anchor deployment operations.

The second situation where seabed interaction is of interest is during anchor breakout. A LuGre dynamic friction model was used to model the anchor and seabed interaction, where the model parameters were selected based on an emprical dataset from an onshore anchor breakout test. Anchor breakout was considered in *Case Study 4*. The friction parameters were selected so that the anchor did not move until a certain cable tension level was reached, and then the velocity of the anchor increased linearly with increasing cable tension. The linear relationship does not necessaily reflect reality, but the simplification was undertaken due to lack of experimental data. However, the use of such dynamic friction models for modeling anchor and seabed interactions is promising, but further work must be undertaken to produce more realistic friction profiles for various anchor types, anchor sizes and seabed conditions. This requires that a more extensive literature search for experimental and empirical data than what was performed in this thesis is undertaken.

9.5   Operational Limitations of AHVs

In *Case Study 1* and *Case Study 2* it was shown that the vessel had to use maximum power in surge just before the anchor landed on the seabed. This is not necessarily the case for all anchor handling operations, but the results emphasize the importance of evaluating the operational limits of the vessels involved in such operations.

The failure scenario in *Case Study 3* illustrated that a thrust loss of 50 % in sway force and yaw moment made the vessel unable to maneuver freely. The vessel drifted away from the preplanned path and any attempt to change the heading resulted in thrust saturation both in sway, surge and yaw. In reality, the use of thrusters to control the vessel heading will result in a reduction of the bollard pull. The simulator does not account for this effect, but this leads to the conclusion that a real anchor handling vessel would have had even less power available for maneuvering. The only perceivable solution to the drifting situation experienced in *Case Study 3* would have been to land the anchor on the seabed, even though this would have been characterized as a failure of the anchor deployment operation

Before the *Bourbon Dolphin* capsized, the vessel experienced a similar situation as the one depicted in *Case Study 3*. *Bourbon Dolphin* drifted out of course and had to change its heading in an attempt to get back on course. One of the key conclusions in the report on the loss of the *Bourbon Dolphin* [29] stated that the Rig Move Procedure was incomplete. The weather criterias were not defined and the forces were calculated for better weather conditions than the vessel infact operated in. In situations were the vessel drifts uncontrollably or some other problem is faced, there should be clear and concise guidelines on how to handle the situation. The use of anchor handling simulators like the one implemented in this thesis could potentially serve as an extra resource in the planning of anchor handling operations.

Chapter 10

Conclusion and Further Work

10.1 Conclusion

Mathematical models of ballast tanks, anti-roll tanks, cables, seabed and anchor interaction, winch systems, guide pins and a supply vessel have been integrated and implemented in Matlab and Simulink, resulting in an anchor handling vessel simulator capable of simulating both anchor deployment and anchor recovery operations.

Mooring chains and work wires were successfully modeled using catenary equations in combination with a quasi-static polynomial approach and look-up tables. The polynomial order required for a specific catenary configuration is a design factor depending on the properties of the cable itself, the cable spans and the cable lengths of the data set. The disadvantage of using the quasi-static polynomial approach is that all cable data must be preprocessed prior to simulations, which can be very time-consuming for large data sets.

A catenary model for two cables with different properties and one point load, imitating the effect of an anchor, was developed based on existing catenary models in the literature. The model requires that the mass of cable B is greater or equal to the mass of cable A. In practice this means that the mooring chain must be implemented as cable B and the work wire as cable A.

The simulator has two main limitations. The first is the linear roll moment of the vessel, which in effect means that the roll motion of the vessel is invalid for large roll amplitudes. The second is the relative simple implementation of the anchor and seabed interaction during anchor breakout. A LuGre dynamic friction model was adapted to empirical data of breakout forces and speeds, and further simplified to give a linear relationship between the friction force and anchor speed.

A simulator module for guide pins was developed based on functional descriptions. Simulations indicated that the implemented algorithm successfully restricted the lateral cable

motion at the stern of the vessel for different guide pin configurations.

A set of case studies was carried out to evaluate the vessel performance and its operational limits during anchor handling operations. The simulations showed that the vessel was successful in deploying an anchor in ideal and rough weather conditions with optimal vessel configuration. It was also shown that incorrect use of ballast tanks, no use of anti-roll tanks and damage on guide pins in rough weather conditions resulted in large roll amplitudes with uncontrollable cable forces. Partial loss of thrust forces caused the vessel to drift uncontrollably. The results of the case studies emphasize the importance of evaluating both vessel characteristics, weather criterias and chain configurations before anchor handling operations commence.

10.2   Further Work

The implemented anchor handling vessel simulator contains the basic elements necessary to carry out anchor deployment and anchor recovery operations. There are however several elements that are subject to further improvements. The following list contains suggestions for further work that are gathered throughout the course of my work on this thesis.

- The anchor and sebead interaction module should be further improved by adapting it to experimental and empirical data obtained from onshore and offshore anchor breakout tests and measurments. The resulting model should be able to describe the interactions between the anchor and seabed for different anchor types, anchor sizes and seabed conditions.

- At some point during anchor deployment and anchor recovery operations, a part of the mooring chain will be in contact with the seabed, resulting in a reduction of the cable forces acting on the vessel. A simulator module for this phase of the operation should be developed, either based on catenary equations or another cable modeling approach suitable for implemetation in control system designs.

- The implemented simulator modules could be further extended with HIL-testing capabilities. This requires that an extensive reasearch of the possible failure scenarios that can occur during anchor handling operations is carried out.

- The process of generating catenary data for quasi-static simulations should be further improved. A system where all cable data is generated automatically based on the seabed depth and the maximum allowable cable span should be designed. This is not of great academic interest, but a commercial implementation of a quasi-static polynomial approach would require this.

- The method for calculating the cable position in the guide pin module should be expanded. The cable force, relative cable angle, the roll angle of the vessel and possible other elements should be taken into account in the calculations.

References

[1] Ahmed F. Abdel Gawad, Saad A. Ragab, and Ali H. Nayfeh. Roll Stabilization by Anti-Roll Passive Tanks. *Ocean Engineering*, 28(1):457–469, 1999.

[2] American Bureau of Shipping. *Rules for Building and Classing Steel Vessels Under 90 Meters (295 feet) in Length*, 2006.

[3] American Bureau of Shipping. *Rules for Building and Classing Steel Vessels*, 2008.

[4] C. Canudas de Wit, H. Olsson, K. J. Åstrøm, and P. Lischinsky. A new Model for Control Systems with Friction. *IEEE Transactions on Automatic Control*, 40(3):419–425, 1995.

[5] Y. T. Chai and K. S. Varyani. Three Dimensional Lump Mass Formulation of a Catenary Riser with Bending, Torsion and Irregular Seabed Interaction Effect. *Ocean Engineering*, 29:1503–1525, 2002.

[6] R. Dahlberg. Design Procedures for Deepwater Anchors in Clay. *Offshore Technology Conference*, May 1998. OTC 8837.

[7] R. Dahlberg and P.T. Strøm. Unique Onshore Tests of Deepwater Drag-In Plate Anchors. *Offshore Technology Conference*, May 1999. OTC 10989.

[8] Det Norske Veritas. *Offshore Standard DNV-OS-E301 Position Mooring*, October 2008.

[9] Det Norske Veritas. *Rules for Classification of Ships*, 2008.

[10] O. Egeland and J.T. Gravdahl. *Modeling and Simulation for Automatic Control*. Marine Cybernetics, 2002.

[11] 0. M. Faltinsen and A. N. Timokha. *Sloshing*. Cambridge University Press, 2009.

[12] Far Sapphire AHTS Vessel Specification. Website. `http://www.farstad.no/default.asp?menu=97&id=538`.

[13] T.I. Fossen. *Marine Control Systems: Guidance, Navigation and Control of Ships, Rigs and Underwater Vehicles*. Marine Cybernetics, 2002.

[14] T.I. Fossen. *Description of MSS Vessel Models: Configuration Guidelines for Hydrodynamic Codes*, June 2008.

[15] T.I. Fossen. *Modelling and Control of Marine Vessels*. Norwegian University of Science and Technology, 2009.

[16] Gary Ritchie. *Practical Introduction to Anchor Handling and Supply Vessel Operations*. Clarkson Research Services, 2nd edition, 2007.

[17] S. Hana and A.H. Hægeland. Modeling, Control and Simulation of Moonpool Deployment Systems. Master's thesis, Norwegian University of Science and Technology, 2008.

[18] International Mooring Systems. *IMS Product Specification Manual*, 2009. `http://www.internationalmooringsystems.com/imsmembers/downloads/files/manuala.pdf`.

[19] Joint North European Collaboration. *Guidelines for the Safe Management of Offshore Supply and Anchor Handling Operations (NW European Area)*, 2006.

[20] Max Irvine. *Cable Structures*. Massachusetts Institute of Technology, 1981.

[21] Max Irvine and G.B. Sinclair. The Suspended Elastic Cable Under the Action of Concentrated Vertical Loads. *International Journal of Solid Structures*, 12(1):309–317, 1976.

[22] Michael Hancox. *Anchor Handling*, volume 3. Oilfield Publications Limited, 1992.

[23] Mosleh A. Al Shamrani. Finite Element Analysis of Breakout Force of Objects Embedded in Sea Bottom.

[24] Marine Systems Simulator. `www.marinecontrol.org`.

[25] S.R. Neubecker and M.F. Randolph. The Kinematic Behaviour of Drag Anchors in Sand. *Canadian Geotechnical Journal*, 33:584–594, 1996.

[26] Norwegian Maritime Directorate. *Act No. 9 of 16 February 2007 on Maritime Safety*. `http://www.lovdata.no/all/nl-20070216-009.html`.

[27] Norwegian Maritime Directorate. *Statuatory Regulations No. 695 of 15. September 1992 (Building Regulations)*.

[28] Norwegian Maritime Directorate. *Retningslinjer for Gjennomføring av Bestemte Tiltak med Formål å Sikre et Tilstrekkelig Sikkerhetsnivå ved Ankerhåndteringsoperasjoner (AH) som Utføres av Supply eller Taubåter, RSV 04-2008*, 2008.

[29] The Ministry of Justice and the Police. The loss of the bourbon dolphin on 12 april 2007, 2008.

[30] Ole Morten Aamo and Thor Inge Fossen. Finite Element Modelling of Mooring Lines. *Mathematics and Computers in Simulations*, 53:415–422, 2000.

[31] Two Dimensional Weighted Polynomial Fitting and Evaluation. Website. `http://www.mathworks.com/matlabcentral/fileexchange/loadFile.do?objectId=13719&objectType=file`.

[32] V. Rapoport and A. Young. Prediction of Breakout Resistance for Objects Embedded into Seafloor Soil. *OCEANS*, 15:567–572, August 1983.

[33] Simulink Module for Real Time Simulations. Website. `http://www.mathworks.com/matlabcentral/fileexchange/21908`.

[34] Reza Moaleji and Alistair R. Greig. On the Development of Ship Anti-Roll Tanks. *Ocean Engineering*, 34(1):103–121, 2007.

[35] R. Ruinen and G. Degenkamp, editors. *Anchor Selection and Installation for Shallow and Deepwater Mooring Systems*, Stavanger, June 2001. Proc. ISOPE Offshore and Polar Engineering Conf.

[36] A. Sawicki and J. Mierszynski. Mechanics of the Breakout Phenomenon. *Computers and Geotechnics*, 30(3):231–243, 2003.

[37] Shan Huang. Dynamic Analysis of Three-Dimensional Marine Cables. *Ocean Engineering*, 21:587–605, 1994.

[38] Ø.N. Smogeli, T. Perez, T.I. Fossen, and A. J. Sørensen. The Marine Systems Simulator State-Space Model Representation for Dynamically Positioned Surface Vessels. In *International Maritime Association of the Mediterranean IMAM Conference*, 2005.

[39] Svein I. Sagatun. The Elastic Cable Under the Action of Consentrated and Distributed Forces. *Journal of Offshore Mechanics and Arctic Engineering*, 123:43–45, 2001.

[40] M. S. Triantafyllou. *Cable Mechanics with Marine Applications*. Department of Ocean Engineering, Massachusetts Institute of Technology, May 1990.

[41] Tristan Perez. *Ship Motion Control. Course Keeping and Roll Stabilisation Using Rudder and Fins*. Springer, 2005.

[42] Vryhof. *Anchor Manual*, 2005. `www.vryhof.com/pdf/anchor_manual.pdf`.

[43] International Maritime Organization. Website. `http://www.imo.org`.

[44] J. M. Wingnet and R. L. Huston. Cable Dynamics - A Finite Segment Approach. *Computers and Structures*, 6:475–480, 1976.

[45] X.X. Zhou, Y.K. Chow, and C.F. Leung. Numerical Modeling of Breakout Process of Objects Lying on the Seabed Surface. *Computers and Geotechnics*, 35(5):686–702, 2008.

Appendix A

Additional Vessel Model Information

A.1 Position and Velocity Vectors

The elements of the vessel's position and orientation vector are

$$\boldsymbol{\eta} = \left[\ (\mathbf{p}^n)^\top, \ \ \boldsymbol{\Theta}^\top \ \right]^\top = \left[\ n, \ \ e, \ \ d, \ \ \phi, \ \ \theta, \ \ \psi \ \right]^\top \tag{A.1}$$

and the elements of the linear and angular velocity vector are

$$\boldsymbol{\nu} = \left[\ (\mathbf{v}_o^b)^\top, \ \ (\boldsymbol{\omega}_{nb}^b)^\top \ \right]^\top = \left[\ u, \ \ v, \ \ w, \ \ p, \ \ q, \ \ r \ \right]^\top \tag{A.2}$$

The relative velocity is defined as

$$\boldsymbol{\nu}_r = \boldsymbol{\nu} - \boldsymbol{\nu}_c \tag{A.3}$$

where the current velocity vector $\boldsymbol{\nu}_c$ is defined as

$$\boldsymbol{\nu}_c == \left[\ u_c, \ \ v_c, \ \ 0, \ \ 0, \ \ 0, \ \ 0 \ \right]^\top \tag{A.4}$$

for a two-dimensional irrotational current [13]. The elements of (A.4) are

$$u_c = V_c \cos(\beta_c - \psi) \tag{A.5}$$
$$v_c = V_c \sin(\beta_c - \psi) \tag{A.6}$$

where β_c is the side-slip angle of the ship defined in the body-fixed reference frame and V_c is the current velocity.

A.2   Rotation and Transformation Matrices

The generalized velocity transformation matrix between n-frame and b-frame is [13]

$$\mathbf{J}(\mathbf{\Theta}) = \begin{bmatrix} \mathbf{R}_n^b(\mathbf{\Theta}) & \mathbf{0}_{3\times 3} \\ \mathbf{0}_{3\times 3} & T_{\mathbf{\Theta}}(\mathbf{\Theta}) \end{bmatrix} \tag{A.7}$$

where Euler angle rotation matrix defined as

$$\mathbf{R}_b^n(\mathbf{\Theta}) = \begin{bmatrix} c\psi c\theta & -s\psi c\phi + c\psi s\theta s\phi & s\psi s\phi + c\psi c\phi s\theta \\ s\psi c\theta & c\psi c\phi + s\phi s\theta s\psi & -s\psi s\phi + s\theta s\psi c\phi \\ -s\theta & c\theta s\phi & c\theta c\phi \end{bmatrix} \tag{A.8}$$

and the Euler angle attitude transformation matrix is defined as

$$\mathbf{T}_{\mathbf{\Theta}}(\mathbf{\Theta}) = \begin{bmatrix} 1 & s\phi t\theta & c\phi t\theta \\ 0 & c\phi & -s\phi \\ 0 & s\phi/c\theta & c\phi/c\theta \end{bmatrix}, \qquad \phi \neq \pm\frac{\pi}{2} \tag{A.9}$$

Appendix B

Simulator Modules

B.1 Preprocessing of Cable Data

All cable data must be preprocessed prior to simulations. Three MATLAB m-functions are used to process this data for each implemented catenary model. Table B.1 lists the catenary models that are implemented in the simulator. Table B.2 lists the m-functions used to preprocess all cable data prior to simulations for each catenary configuration

Abbreviation	Catenary configuration	Section Reference
C1	General elastic catenary configuration	3.2.2
C2	Double catenary configuration	3.2.4
C3	Inclined elastic catenary configuration	3.2.5

Table B.1. Overview of catenary configurations that are implemented in the simulator.

Model	m-function	Description
C1	C1_CatenaryModel.m	Implementation of Equations (3.16)-(3.17)
C1	C1_GenerateData.m	Generate cable data
C1	C1_CreatePolynomial.m	Convert generated data into a polynomial
C2	C2_CatenaryModel.m	Implementation of Equations (3.30)-(3.33)
C2	C2_GenerateData.m	Generate cable data
C2	C2_CreatePolynomial.m	Convert generated data into a polynomial
C3	C3_CatenaryModel.m	Implementation of Equations (3.36)-(3.37)
C3	C3_GenerateData.m	Generate cable data
C3	C3_CreatePolynomial.m	Convert generated data into a polynomial

Table B.2. Listing of m-functions used for generation of cable data and polynomials prior to simulations.

B.2 Manual Control Module

The manual control module is used to set signals and control parameters during simulations. Table B.3 lists the parameters that are manually controlled and described their use. The control interface is implemented using manual switches (MS) and slider gains (SG), illustrated in Figure B.1. The signals are then routed to the appropriate destinations by means of Goto and From blocks in Simulink.

(a) Slider gain.   (b) Manual switch.
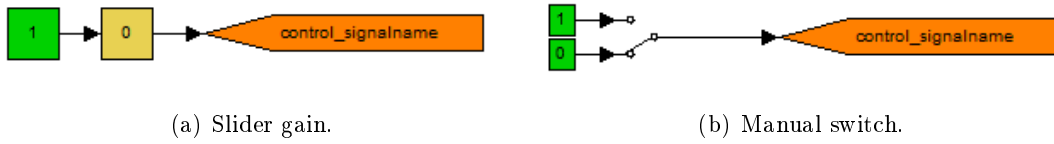
Figure B.1. Control signals used in the Manual Control Module.

Signal Name	Type	Values	Description
cable_plot_active	MS	0/1	Profile plot of cable on/off
animation_active	MS	0/1	Vessel states animation on/off
cable_forces_active	MS	0/1	Cable forces on/off
heading_mode	MS	0/1	Heading reference equal to cable angle manual set-point
heading_angle_ref	SG	-	Manual heading set point
x_ref	SG	-	DP x-axis set point
y_ref	SG	-	DP y-axis set point
freeze_ref	MS	-	Freeze x- and y-ref signal
ahv_winch_speed_or_pos	MS	0/1	AVH winch speed or position controller
ahv_winch_pos_ref	SG	0/1	AVH winch position controller reference
ahv_winch_speed_ref	SG	-	AHV winch speed controller reference
oi_winch_speed_or_pos	MS	0/1	OI winch speed or position controller
oi_winch_pos_ref	SG	-	OI winch position controller reference
oi_winch_speed_ref	SG	-	OI winch speed controller reference
ballast_tanki_h	SG	-	Water height set-point for ballast tank i
catenary_mode_h	MS	1/2/3	Select C1,C2,C3 catenary mode
simulator_mode	MS	0/1	Anchor deployment of recovery

Table B.3. Control signals in the Manual Control Module.

B.3   Cable Module

A conceptual block diagram of the cable module is presented in Figure B.2, resembling the final module implementation in Simulink. The mooring chain and work-wire length is adjusted according to the OI winch and AHV winch speed. The position of the cable attachment point of the cable on the vessel and the relative cable angle is calculated as shown in Section 5.4.
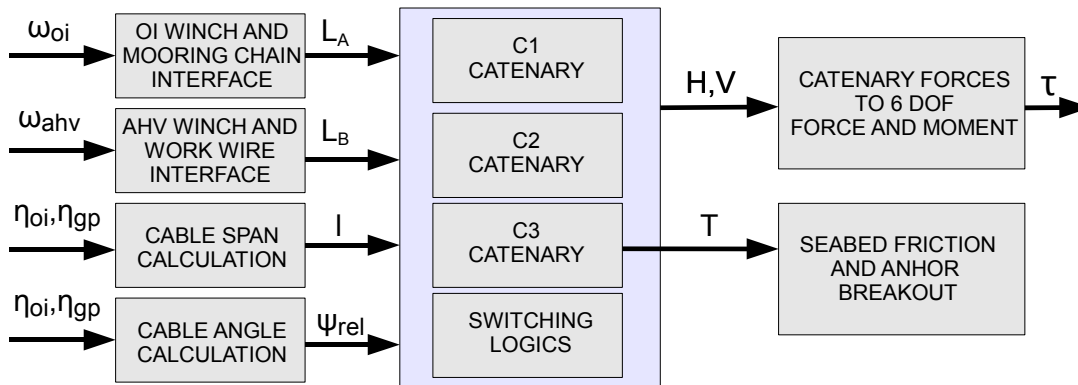
Figure B.2. Block diagram of the cable module.

Three catenary equation configurations are implemented, see Table B.1. A manual switching mechanism is used to select the current catenary representation. For instance, a switch from C1 to C2 means that the anchor is connected to the work wire and deployed from the vessel. However, when C2 is during anchor deployment and the anchor lands on the seabed, the simulator automatically switches to C3. The profile of the cable configuration can be visualized at any time during the simulation, but note that this results in a drastic reduction of simulation speed.

Each of the catenary modules in Figure B.2 is implemented using MATLAB m-functions, where the correct polynomial is evaluated and the catenary forces are calculated. The m-files used during simulations are listed in Table B.4

Catenary model	m-function	Description
C1	C1_GetForces.m	Force calculation
C1	C1_PlotProfile.m	Profile visualization
C2	C2_GetForcesAndAnchorPosition.m	Force calculation
C2	C2_PlotProfile.m	Profile visualization
C3	C3_GetForces.m	Force calculation
C3	C3_PlotProfile.m	Profile visualization

Table B.4. Catenary m-files used by the simulator.

B.4 Guide Pin Module

A conceptual block diagram of the guide pin module is presented in Figure B.3, resembling the final module implementation in Simulink. The module is an implementation of the equations and algorithms presented in Section 6.2.
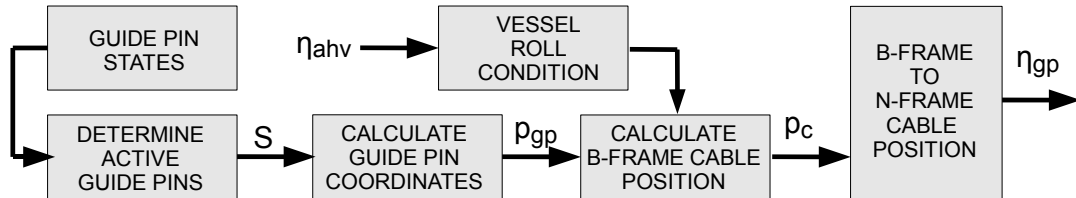
Figure B.3. Block diagram of the guidepin module.

B.5 Winch Module

A conceptual block diagram of the winch system module is presented in Figure B.4, resembling the final module implementation in Simulink. The module is an implementation of the equations presented in Section 6.1. Note that two winch system modules are implemented, as illustrated in Figure 8.1. The AHV winch system is used to control the length of the anchor handling vessel's work wire whereas the OI winch module is used to control the length of the mooring chain. The modules are identical, except from the fact that the inputs differ.
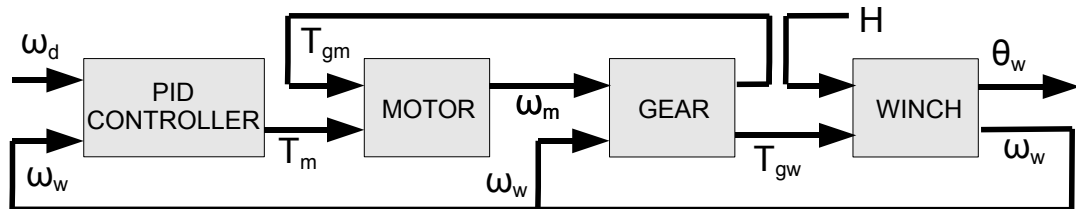
Figure B.4. Block diagram of the winch module.

B.6 Ballast Tank Module

A conceptual block diagram of a ballast tank module is presented in Figure B.4, resembling the final module implementation in Simulink. A ballast system with n_b tanks have n_b such block diagrams associated with it. The output of the complete ballast system is

the sum of the outputs of each individual ballast tank. The module is an implementation of the equations presented in Section 7.1.
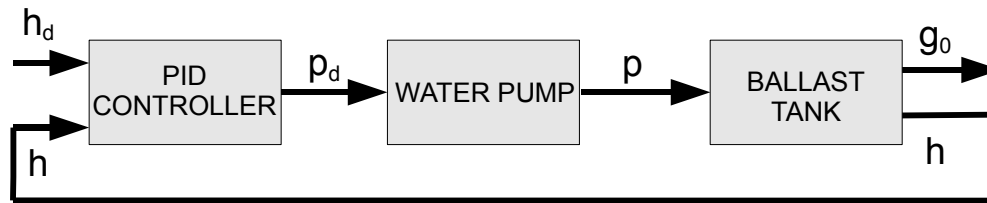
Figure B.5. Block diagram of a ballast tank.

B.7   Anti-Roll Tank Module

No conceptual block diagram is provided for the anti-roll tank module since the module has a straight forward implementation. The effect of the implemented free-surface tank is described by the free surface correction of Equation (7.21) and the roll moment of the tank given by Equation (7.23).

B.8   Real-Time Simulation Block

The simulator is extended with a real-time simulation block downloaded from the *Mathworks* file exchange central [33]. It is convenient to perform the simulations in real time since manual inputs in the manual control module are required during the simulations. The real-time block can be activated and deactived in the manual control module. Activation and deactivation must only be performed prior to simulation, as MATLAB will crash if it is done during simulation. The real-time block has no effect if the simulation already is slower than real time.

Appendix C

Numerical Data

C.1 MSS Supply Vessel Parameters

The vessel data used in the simulations are provided by the MSS-library. The data is loaded into workspace by invoking the MATLAB-functions load(supply) and load(supplyABC). The various elements can then be explored by writing display(vessel) and display(vesselABC) in the command window. The main particulars of the supply vessel is listed in Table C.1.

Parameter	Value	Unit	Definition
m	$6.3622 \cdot 10^6$	[kg]	Mass
ρ	1025	[kg/m^3]	Water density
∇	$6.207 \cdot 10^3$	[m^3]	Displacement volume
T	6	[m]	Draught
B	19.2	[m]	Breadth of ship
S	$1.8202 \cdot 10^3$	[m^2]	Area of wetted surface
L_{pp}	82.8	[m]	Length between perpendiculars
L_{wl}	82.8	[m]	Length of water line
GM_L	103.862	[m]	Longitudinal metacentric height
GM_T	2.144	[m]	Transverse metacentric height
CG_L	-5.3859	[m]	Longitudinal centre of gravity
CG_T	0	[m]	Transverse centre of gravity
CG_V	7.3	[m]	Vertical centre of gravity
CB_L	-5.3860	[m]	Longitudinal centre of buoyancy
CB_T	0	[m]	Transverse centre of buoyancy
CB_V	3.334	[m]	Vertical centre of buoyancy

Table C.1. Main parameters of the supply ship used in simulations.

C.2 Wave Parameters

Parameter	Value	Parameter	Value
Significant Wave Height H_s [m]	4	Number of grid frequencies	20
Peak frequency ω_0 [rad/s]	0.67	Number of grid directions	10
Mean wave direction [deg]	190	Wave component energy limit	0.003
Wave spreading factor	3	Frequency cutoff factor	3
Water depth [m]	700	Direction cutoff	0

C.3 Wave Filter Parameters

$$\lambda = \text{diag} \begin{bmatrix} 0.1 & 0.1 & 0.1 \end{bmatrix} \qquad \omega_0 = \text{diag} \begin{bmatrix} 0.67 & 0.67 & 0.67 \end{bmatrix}$$

$$K_4 = \text{diag} \begin{bmatrix} 100000 & 100000 & 100000 \end{bmatrix} \qquad K_3 = \text{diag} \begin{bmatrix} 66000 & 66000 & 66000 \end{bmatrix}$$

$$\omega_c = \text{diag} \begin{bmatrix} 1.04 & 1.04 & 1.04 \end{bmatrix} \qquad T_b = \text{diag} \begin{bmatrix} 10000 & 10 & 1000000000 \end{bmatrix}$$

$$\boldsymbol{M} = \begin{bmatrix} 0.0001 & 0 & 0 \\ 0 & 0.0007 & 0.0083 \\ 0 & 0.0083 & 4.4971 \end{bmatrix} \cdot 10^8 \qquad \boldsymbol{D} = \begin{bmatrix} 0.0072 & 0 & 0 \\ 0 & 0.0079 & -0.0026 \\ 0 & -0.0026 & 3.57 \end{bmatrix} \cdot 10^9$$

C.4 Controller Parameters

PID Controller Parameter			
Controller	K_p	K_d	K_i
AHV winch speed controller	$3.93 \cdot 10^5$	$4.93 \cdot 10^5$	$4 \cdot 10^5$
OI winch speed controller	$3.93 \cdot 10^5$	$4.93 \cdot 10^5$	$4 \cdot 10^5$
Ballast tank 1,2,3,4 controllers	25	100	0
DP Surge	$9 \cdot 10^5$	$1 \cdot 10^7$	$5 \cdot 10^3$
DP Sway	$2.5 \cdot 10^5$	$4.5 \cdot 10^6$	$1 \cdot 10^3$
DP Yaw	$5 \cdot 10^7$	$8 \cdot 10^6$	$5 \cdot 10^4$

C.5 Simulation Parameters

This section lists all the parameters used for the case study simulations in Section 8.2. Note that not all modules are used in every case study.

AHV and OI Winch System Parameters										
Motor	Gear				Winch			Controller		
J_m	n_g	K_g	D_g	δ_g	J_w	d_w	r_d	K_p	K_d	K_i
15000	10	10	5000	0.2	3000	3000	0.98	$3.9 \cdot 10^5$	$4.9 \cdot 10^5$	$4 \cdot 10^5$

Ballast Tank System Parameters								
Ballast Tanks						Water Pumps		
Tank Number	A_b	h_b	x_b	y_b	z_b	Pump Number	T_p	$p_{p,min}$	$p_{p,max}$
1	36	5	30	5	5	1	7	-2	2
2	36	5	-30	5	5	2	7	-2	2
3	36	5	-30	-5	5	3	7	-2	2
4	36	5	30	-5	5	4	7	-2	2

Guide Pin System Parameters					
Guide Pin Number	x_g^b	y_g^b	z_g^b	Rising slewrate	Falling Slewrate
1	-41.4	-2.5	0	Inf	-Inf
2	-41.4	-2	0	Inf	-Inf
3	-41.4	2	0	Inf	-Inf
4	-41.4	2.5	0	Inf	-Inf

Free Surface Tank Parameters								
ω_4	σ_4	ϵ_t	K_{ta}/A_4	ζ_4	FSC	b_f	l_f	h_w
0.5478	0.5478	$-\pi/2$	$1.2 \cdot 10^8$	0.4976	0.4288	17.2	6.28	1.02

Cable Parameters					
Cable Type	m [kg/m]	m_s [kg/m]	d [mm]	A [m^2]	E [Pa]
Work Wire	24.7	20.83	77	0.0047	$196 \cdot 10^9$
Mooring chain	92	80	84	0.0111	$196 \cdot 10^9$

LuGre Dynamic Friction Model Parameters							
m_a	d_a	F_s	F_c	v_s	σ_0	σ_1	σ_2
18000	20000	$6 \cdot 10^5$	$6 \cdot 10^5$	0.1	$5 \cdot 10^7$	$1 \cdot 10^4$	$4 \cdot 10^6$

Appendix D

Contents of Attached CD-ROM

The contents of the attached CD-ROM are:

- The pdf-file MasterThesis.pdf

- The MATLAB/Simulink files of the simulator

- The simulation data from Case Study 1, 2, 3 and 4.

The simulator requires that the MSS GNC and HYDRO Toolboxes are downloaded from www.marinecontrol.org and installed in MATLAB. Both the simulator folder and the MSS Toolboxes must be added to the MATLAB-path.

The contents of the CD-ROM can also be requested by sending an e-mail to:

- lars.andreas.wennersberg@gmail.com.